Design of Low-Noise Fan Engines for Urban Air Mobility and Sound Quality Analysis Using Virtual Flyovers

Stephen Schade

Deutsches Zentrum für Luft- und Raumfahrt
Institut für Antriebstechnik
Berlin

Deutsches Zentrum
DLR für Luft- und Raumfahrt

Forschungsbericht 2025-26

Design of Low-Noise Fan Engines for Urban Air Mobility and Sound Quality Analysis Using Virtual Flyovers

Stephen Schade

Deutsches Zentrum für Luft- und Raumfahrt
Institut für Antriebstechnik
Berlin

108 Seiten
 57 Bilder
 16 Tabellen
220 Literaturstellen

Deutsches Zentrum
DLR für Luft- und Raumfahrt

DLR

Stephen SCHADE
DLR, Institut für Antriebstechnik, Berlin

Auslegung geräuscharmer Fan-Triebwerke für die urbane Luftmobilität und Analyse der Geräuschqualität anhand virtueller Überflüge

Technische Universität Berlin (Dissertation)

Um eine neue Form des urbanen Luftverkehrs zu ermöglichen, werden neue Flugzeugkonzepte mit verteilten Antriebssystemen erforscht, die mit einer größeren Anzahl von Triebwerken ausgestattet sind, beispielsweise mit verteilten, ummantelten Fans. Aufgrund von akustischen und psychoakustischen Effekten werden sich die Geräusche solcher Antriebssysteme von denen bestehender Antriebe unterscheiden, wodurch die Lärmwahrnehmung zu einem entscheidenden Faktor für die gesellschaftliche Akzeptanz wird.

In dieser Arbeit werden tonale Schallminderungseffekte für langsam drehende, ummantelte Fanstufen mit weniger Stator- als Rotorschaufeln untersucht. Es wird analysiert, wie solche Fanstufen für die urbane Luftmobilität ausgelegt werden können, sodass sie nicht nur leiser sind als konventionelle Designs, sondern auch als weniger unangenehm empfunden werden. Dazu wird das Schaufelzahlverhältnis variiert, wodurch drei akustisch vorteilhafte Designräume identifiziert werden. Zwei tonale Schallminderungseffekte werden analytisch, numerisch und experimentell analysiert, und darauf aufbauend zwei Entwurfsregeln abgeleitet.

Die tonalen Schallminderungseffekte werden an zwei Fanstufen mit reduzierter Statorschaufelzahl demonstriert. Diese werden anschließend virtuell in ein verteiltes Antriebssystem eines Flugtaxis integriert. Trotz vergleichbarer aerodynamischer Leistung zeigen sie deutliche Unterschiede in der Schallabstrahlung. Die Geräuschqualität wird über virtuelle Überflugsimulationen bewertet. Die Ergebnisse zeigen eine Reduktion des EPNL um mehr als 6 dB sowie eine deutliche Verringerung von Lautstärke, Tonalität und Rauheit gegenüber einem Referenzdesign.

(Published in english)

Stephen SCHADE
German Aerospace Center (DLR), Institute of Propulsion Technology, Berlin

Design of Low-Noise Fan Engines for Urban Air Mobility and Sound Quality Analysis Using Virtual Flyovers

Technical University Berlin (dissertation)

To enable a new form of urban air mobility, novel aircraft concepts and distributed propulsion systems are investigated. These propulsion systems consist of a higher number of engines, such as distributed, ducted fans. Due to acoustic and psychoacoustic effects, the noise signatures of such propulsion systems will differ from those of conventional ones, making noise perception a critical factor for public acceptance.

This study investigates tonal noise reduction effects for low-speed, ducted fan stages with fewer stator than rotor blades. The objective is to evaluate how such fan stages can be designed to achieve not only lower noise levels but also an improved perceived sound quality. By varying the blade count ratio, three acoustically beneficial design spaces are identified. Two tonal noise reduction mechanisms are analyzed using analytical, numerical, and experimental methods, leading to the derivation of two design rules.

The identified tonal noise reduction effects are demonstrated on two fan stages with reduced stator vane count. These fan designs are virtually integrated into a distributed propulsion system. Despite similar aerodynamic performance, the designs show significant differences in noise radiation. The sound quality is assessed using virtual flyover simulations. The results show a reduction in Effective Perceived Noise Level (EPNL) of more than 6 dB, along with a noticeable decrease in loudness, tonality, and roughness compared to a reference design.

Design of Low-Noise Fan Engines for Urban Air Mobility and Sound Quality Analysis Using Virtual Flyovers

vorgelegt von

Stephen Schade, M. Sc.

ORCID: 0000-0002-6381-0284

an der Fakultät V – Verkehrs- und Maschinensysteme
der Technischen Universität Berlin
zur Erlangung des akademischen Grades

Doktor der Ingenieurwissenschaften
–Dr.-Ing.–

genehmigte Dissertation

Promotionsausschuss:

Vorsitzender: Prof. Dr. Ennes Sarradj
Gutachter: Prof. Dr. Dieter Peitsch
Gutachter: Prof. Dr. Christophe Schram

Tag der wissenschaftlichen Aussprache: 10. Juli 2025

Berlin 2025

Acknowledgements

Abstract

New aircraft concepts and propulsion systems are developed to power aircraft for urban and regional air transportation. Distributed propulsion systems are designed consisting of a larger number of engines, e.g. ducted fans. The main challenges in operating such aircraft are safety, system complexity and noise. Due to new acoustic and psychoacoustic effects the temporal and spectral noise content and the noise signatures of these aircraft will differ from those of existing aircraft. Should they once become reality, the noise perception of such vehicles is a decisive factor for public acceptance, especially if these aircraft are operated at low-altitudes in densely populated areas. Urban air mobility thus creates a new type of noise pollution that affects the noise characteristics of urban environments. Since the propulsion system dominantly contributes the the overall aircraft noise emission, one of the key objectives is to assess noise reduction mechanisms for future engines.

This work investigates tonal noise reduction measures for low-speed, ducted fans with fewer stator than rotor blades and evaluates the impact of these noise reduction effects on the sound quality characteristics of a distributed propulsion system for an urban air mobility vehicle. The tonal rotor–stator interaction noise is typically the dominant noise source for low-speed fans. Regarding the listening impression, a sensitivity of human hearing to tonality exists. Therefore, the research question addressed in this work is, how low-speed fan stages with fewer stator than rotor blades can be designed for urban air mobility applications, which are not only quieter than conventional designs but also perceived as less unpleasant.

Rotor–stator blade count variations are performed, since the blade-to-vane ratio significantly impacts the tonal noise excitation. As a result of the blade count variations, three acoustically beneficial blade count areas are identified for a low-noise fan design with reduced stator vane count. Two tonal noise reduction mechanisms are analytically and numerically verified and experimentally confirmed which en-

sure that blade count combinations located within the identified design spaces have lower tonal noise levels. In order to apply the effects to fan stages with reduced stator vane count, two design rules are derived and validated.

Using the design rules, the tonal noise reduction effects are demonstrated on two fan stages with fewer stator vanes than rotor blades, which are developed for an urban air mobility application. The 3D blade and vane geometries are obtained from a multidisciplinary optimization process targeting similar aerodynamic efficiency and pressure ratio for all fan designs. An essential characteristic of these fans are substantial differences in the acoustic noise signatures, such as the tonal-to-broadband noise ratio and the dominant tonal noise radiation direction, while the aerodynamic performance in terms of efficiency, pressure ratio and thrust remains similar.

Both fan stages with reduced stator vane count as well as a baseline fan design are each integrated into a distributed propulsion system of an urban air mobility vehicle. The distributed propulsion system consists of 26 low-speed fans installed over the wings. The impact of fan design on the noise signature of the distributed propulsion system is assessed using an analytical process to (1) determine the noise emission, (2) propagate the sound through the atmosphere and (3) provide a binaural noise synthesis. The generated audio files are used to estimate the perception of human hearing based on the sound quality metrics loudness, tonality, roughness, sharpness and fluctuation strength.

The results show that the distributed propulsion system generates noise directivities with complex interference patterns due to the large amount of engines. The sound quality analysis indicates that noise signatures with a high level of sharpness are generated, which is about two times higher than for turbofan engines. Moreover, the two fan designs with reduced stator vane count lead to a reduction in effective perceived noise level of more than 6 dB compared to a baseline design. In addition, these two fan designs show a reduction in loudness, tonality and roughness well above one just noticeable difference compared to the baseline design as a result of the applied noise reduction mechanisms. These sound quality improvements lead to a 40 % reduction in the psychoacoustic annoyance metric compared to the baseline design. This work indicates that aerodynamically equivalent fan designs may produce very different noise signatures, demonstrating that there is a wide latitude in the acoustic design of urban air mobility fan stages.

Zusammenfassung

Um eine neue Form des urbanen und regionalen Luftverkehrs zu ermöglichen, werden neue Flugzeugkonzepte entwickelt. Für diese Flugzeuge werden verteilte Antriebssysteme erforscht, die mit einer größeren Anzahl von Triebwerken ausgestattet sind, beispielsweise mit verteilten, ummantelten Fans. Herausforderungen im Betrieb dieser Flugzeuge sind die Sicherheit, die Systemkomplexität und der Lärm. Aufgrund von akustischen und psychoakustischen Effekten, die sich sowohl auf den zeitlichen als auch auf den spektralen Geräuschinhalt auswirken, unterscheiden sich die Geräusche neuer Flugzeugkonzepte von denen bestehender Flugzeuge. Beim Einsatz dieser Flugzeuge in geringen Höhen und dicht besiedelten Gebieten, wird die Lärmwahrnehmung zu einem entscheidenden Faktor für die gesellschaftliche Akzeptanz. Das Antriebssystem trägt zu einem wesentlichen Anteil zur gesamten Geräuschemission von Flugzeugen bei. Daher müssen Schallminderungseffekte für zukünftige Antriebe untersucht werden.

In dieser Arbeit werden Schallminderungseffekte für langsam drehende, ummantelte Fanstufen mit weniger Stator- als Rotorschaufeln untersucht und die Auswirkungen dieser Effekte auf die Geräuschqualität eines verteilten Antriebssystems eines Flugtaxis bewertet. Der tonale Rotor-Stator-Interaktionsschall ist typischerweise die dominante Schallquelle für langsam drehende Fanstufen. Hinsichtlich des Höreindrucks besteht eine Empfindlichkeit des menschlichen Gehörs gegenüber Tonalität. Die Forschungsfrage dieser Arbeit lautet daher: Wie können langsam drehende Fanstufen mit weniger Stator- als Rotorschaufeln für die urbane Luftmobilität ausgelegt werden, sodass diese nicht nur leiser sind als konventionelle Designs, sondern auch als weniger unangenehm empfunden werden?

Da das Schaufelzahlverhältnis einen wesentlichen Einfluss auf die tonale Schallanregung hat, wird die Anzahl der Rotor- und Statorschaufeln variiert. Als Ergebnis der Schaufelzahlvariationen werden drei akustisch vorteilhafte Bereiche für

ein geräuscharmes Fandesign identifiziert. Darüber hinaus werden zwei Effekte zur Reduktion der tonalen Schallanregung analytisch und numerisch verifiziert und experimentell bestätigt. Aufgrund dieser Effekte weisen Schaufelzahlkombinationen, die sich innerhalb der identifizierten Designräume befinden, geringere tonale Schallpegel auf. Um die tonale Schallreduktion auf Fanstufen mit reduzierter Statorschaufelzahl anzuwenden, werden zwei Entwurfsregeln abgeleitet.

Durch Anwendung der Entwurfsregeln werden zwei Fanstufen mit weniger Stator- als Rotorschaufeln, für eine Anwendung in der urbanen Luftmobilität, ausgelegt. Die 3D Geometrien der Schaufeln sind das Ergebnis eines multidisziplinären Optimierungsprozesses, für den der Wirkungsgrad und das Druckverhältnis als Zielfunktionen vorgegeben werden. Ein wesentliches Merkmal dieser Fanstufen ist, dass sich bei ähnlicher aerodynamischer Leistung die Schallabstrahlung der einzelnen Designs deutlich voneinander unterscheidet, beispielsweise hinsichtlich des Verhältnisses von tonalem zu breitbandigem Schall und der dominanten tonalen Schallabstrahlungsrichtung.

Beide Fanstufen sowie ein Referenz-Design werden jeweils in ein verteiltes Antriebssystem eines Flugtaxis integriert. Das Antriebssystem besteht aus 26 Fans, die oberhalb der Tragflächen verteilt sind. Die Auswirkung des Fandesigns auf die Geräusche des Antriebssystems wird mit einem analytischen Prozess bewertet, mit dem (1) die Schallemission und (2) die Ausbreitung des Schalls in der Atmosphäre berechnet werden sowie (3) eine binaurale Geräuschsynthese durchgeführt wird. Die Audiosignale werden verwendet, um die Geräusche basierend auf den Metriken Lautheit, Tonalität, Rauheit, Schärfe und Fluktuationsstärke zu beurteilen.

Die Ergebnisse zeigen, dass das verteilte Antriebssystem, aufgrund der großen Anzahl von Triebwerken, Richtcharakteristiken mit komplexen Interferenzmustern erzeugt. Die Analyse der Geräuschqualität verdeutlicht, dass Geräuschsignaturen mit einer hohen Schärfe erzeugt werden, die etwa doppelt so hoch ist wie bei Turbofan-Triebwerken. Darüber hinaus weisen die beiden Fandesigns mit reduzierter Statorschaufelzahl eine Verringerung des effektiv wahrgenommenen Schallpegels (EPNL) von mehr als 6 dB im Vergleich zum Referenzdesign auf. Zusätzlich erreichen diese beiden Fandesigns eine Verringerung der Lautstärke, Tonalität und Rauheit im Vergleich zum Referenzdesign, die jeweils deutlich über einem gerade wahrnehmbaren Unterschied liegt. Diese Verbesserungen der Geräuschqualität führen zu einer Verringerung der psychoakustischen Belästigungsmetrik um 40 %

im Vergleich zum Referenzdesign. Diese Arbeit verdeutlicht, dass aerodynamisch ähnliche Fandesigns sehr unterschiedliche Geräuschsignaturen erzeugen können, was wiederum bedeutet, dass es einen großen Designraum bei der akustischen Auslegung von Fanstufen für die urbane Luftfahrt gibt.

Graphical abstract

Figure 1 shows the graphical abstract of this cumulative dissertation.
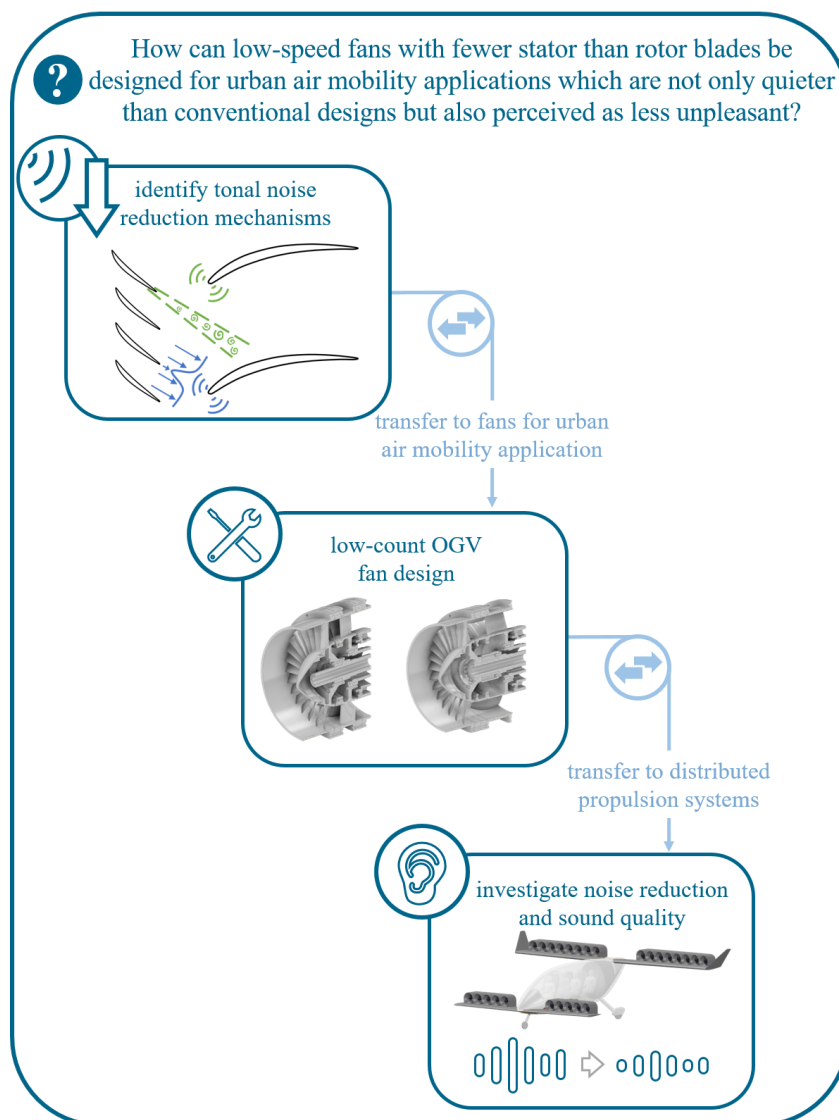
Figure 1: Graphical abstract.

Contents

II

List of Abbreviations

AAM	Advanced Air Mobility
CORAL	airCraft engine nOise auRALization
CRAFT	Co-/Counter Rotating Acoustic Fan Test
DLR	German Aerospace Center
EASA	European Union Aviation Safety Agency
EDF	Electric Ducted Fan
EPNL	Effective Perceived Noise Level
FAA	Federal Aviation Agency
FAR	Federal Aviation Regulation
HRIR	Head Related Impulse Response
NASA	National Aeronautics and Space Administration
OGV	Outer Guide Vane
PNL	Perceived Noise Level
PNLT	Tone-corrected Perceived Noise Level
PropNoise	Propulsion Noise
UAM	Urban Air Mobility
UHBR	Ultra High Bypass Ratio
VIOLIN	Virtual acoustIc flyOver simuLatIoN
VTOL	Vertical Take-Off and Landing

Structure of this dissertation

This cumulative dissertation is organized as follows. Chapter 1 is the introduction. Section 1.1 provides an overview of the research area in which this work is integrated. Section 1.2 reviews relevant work from literature and outlines the research demand. Section 1.3 summarizes the research motivation and states the research question and objectives. Section 1.4 provides the contribution of each publication to answer the research question. Chapter 2 shows the three journal papers in chronological order. In Chap. 3 the results and limitations are discussed and in Chap. 4 the main conclusions are summarized. Based on the limitations an outlook for future studies is formulated in Chap. 5.

Chapter 1

Introduction

1.1 Research context

This section outlines the research context in which this work is embedded. Section 1.1.1 describes the motivation and challenges for urban air mobility. In Sec. 1.1.2, our current understanding about the acoustic characteristics of distributed propulsion systems is summarized.

1.1.1 Urban air mobility – vision and challenges

In the future, small aircraft, for instance so-called air taxis, are intended to provide a new form of local air transportation, which is referred to as Urban Air Mobility (UAM). The European Union Aviation Safety Agency (EASA) defines UAM as a "new, safe and more sustainable" type of transportation, which is intended to carry passengers as well as cargo within densely populated regions [25]. According to a definition by the National Aeronautics and Space Administration (NASA), "UAM is the concept of expanding transportation networks to include short flights that transport people and goods around metropolitan areas. UAM is part of a larger paradigm shift toward AAM [(Advanced Air Mobility)], in which new technologies and business models are enabling transformational applications of aviation [...]" [39]. The feasibility, economics and ground infrastructure intended for a future on-demand air transportation in metropolitan areas are reviewed by the private company UBER Elevate [27]. If certain challenges, such as noise emissions, safety and costs, are successfully resolved, UBER draws the vision that UAM may

be a widely used form of urban transportation [27]. Based on these definitions, Fig. 1.1 sketches possible UAM use cases.
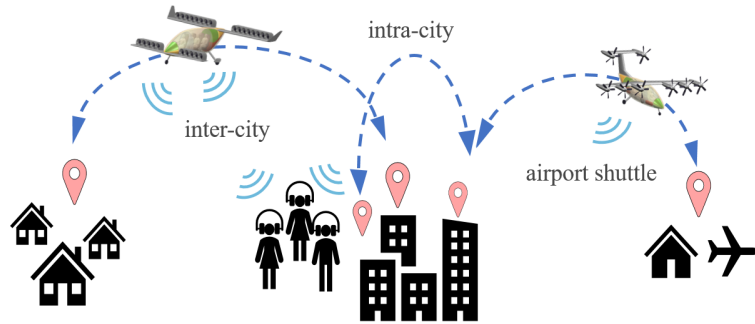
Figure 1.1: Examples of targeted UAM use cases.

UAM is commonly considered as one step towards the electrification of aviation [25]. Therefore, it is expected that new aircraft powered by electrical propulsion systems may mainly conduct these air taxi operations [39]. Moreover, vertical take-off and landing (VTOL) capabilities represent a major technology for UAM. Within industry, several electrically powered aircraft are being developed for UAM applications. Examples include the *Lilium jet* (see Fig. 1.2(a)) and the *Joby S2* (see Fig. 1.2(b)) VTOL aircraft. For the Lilium jet, Nathen [63] describe the design and performance of the aircraft, which is powered by a ducted, vectored thrust system consisting of several distributed fans. For the Joby S2, Stoll *et al.* [79] describe the design of the aircraft, which is powered by electrical, distributed propellers.

(a) Lilium jet [54]

(b) Joby Aviation aircraft [5]

Figure 1.2: Industry examples of UAM VTOL aircraft concepts.

Based on the findings from Pak *et al.* [65], the three key challenges (1) profitability, (2) system complexity and (3) community acceptance must be resolved so that UAM can be established. Community acceptance is, according to their

assessment, mainly driven by safety and noise. Noise as a key concern is also confirmed by the results of two public surveys conducted by Eißfeldt and Stolz [26] and EASA [24]. The study conducted by EASA indicates a negative correlation between annoyance and familiarity of a sound [24]. This means that citizens would rate UAM noise emissions more annoying compared to other noise signatures at the same level due to the unfamiliarity of the sound. This is particularly important as Rizzi *et al.* [71] expect that UAM noise signatures considerably vary compared to those from existing aircraft and helicopters due to different temporal and spectral characteristics resulting in a different aural impression. Thus, human annoyance ratings may vary between UAM and existing aircraft. However, the subjective annoyance ratings do not only depend on the noise signature, but also on non-acoustic factors, such as the time of day and the respective situation, in which the sound is experienced [6]. As a result, assessing noise reduction mechanisms for UAM vehicles is a high level objective that needs to be addressed at an early stage in the design process [71].

As an intermediate summary, UAM is a new form of mobility creating a new type of noise pollution, which affects the noise characteristics of our urban environments. A major challenge for future aviation is to reduce noise emissions since noise emissions are an obstacle to public acceptance. However, if noise emissions of future generations of aircraft are reduced substantially, it can be expected that a larger number of these aircraft enter the market leading to a larger number of flights. This will in turn result in a higher impact on people and environment in absolute terms. As a result, acoustics is a controversial topic, since quieter aircraft have a positive impact on human perception and health on the one hand, but can also increase the overall fleet size, which in turn may rise again the absolute noise levels in urban environments.

1.1.2   Acoustics of distributed propulsion systems

Distributed propulsion systems are arrays of propulsion units consisting of several engines, such as ducted fans or open propellers, which are installed above or along the wing or at the wingtips [44]. These propulsion systems may offer the potential for acoustic benefits through the propulsor arrangement and lower tip speeds, while achieving higher operational flexibility and system redundancy due to the larger amount of engines [44]. Examples of DLR UAM vehicles equipped with distributed

propulsion systems are shown in Fig. 1.3.

(a) HorizonUAM multicopter [3]

(b) HorizonUAM tilt-rotor vehicle [65]

(c) VIRLWINT tilt-duct vehicle [72]

(d) VIRLWINT tilt-rotor vehicle [72]
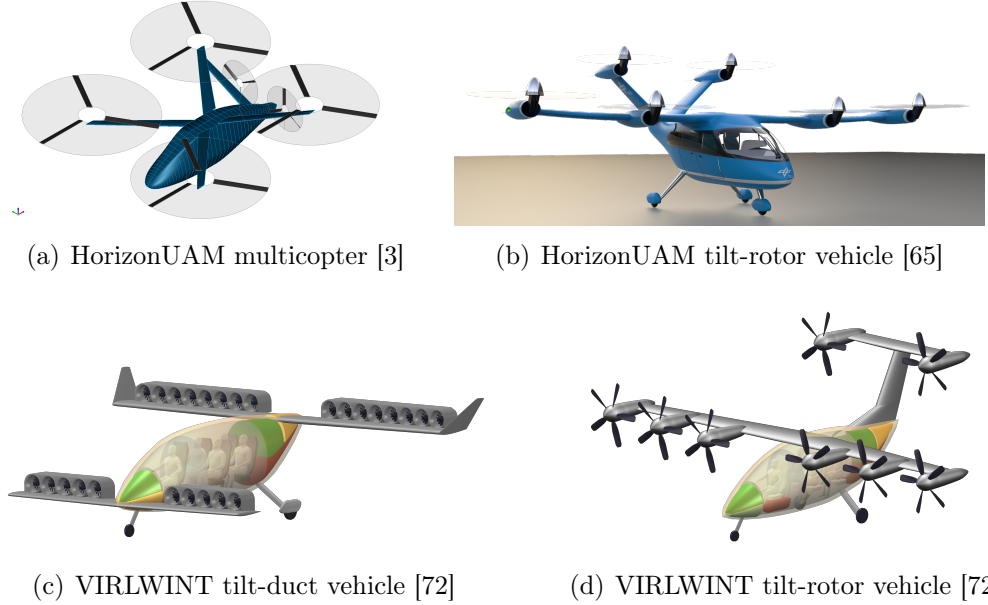
Figure 1.3: DLR UAM vehicle concepts with distributed propulsion systems obtained from the DLR-funded projects VIRLWINT and HorizonUAM.

Kim *et al.* [44] review different concepts of distributed propulsion systems and evaluate aeroacoustic challenges and advantages. For instance, boundary layer ingestion may on the on hand increase the propulsive efficiency of ducted fans [44] but might also intensify the tonal noise excitation on the other hand [48, 17]. Studies on the aerodynamic and acoustic interaction between propulsion units indicate that the arrangement and number of propulsors may significantly influence the noise emission [35, 8, 67]. The sound fields emitted from the engines may interfere with each other during noise propagation through the atmosphere. This leads to destructive or constructive interferences and thus to amplification or cancellation of the sound waves [35]. For the aural impression, this means that the sound pressure amplitudes may vary considerably within short periods of time. This effect can be further intensified due to potential rotational speed deviations between individual propulsors. Moreover, the diameter of the propulsors and their rotational speed influence the frequency spectrum of the noise emission. Compared to turbofan engines, the noise emission spectrum may be shifted to higher frequencies in the case of multiple distributed fans with small diameters. Moreover, the flight

speed and propagation distance between sound source and observer are reduced, which may also modify the aural impression compared to existing aircraft.

As a result of these effects, which affect both the temporal and spectral noise signature, the subjective noise perception of distributed propulsion systems is expected to differ from those of existing propulsion systems [71]. This is expressed not only by differences in the sound level, but particularly in terms of the listening experience, which is determined by the psychoacoustic characteristics of a sound.

The research context outlined in this Section and in Sec. 1.1.1 can be summarized as follows. UAM is only feasible in the future if the key challenges of safety, system complexity and, in particular, noise are solved for the operation of air taxis. With regard to noise, the use of distributed propulsion systems brings the additional challenge that the temporal and spectral noise content may differ from that of existing aircraft resulting in different psychoacoustic noise signatures. If these aircraft will be operated at low altitudes in urban, possibly densely populated areas, noise emissions and noise exposure will therefore become a decisive factor regarding the public acceptance towards these aircraft.

Within these fields of research this work investigates noise reduction mechanisms for low-speed, ducted fan stages and evaluates the impact of these noise reduction effects on the sound quality characteristics of a distributed propulsion system for an UAM VTOL vehicle.

1.2 Literature review and research demand

This section reviews the relevant literature on the topic and derives the research demand. Since the distributed propulsion system considered in this work consists of ducted fans, Sec. 1.2.1 reviews applications of low-speed fans in urban and regional air mobility. Section 1.2.2 describes the excitation mechanism of the dominant noise source for these fan stages. Sections 1.2.3 and 1.2.4 evaluate different design approaches for ducted fans with regard to the number of rotor and stator blades, as the blade-to-vane ratio significantly influences the fan acoustics. Section 1.2.5 outlines the advantages of auralization methods and sound quality metrics compared to the evaluation of single noise levels with regard to noise signatures obtained from distributed propulsion systems.

1.2.1 Low-speed, ducted fan stages

The term ducted or shrouded fan is used in the literature to describe both ducted propellers and ducted rotor-stator fan stages. The latter are examined in this work and are subsequently denoted as ducted fans or low-speed ducted fans.

A range of novel aircraft concepts and prototypes for urban and regional air mobility applications are currently under development, incorporating low-speed ducted fans or electric ducted fans (EDFs) in case of an electric powertrain. For urban air mobility applications, the *Lilium Jet* serves as a representative example, which is powered by multiple EDFs distributed across the canard and main wings [63]. Another UAM vehicle powered by EDF is the *APELEON X1* demonstrator. Schoder et al.[75] propose a low–cost experimental measurement setup to quantify the acoustic characteristics of EDFs at an early prototyping stage, which they apply to the noise emission analysis of the APELEON X1 fan units. For regional air mobility, notable concepts include the *NASA N3-X* blended wing body design [9, 43] and the *ESAERO ECO-150*. Schiltgen et al. [74] design the low-speed fan stages for the ECO-150 aircraft and integrate them into the leading edge of the wing to enable a distributed split-wing propulsion system. Further research on EDF applications extends to VTOL drones. *StriekAir* develops a VTOL drone, for which Casagrande Hirono et al.[14] examine the aeroacoustic characteristics of three EDF designs with different rotor and stator blade counts.

Castegnaro [15] provides an historical overview of fan design developments, summarizing various design methodologies for low-speed fans. Zhang and Barakos [93] review analytical, numerical, and experimental studies on ducted fans and see a future application of such fans also for rotorcraft configurations, as for example compound helicopters.

1.2.2 Rotor–stator interaction noise

Fan noise can be classified into two main noise excitation mechanisms: self-noise and interaction noise. Firstly, self-noise includes sources arising from the aerodynamic flow around the blades. For instance, resulting from the flow redirection and flow displacement by the blades, which generate a stationary pressure field around the blades. Due to the rotation of the rotor, a fluctuating pressure field is created leading to a noise excitation. However, as derived by Moreau and Guérin [58], this

source radiates noise less efficiently at subsonic conditions, as encountered for low-speed fan stages, and is for this reason not explained further. Likewise, broadband trailing edge noise, which is another self-noise source, is not considered, as this source is not dominant for the considered case. Since noise reduction effects at the source are investigated in this work, clean fan inflow conditions are assumed. The assessment of inflow distortions is out of scope for this work.

The second type of noise source is called interaction noise as this source results from the interaction of the flow of the rotor with the downstream leading edge of the stator. The rotor wakes periodically impinge on the stator leading edges, which generates unsteady forces on the stator vanes. These unsteady forces are induced by an inhomogeneous velocity distribution (sketched in blue in Fig. 1.4) on the one hand and increased turbulence within the rotor wakes (sketched in green in Fig. 1.4) on the other. Due to the periodic interaction of the wakes with the stator leading edges, unsteady pressure fluctuations are induced causing a variation of airfoil lift. As a result, a dipole noise source is generated located at the stator leading edge. Depending on these flow disturbances the interaction noise source is subdivided into a broadband and a tonal component. The tonal and broadband excitation mechanisms are visualized in Fig. 1.4 and described in the following.
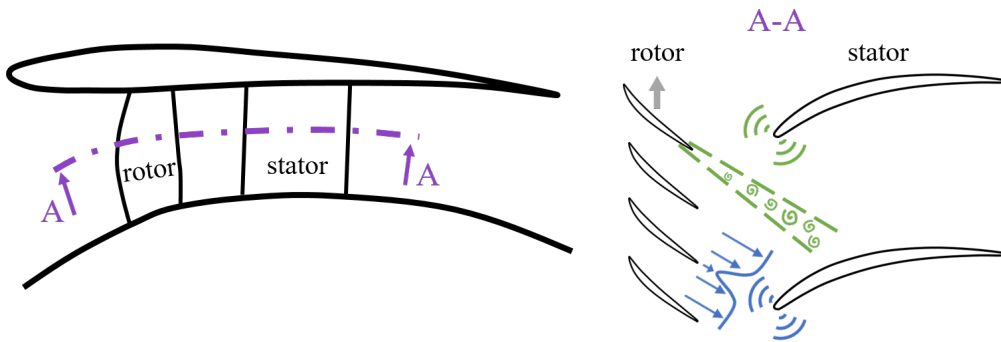
Figure 1.4: Schematic illustration of the tonal (blue) and broadband (green) excitation mechanisms of the rotor–stator interaction noise source.

Broadband component

As a result of the rotor wake turbulence a flow perturbation is produced in terms of a stochastic distribution of turbulent eddies. Due to the interaction of these stochastic fluctuations with the stator leading edge, pressure fluctuations are ex-

cited within a broad frequency range. As an example, a schematic broadband frequency spectrum is shown in green in Fig. 1.5. Broadband interaction noise directly scales with the number of stator vanes [19, 57, 62]. If the number of stator vanes is halved, the overall broadband levels are reduced in good approximation by 3 dB, which is experimentally verified by Woodward *et al.* [91] and analytically found by Jaron [40].

Tonal component

Tonal rotor–stator interaction noise results from the periodic impingement of the wakes generated by the upstream rotors on the leading edges of the downstream stators. The excited tonal frequencies are determined from the number of rotor blades multiplied with the rotor's rotation frequency. These frequencies are denoted as blade passing frequencies (BPFs). Fan tones at the BPF and its second and third harmonics are exemplarily visualized in blue in Fig. 1.5. The excited acoustic modes can be determined as a function of the rotor and stator blade numbers using the relation derived by Tyler and Sofrin [85].
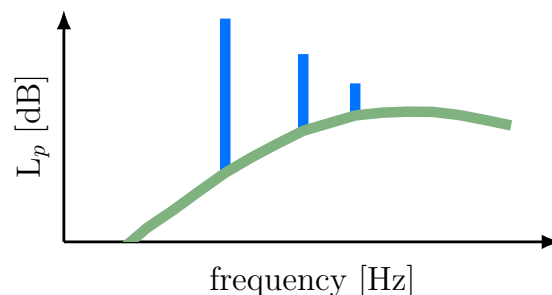
Figure 1.5: Schematic sketch of a broadband frequency spectrum (green) including tones at the blade passing frequency and at two of its harmonics (blue).

The tonal noise excitation is either cut-on or cut-off depending on the rotor and stator blade counts, where cut-on and cut-off refer to the propagation capability of acoustic energy. In an acoustic cut-on scenario, the pressure fluctuations excite acoustic waves at harmonics of the blade passing frequency. These acoustic waves then propagate upstream and downstream. By contrast, in an acoustic cut-off scenario, the periodic impingement of the wakes still induces an acoustic excitation, however, the acoustic energy remains confined to the stator leading edge region (noise source region). Thus, no acoustic energy is propagated upstream or

downstream. The cut-off condition is a common mechanism used in acoustic fan design to eliminate noise excitation at the BPF tone. Conventionally, to cut off the BPF tone, the stator vane count is chosen significantly larger (by a factor > 1.5) than the rotor blade count. However, for low-speed fan stages, certain rotor–stator blade count combinations exist where a cut-off condition can be realized although the stator vane count is lower than the rotor blade count [12, 60, 13]. This is called an inverse cut-off.

For low-speed fan stages, interaction noise in general and its tonal component in particular are typically the dominant noise source. Commonly, the blade passing frequency tone and its harmonics dominate the noise generation spectrum. This is found in the experimental results of Schoder *et al.* [75] on an electric ducted fan or in the studies on NASA's Q-Fan conducted by Worobel *et al.* [92] and Metzger *et al.* [55] as well as in the experimental results on DLR's low-speed fan CRAFT conducted by Klähn *et al.* [46] and Tapken *et al.* [82]. This emphasizes the relevance of investigating tonal noise reduction mechanisms at the source for low-speed fan stages.

1.2.3 Conventional fan designs

Typically, fan stages are designed with more stator than rotor blades. The key driver for this design decision is acoustics, as the blade-to-vane ratio influences the noise emission of fan stages. With a considerably larger number of stator vanes compared to the rotor, the tonal rotor-stator interaction noise is reduced by design since the cut-off condition is achieved for the BPF tone (see Sec. 1.2.2). The reduction in tonal noise is counteracted by an increase in broadband rotor-stator interaction noise as a result of its proportionality to the stator vane count (see Sec. 1.2.2). Due to the higher number of stator vanes, the stator has smaller chord lengths and smaller pitchwise distances between neighboring vanes compared to the rotor. This may increase the complexity of manufacturing, especially for small fan diameters, as might be the case for an application in urban air mobility. In addition, high blade numbers may increase the maintenance effort and costs.

In this work, these types of fan stages with more stator than rotor blades are referred to as conventional fan designs.

1.2.4 Low-count OGV fan designs

By contrast to conventional fan designs, fan stages can also be equipped with fewer stator than rotor blades. These designs are known as low-count OGV (outer guide vane) fan stages and are the main research subjects of this work.

Low-count OGV fans have considerably thicker stator vanes with longer chord lengths compared to the rotor. Dittmar *et al.* [19] showed that with a reduced number of stator vanes acoustic damping material could be applied to the vane surfaces as a result of the increased thickness and length of the vanes and suggested that load carrying struts could be replaced in case of long-chord stator vanes. Moreover, a lower number of vanes could also reduce manufacturing and maintenance costs. When operating with an electric motor, which is located in the aircraft fuselage, fewer and therefore thicker stator vanes may offer the additional advantage of guiding the motor shaft directly through one of the stators. This approach is followed in the design shown by Weintraub *et al.* [90] for a hybrid electrically operated ducted fan.

Regarding the acoustic characteristics of low-count OGV fans, contrary to conventional designs, the broadband interaction noise source is reduced by design due to the lower number of stator vanes (see Sec. 1.2.2). However, by contrast to conventional high-speed fans, the cut-off condition of the BPF tone can no longer be achieved as a result of the reduced stator vane count. Therefore, high-speed low-count OGV fans are cut-on designs, meaning that the BPF tone and its harmonics become dominant. This may lead to a rather tonal noise emission. Consequently, due to (1) the reduction of broadband interaction noise by design and (2) the cut-on condition of the BPF tone and its harmonics, a high tonal-to-broadband noise ratio is expected. As a result, there is no inherent tonal advantage as for conventional designs due to the propagating tonal duct modes, which are no longer cut-off. Thus, for low-count OGV fan stages there is the demand to investigate tonal noise reduction mechanisms.

In the literature, only few studies are available so far that examine low-count OGV fan stages and tonal noise reduction methods for these fans. The fundamental work is the study by Schwaller *et al.* [76], who acoustically analyzed high-speed fans with several blade-to-vane ratios and concluded that with a reduced number of stator vanes, both the tonal and broadband noise decreases at higher frequencies. Based on these results, Kröger *et al.* [51] performed an aerodynamic optimization of

an OGV with reduced vane count and concluded that high-speed fan designs with reduced OGV count are feasible with regard to good aerodynamic performance. Giacché *et al.* [32] then provided an acoustic optimization for this OGV. In the acoustic optimization, a non-uniform distribution of sweep at the stator leading edge was applied to mitigate the tonal penalty existing for high-speed, low-count OGV fans. Dittmar and Woodward [20] applied a different approach to reduce tonal noise for low-count OGV fans. While significantly reducing the number of stator vanes they additionally increased the number of rotor blades. Dittmar and Woodward [20] concluded that using this approach, low-count OGV fans provide a high potential for perceived noise reduction because, on the one hand, a higher number of rotor blades shifts the fan tones to higher frequencies which are outside of the sensitive range for human hearing and, on the other hand, a reduced number of stator vanes decreases the rotor–stator interaction broadband noise.

Based on this literature review, the hypothesis for this work is formulated that if the tonal noise penalty can already be mitigated at the source, low-count OGV designs offer the potential for quiet fans, as broadband noise is directly decreased by design. Therefore, two effects are examined in order to reduce tonal noise excitation for low-count OGV fans. On the one hand, the inverse cut-off effect is investigated. This effect could be a promising tonal noise reduction mechanism for low-speed, low-count OGV fans, as with reduced rotor tip Mach number a cut-off condition can be achieved even with fewer stator vanes than rotor blades (see publication I). In this case, low-count OGV designs benefit from the cut-off condition in a similar way to conventional designs. Broszat *et al.* already numerically verified the tonal noise reduction potential of the inverse cut-off effect for a low-pressure turbine stage [12], experimentally confirmed the reduction potential and concluded that this effect can efficiently reduce tonal noise, although in the experiments the absolute noise level reduction was lower due to background noise [13]. Moreau *et al.* [60] acoustically re-designed a ventilator, which entrains the flow in a wind tunnel, and used the inverse cut-off effect to mitigate tonal noise produced by the ventilator of the wind tunnel. To the best of the author's knowledge, this effect has not yet been demonstrated on a low-count OGV fan intended for an UAM distributed propulsion system. On the other hand, for those low-count OGV fans where the cut-off condition is not reached, an additional effect is investigated that reduces the noise excitation at the blade passing frequency

11

tone. This approach is based on a well-considered choice of the rotor and stator blade numbers to reduce the tonal noise excitation although the BPF is cut-on. The physical explanation of this effect is based on the propagation direction of the excited acoustic waves relative to the main dipole radiation axis. Provided that the propagation direction of acoustic modes, expressed by the modal phase propagation angle, is perpendicular to the dipole radiation axis, a minimum of acoustic energy is excited [21]. The definition of the modal phase propagation angle is derived by Moreau *et al.* [59]. Since the propagation direction depends on the excited acoustic interaction modes and the mode orders in turn depend on the blade numbers, the effect can be controlled by a well-considered choice of the rotor–stator blade count. Duncan and Dawson [21] first theoretically investigated this effect and named this mechanisms "Venetian blind" effect. Jaron [40] also observed this effect when investigating an UHBR (ultra high bypass ratio) fan stage, but has not yet transferred it to a low-speed, low-count OGV fan. Moreover, the physical mechanism of the effect resulting from the modal propagation angle is similar to an effect known as "modal condition", which is identified with regard to the transmission of sound waves through rotor / stator blade / vane rows [37, 7].

1.2.5 Noise assessment methods

The acoustic development of propulsion systems is commonly based on the assessment of single noise levels. Based on these noise levels, different designs are acoustically evaluated and compared. In this process, the design with the lowest level is prioritized. Typically, the sound pressure level L_p is considered as an evaluation criterion. Therefore, the sound pressure p is determined relative to a reference value p_{ref} and expressed on a 10-logarithmic scale. The resulting value is called sound pressure level $L_p = 10 \cdot \log(p^2/p_{\mathrm{ref}}^2)$, whereby the reference pressure is defined as the hearing threshold at $2 \cdot 10^{-5}\,\mathrm{Pa}$, which represents a theoretical limit of hearing sensitivity of the human ear.

Likewise, a single noise level is evaluated for the acoustic aircraft certification. Here, the time-dependent noise levels obtained from flyovers are analyzed at three reference locations, defined for the flight segments corresponding to approach, sideline and cutback. From these time histories, a single noise level is derived in each case and these three levels are then accumulated to one noise certification value. The evaluation criterion is the Effective Perceived Noise Level (EPNL) [64]. For

the EPNL calculation, the time-dependent sound pressure levels are first converted to perceived noise levels (PNL(t)) and then to tone-corrected perceived noise levels (PNLT(t)) by applying a correction for tonal peaks. A further correction factor is determined for the duration of noise exposure. This factor is obtained from the temporal integration of a $10\,\mathrm{dB}$ area below the maximum perceived noise level. The EPNL is then determined as the sum of the maximum PNLT and the integrated duration correction factor. For successful certification, a defined EPNL upper limit should not be exceeded. Thereby the certification ensures that the noise levels of newly certified aircraft are lower than those of earlier certified aircraft. Regarding the acoustic certification of future aircraft with VTOL capabilities, the EASA currently develops a new certification standard and suggests to use the EPNL also for VTOL aircraft as the main noise certification criterion [23].

These established metrics, such as the EPNL metric, reduce the noise exposure to a single noise level and therefore do not fully capture psychoacoustic characteristics nor the subjective human noise perception. The United States Federal Aviation Agency (FAA) outlines this limitation in their Federal Aviation Regulations (FAR) Part 36 by highlighting that "No determination is made, under this part, that these noise levels are or should be acceptable or unacceptable for operation at, into, or out of, any airport" [30]. This means that the design with minimum EPNL may not necessarily be perceived as the most pleasant design by human noise perception. Especially, for a new generation of aircraft, which may have VTOL capabilities and are powered by distributed propulsion systems consisting of a large number of engines, the resulting noise signatures might sound different and unfamiliar compared to already existing aircraft [71, 22]. Therefore, existing acoustic certification procedures and noise evaluation methods require further development.

One approach is to evaluate the noise emission based on sound quality metrics as these metrics are intended to provide an estimation of the perception of human hearing. Typically, loudness, sharpness, tonality, roughness and fluctuation strength as well as a combination of these metrics denoted as psychoacoustic annoyance are assessed. Loudness [1] indicates the noise magnitude, sharpness [87] represents high-frequency noise content, tonality [4] indicates the presence of tonal components, roughness [16] indicates fast changes in frequency or amplitude with modulation frequencies up to $300\,\mathrm{Hz}$, and fluctuation strength [86] indicates slow

changes in frequency or amplitude with modulation frequencies up to 20 Hz. Although these metrics provide an estimation of the sound characteristics, these metrics and especially the psychoacoustic annoyance metric may not completely capture the subjective human noise perception. Therefore, a further approach is to establish a feedback loop between acoustic design and laboratory listening experiments. Typically, synthesized audio files are used as stimuli for listening tests and based on the obtained subjective noise ratings conclusions are drawn for the acoustic design. As a result, human noise perception can directly influence the acoustic design of, for example, propulsion systems. In literature, this approach is denoted as perception-influenced design [68]. By applying this approach, human noise perception can already be considered at an early stage in the design process, so that the evaluation of single noise levels is replaced by the assessment of the aural impression.

Particularly for noise signatures obtained from future aircraft, it is part of current research (1) to develop new metrics for community noise assessment, (2) to investigate which method provides an acceptable measure of noise and (3) to evaluate whether the EPNL metric correlates with human noise perception [83, 50]. Rizzi [68] provides a review of current aircraft noise assessment metrics, compares a metrics-driven design approach (based on individual noise levels) with perception-influenced design and formulates a strategy towards the application of perception-influenced design based on four case studies. In [68, 69], Rizzi as well as Rizzi and Christian conclude that a low-noise design, as obtained from EPNL reduction, may not necessarily be equivalent with a low-perceived noise design. The authors, however, put forward that meeting noise certification requirements and achieving desirable noise perception attributes at the same time is feasible and suggest to account for psychoacoustic metrics, which also consider tonal amplitudes as well as spectral and temporal patterns [68, 69]. Pieren *et al.* [66] demonstrate a perception-influenced evaluation of different aircraft noise reduction measures, whereby synthesized flyovers of different aircraft types are used as stimuli for a laboratory listening experiment to assess the human noise perception.

In order to investigate psychoacoustic and aural characteristics of noise, auralization can provide a valuable tool to support the acoustic design of aircraft and propulsion systems at an early stage in the design process and to develop psychoacoustic annoyance metrics [2]. Auralization enables perception-influenced

design as it is a method to transform analytical or numerical data, such as time dependent sound pressure levels obtained from virtual flyover simulations, in audible sound files, as for example mp3 or wav audio files, which may then be used as stimuli for listening experiments with human subjects [88]. Rizzi and Sahai [70] provide an overview of different auralization strategies and apply an auralization process to noise obtained from different aircraft concepts ranging from a large transport aircraft to a smaller UAV. Arntzen *et al.* [2] present an auralization process and its application to a medium range aircraft. The authors conclude that auralization is a powerful tool for aircraft designers in order to evaluate the effectiveness of noise reduction mechanisms. Torija *et al.* [84] and Boucher *et al.* [10] use auralization data as stimuli for listening tests to derive new psychoacoustic annoyance metrics based on human responses.

Based on this literature study, it becomes evident that classical metrics such as EPNL cannot or only partially capture the subjective aural perception and are therefore not necessarily suitable for the certification of future UAM aircraft with distributed propulsion systems. There is a demand to investigate acoustic and psychoacoustic noise reduction effects for distributed propulsion systems and to evaluate their noise signatures by means of sound quality metrics and laboratory listening experiments. This is enabled by the development of auralization methods since audio files allow to evaluate the aural impression instead of individual sound levels. Using virtual flyover simulations and auralizations, comprehensive data can be provided in order to conduct laboratory listening experiments and to derive new acoustic and psychoacoustic metrics. With regard to public relations, auralization can also contribute to increase public's identification, awareness and understanding of acoustic design mechanisms, as changes in the noise signature can intuitively be detected using audio files even for non-experts.

Based on these findings, a central aspect of this work is the development of an analytical auralization process and, in particular, the development of a tool for virtual flyover simulations called VIOLIN. The auralization process consists of a coupling between three individual in-house tools, whereby PropNoise (PropulsionNoise) [57, 40] is used to determine the noise sources for each engine, VIOLIN (Virtual acoustIc flyOver simuLatIoN) is used to propagate the noise emission through the atmosphere and CORAL (airCraft engine nOise auRALization) [61] is used to synthesize the incoming signal at a microphone position and save it as

an audio file. A schematic illustration of this process in shown in Fig. 1.6. An overview of the coupling between these tools is provided in [61] and the impact of rotational speed deviations on the noise signature of a distributed propulsion system is investigated in [73] based on synthesized flyover sounds obtained from this method. A description of the noise propagation approach in VIOLIN between source and receiver as well as the required extensions for distributed propulsion are presented in publication III of this work.
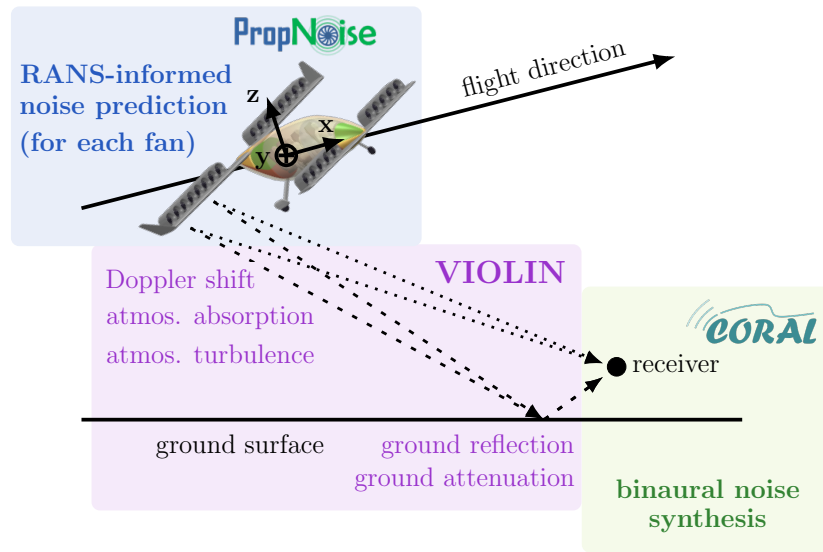
Figure 1.6: Analytical auralization process chain.

As an advantage of the analytical modeling approach, turnaround times in the range of a few minutes are achieved. Thus, this method allows to assess psychoacoustic aspects early in the fan engine development process and to examine changes in the fan design not only in terms of the pure sound level, but also in terms of the time-histories, the resulting sound signatures and via headphones using audio files. The audio files can then be used for listening tests with human subjects or for calculating psychoacoustic sound quality metrics.

1.3 Research question and research objectives

Summarizing the literature review in Sec. 1.2, there is a demand for further research into tonal noise reduction mechanisms for low-speed, low-count OGV fans, with a particular focus on tonal noise mitigation at the source. Additionally, the development of auralization methods is essential to investigate the noise signatures of future propulsion systems. An analysis of psychoacoustic sound quality characteristics of distributed propulsion systems is required to enhance the understanding of their impact on human noise perception.

Based on these research demands, the primary motivation for this work is that, from an acoustic perspective, low-count OGV fans offer a promising design option for low-speed fan engines of future propulsion systems for UAM applications. The reason is that low-speed, low-count OGV fan stages provide the perspective to cut-off or mitigate the BPF tone, even though the stator vane count is lower then rotor blade count. In addition, broadband noise is already decreased by design due to the lower number of stator vanes. It is relevant to investigate low-tonal noise fan designs, as in human noise perception tonal sound components often produce a more annoying impression. Low-tonal noise fan designs may not only reduce the sound level, but may also decrease the subjective human noise annoyance. Besides these acoustic aspects, low-count OGV designs offer additional advantages with regard to economical and mechanical aspects compared to conventional fan designs.

The main research question for this work is therefore formulated as follows: How can low-speed fan stages with fewer stator than rotor blades be designed for UAM applications, which are not only quieter than conventional designs but also perceived as less unpleasant? To address the research question, three sub-questions are defined, whereby each question is examined in one of the three publications:

1. Which tonal noise reduction measures can be taken for low-speed, low-count OGV fan stages? (addressed in publication I)

2. How can the effects be applied to fan designs for an urban air mobility vehicle? (addressed in publication II)

3. Which tonal noise level reduction potential arises and what is the impact on the psychoacoustic characteristics for a propulsion system consisting of distributed ducted fans? (addressed in publication III)

For each sub-question, an associated objective is derived and formulated as follows:

1. The investigation of acoustic effects to reduce tonal rotor–stator interaction noise at source for low-count OGV fans.

2. The design of low-speed, low-count OGV fan stages for an urban air mobility application.

3. The virtual integration of the fan stages into a distributed propulsion system of an UAM vehicle and the assessment of the sound quality using psychoacoustic metrics based on synthesized flyovers.

Based on these objectives, the main scientific contribution of this work consists of (1) the investigation of two tonal noise reduction mechanisms, (2) the application of these measures on two new low-count OGV fan stages designed for a distributed propulsion system of an UAM aircraft and (3) the assessment of the noise signatures of the distributed propulsion system with respect to the different fan designs. An essential characteristic of these fan designs is that a similar aerodynamic performance is achieved while the acoustic radiation characteristics are very different.

1.4 Contribution of the publications to answer the research question

The thesis consists of three journal publications. In this section, the contributions of each journal publication in assessing the previously formulated research questions and objectives are presented.

1.4.1 Contribution of publication I

The main objective of publication I is to analytically and numerically investigate acoustic effects to reduce tonal rotor–stator interaction noise at source for low-count OGV fans. This publication addresses the question of which tonal noise reduction mechanisms can be taken for low-speed low-count OGV fan stages (see question and objective 1) in Sec. 1.3). Figure 1.7 shows the graphical abstract for publication I.
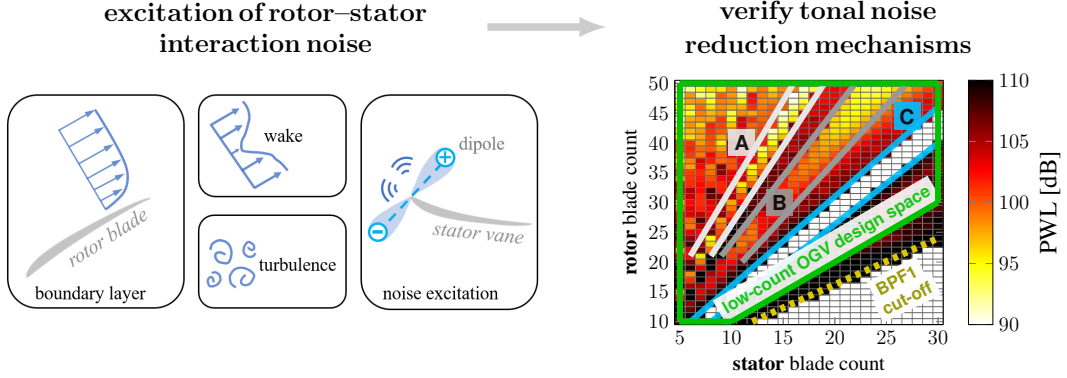
Figure 1.7: Graphical abstract publication I.

In order to investigate the formulated objective, rotor and stator blade count variations are performed to evaluate the tonal noise excitation of a large variety of different blade count pairings. For each rotor and stator blade count combination, the tonal noise levels are predicted analytically. Within the low-count OGV design space (fewer stator than rotor blades), three acoustically beneficial blade count areas are identified based on the analytical noise prediction (see Fig. 1.7). Two

effects are found, which ensure that blade count combinations located within the identified areas have lower tonal noise levels compared to other combinations.

The first effect is the impact of the modal phase propagation angle on tonal noise excitation. Within the identified areas the tonal noise excitation is particularly affected by the difference between the phase propagation angle of the dominantly excited mode and the stator leading edge angle. The results indicate that a weaker tonal noise excitation occurs if exactly those modes are dominantly excited whose propagation angles are preferably parallel to the stator leading edge angle. In this case the modal propagation angle is almost perpendicular to the dipole radiation axis, which in turn is perpendicular to the stator leading edge angle. Thus, less acoustic energy is generated. The existence of this effect as well as the trends obtained from analytical noise prediction are numerically confirmed using unsteady Harmonic Balance simulations.

The second effect impacting the tonal noise excitation is the inverse cut-off of the blade passing frequency tone. Typically, a cut-off of the blade passing frequency tone is achieved if the stator vane count is significantly larger than the rotor blade count so that the resulting interaction modes are not able to propagate (see Sec.1.2.2). However, the study indicates that additional (inverse) cut-off areas exist for fans with fewer stator than rotor blades given that the rotor tip Mach number is lower than a critical Mach number. Therefore, the application of this effect is limited to low-speed fans. In order to transfer this effect to other low-speed fan stages, a design rule is derived to estimate the critical tip Mach number as a function of the axial Mach number, the tonal mode order and the rotor blade count.

All in all, to provide a first step in answering the main research question formulated in Sec. 1.3, publication I provides the analytical verification and numerical validation of two acoustic effects to efficiently reduce the tonal noise excitation of low-speed fans with fewer stator than rotor blades. The study I focuses on noise generation and has a theoretical and general character, providing the theoretical basis for study II.

1.4.2 Contribution of publication II

Publication II is based on two main objectives: The first objective is to provide an experimental validation of the impact of the modal propagation angle on tonal noise excitation. The second objective is to demonstrate the two tonal noise reduction mechanisms identified in publication I on two low-count OGV fan stages intended for an urban air mobility application. Publication II addresses the question of how the effects can generally be transferred to low-count OGV fan stages and how they can be applied in a design-to-noise procedure (see question and objective 2) in Sec. 1.3). The concept of publication II is illustrated in Fig. 1.8 showing the graphical abstract.
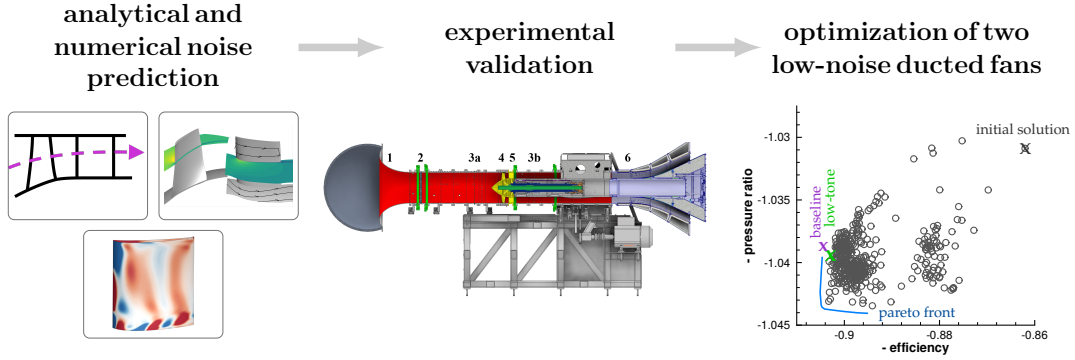
Figure 1.8: Graphical abstract publication II.

In this publication, an experimental verification of the impact of the modal propagation angle on tonal noise excitation is provided using a conventional fan design with more stator than rotor blades (treated as baseline configuration). This fan has 18 rotor blades and 21 stator vanes. Analytical and numerical results indicate that a tonal advantage should be achieved if the propagation angle of the dominantly excited acoustic mode is aligned with the stator leading edge stagger angle (see publication I). This is confirmed with experimental data showing a reduction potential of tonal interaction noise larger than $10\,\mathrm{dB}$ if the excited acoustic modes propagate parallel to the stator leading edge angle. For the baseline configuration, the upstream propagating mode is almost aligned with the stator leading edge angle. Thus, the tonal noise reduction is achieved upstream, which is confirmed by the experimental results.

In order to apply this noise reduction measure to other fan stages, a design rule

is derived, which allows to estimate the noise reduction potential as a function of the stator leading edge angle, the number of rotor blades and the propagation angle of the dominantly excited interaction mode. Under the condition that the stator leading edge angle is predefined, this design rule can be used to iterate the blade numbers until exactly those modes are dominantly excited whose propagation angles are parallel to the leading edge angle.

This procedure is applied to transfer the effect to two low-count OGV fan stages. For the first new fan stage, the tonal noise reduction mechanism is combined with a broadband noise reduction mechanism. The number of stator vanes is decreased from 21 to 10 to achieve a reduction in broadband noise and the rotor blade count is increased from 18 to 31 to ensure that the modal propagation angle reduces the tonal noise excitation. This fan stage is denoted as low-broadband design. With this fan design it is demonstrated that the modal propagation angle not only reduces tonal noise but also affects the dominant tonal noise radiation direction. For the low-broadband fan, an opposite dominant tonal noise radiation direction is realized compared to the baseline fan due to the impact of the modal propagation angle on noise excitation. Thus, compared to the baseline fan, the tonal noise reduction is achieved downstream.

For the second low-count OGV fan, two tonal noise reduction mechanisms are combined: Firstly, the blade numbers are chosen such that the blade passing frequency tone is inverse cut-off and, secondly, the excitation of the second harmonic is decreased upstream using the modal propagation angle. This fan stage has 31 rotor blades and 21 stator vanes. The combination of both effects in one fan stage leads to an almost full suppression of tonal noise, so that this design is named low-tone fan.

Both new low-count OGV fan stages are intended for experimental testing in DLR's CRAFT (Co-/Counter Rotating Acoustic Fan Test) facility. In order to allow the manufacturing of the rotor and stator geometries, the 3D blade shapes are determined using a multidisciplinary optimization process. The primary objective for the optimization is that the low-count OGV fan stages are operated at similar aerodynamic conditions as the baseline fan. This is essential as the targeted acoustic comparison is only valid if all fans provide similar performance key figures, such as the thrust.

All in all, to provide a second step in answering the main research question

formulated in Sec. 1.3, publication II provides an experimental validation of the impact of the modal propagation angle on tonal noise excitation using a conventional fan design. In study II, the identified noise reduction mechanisms from study I are transferred to two low-count OGV fan stages representative for an urban air mobility application. The fan stages are designed for an UAM vehicle powered by 26 distributed, ducted fans. Thus, study II provides the integration of the identified tonal noise reduction mechanisms into realistic fan designs for urban air mobility and forms the basis for the psychoacoustic assessment in study III.

1.4.3 Contribution of publication III

The primary objective of publication III is to virtually integrate the fan stages into a distributed propulsion system of an UAM vehicle and examine the noise signature obtained from synthesized flyovers using sound quality metrics. Publication III therefore examines the question of what noise reduction arises from the integration of the individual low-count OGV fans into a distributed propulsion system and what psychoacoustic noise characteristics are achieved as a result (see question and objective 3) in Sec. 1.3)? The overall study concept is visualized in Fig. 1.9 showing the graphical abstract of publication III.
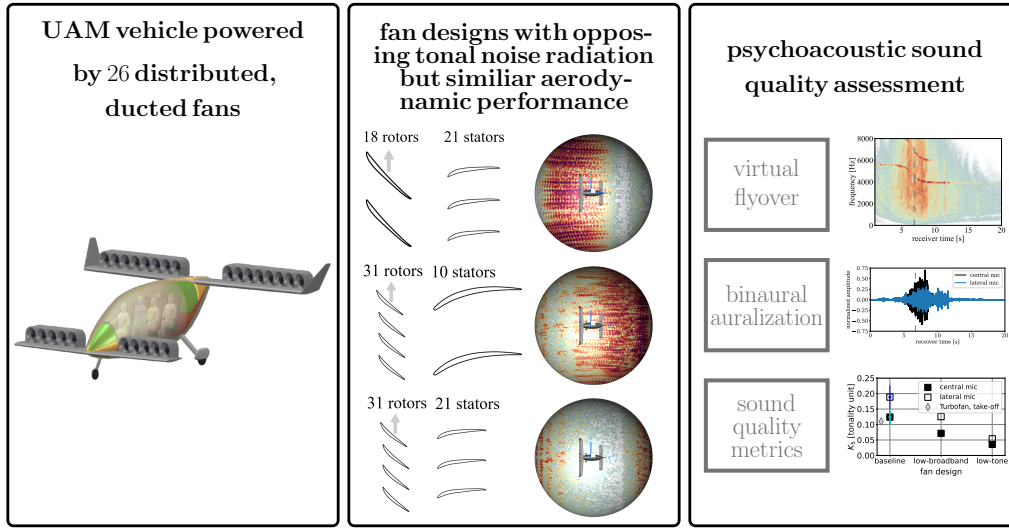
Figure 1.9: Graphical abstract publication III.

Publication III examines the impact of fan design on noise perception of a distributed propulsion system consisting of 26 low-speed, ducted fan stages. The propulsion system is either equipped with one of the two low-count OGV fans or with the baseline design. These fans are suitable for a psychoacoustic evaluation due to their different tonal to broadband noise ratio, different dominant tonal noise radiation directions but similar aerodynamic performance.

The distributed propulsion system powers an UAM concept vehicle denoted as tilt-duct vehicle. This vehicle has VTOL capabilities and carries a payload of up to 450 kg over a range of 100 km at a cruise speed of 200 km/h [72]. An analytical auralization process is first extended for distributed propulsion systems and is then applied to determine the noise emission, propagate the sound through the

atmosphere and provide a binaural noise synthesis. In order to gain an estimation of the perception of human hearing several sound quality metrics are assessed. Firstly, a validation and comparison of noise immission and sound quality metrics with an A320 turbofan engine at take-off is provided. Secondly, the auralization process is applied to the distributed propulsion system of the UAM vehicle.

The study indicates that the distributed propulsion system generates noise signatures with complex directional characteristics and high sharpness. The two low-count OGV fan stages considerably decrease the EPNL and reduce the tonality, loudness and roughness by more than one noticeable difference compared to the baseline fan leading to a reduced psychoacoustic annoyance. Comparable or even lower values compared to turbofan engine at take-off are achieved.

All in all, to provide a third step in answering the main research question formulated in Sec. 1.3, publication III provides an analytical auralization process for calculating the noise immission of distributed propulsion systems. Using this process, study III investigates the impact of different fan designs on the noise signatures obtained from the distributed propulsion system of the UAM vehicle and provides a comparison with the noise characteristics of a conventional turbofan engine. As the noise signatures of distributed propulsion systems for UAM applications are mainly unknown so far, this is an essential step towards understanding their noise characteristics.

Chapter 2

Publications

This chapter contains the three journal publications in chronological order shown in the original journal layout.

Publication I

S. Schade, R. Jaron, A. Moreau, S. Guérin. Mechanisms to reduce the blade passing frequency tone for subsonic low-count OGV fans. *Aerospace Science and Technology*, Volume 125, SI: DICUAM 2021, 2022, ISSN 1270-9638. doi: 10.1016/j.ast.2021.107083

Publication II

S. Schade, R. Jaron, L. Klähn, A. Moreau. Smart Blade Count Selection to Align Modal Propagation Angle with Stator Stagger Angle for Low-Noise Ducted Fan Designs. *Aerospace* 2024, 11, 259. doi: 10.3390/aerospace11040259

Publication III

S. Schade, R. Merino-Martinez, A. Moreau, S. Bartels, R. Jaron. Psychoacoustic evaluation of different fan designs for an urban air mobility vehicle with distributed propulsion system. *J. Acoust. Soc. Am.* 26 March 2025; 157 (3): 2150–2167. doi: 10.1121/10.0036228

2.1 Publication I

Mechanisms to reduce the blade passing frequency tone for subsonic low-count OGV fans

Stephen Schade [*], Robert Jaron, Antoine Moreau, Sébastien Guérin

German Aerospace Center (DLR), Müller-Breslau-Straße 8, 10623 Berlin, Germany

A R T I C L E   I N F O

A B S T R A C T

Conventionally, fan stages are designed with more stator vanes than rotor blades. These fan stages provide a tonal noise advantage as the blade passing frequency tone is cut-off. Contrary to conventional cut-off designs, low-count OGV (Outlet Guide Vane) designs are fan stages with fewer stator vanes than rotor blades. Low-count OGV designs benefit from lower broadband noise due to the reduced number of stator vanes. However, the blade passing frequency tone may no longer be cut-off. Therefore, we assess tonal noise reduction mechanisms for subsonic low-count OGV fan stages. We use an analytical and a numerical method to predict the rotor–stator interaction noise for different blade count pairings. The results indicate that the mode phase propagation angle and the cut-on factor are two acoustic parameters that dominantly influence the noise excitation. For certain blade count pairings an acoustic benefit exists if the mode phase propagation angle is congruent to the stator leading edge angle and / or if the mode is away from the cut-off limit. Moreover, reducing the rotor tip speed allows, for some configurations, a cut-off design even with fewer stator vanes than rotor blades (inverse cut-off). Overall, the study shows promising possibilities to reduce tonal interaction noise for low-count OGV fan stages.

1. Introduction

The noise impact of urban air mobility (UAM) airplanes has attracted increasing attention as these airplanes are expected to take off and land in highly populated areas. Especially for electrically powered airplanes operating in urban areas, fan noise will be a crucial challenge. Current UAM airplane concepts include, in addition to open-rotor variants, airplanes equipped with low-speed shrouded fan stages. These fan stages may be arranged either as a double configuration or as a distributed propulsion system. A significant contribution to the overall noise impact of the aircraft will be caused by the fan stages [1,2]. Rizzi et al. [3] highlighted the demand to "document noise reduction technologies available for UAM" as one "high-level goal" for the development of UAM airplanes. Referring to this demand, we intend to investigate and evaluate noise reduction mechanisms for low-speed shrouded fan stages of small airplanes. Our objective is to provide a step towards the design-to-noise of fan stages.

Conventionally, fan stages are designed with significantly more stator vanes than rotor blades. This approach leads to an advantage regarding tonal interaction noise since the blade passing frequency tone, which is usually dominant, is cut-off. Although cut-off designs have a tonal advantage, these designs are not beneficial regarding broadband noise. The broadband noise source can be efficiently decreased by reducing the stator vane count since this noise source roughly scales with the number of stator vanes [4].

Contrary to a conventional cut-off design, a low-count OGV (Outlet Guide Vane) design is a fan stage with fewer stator vanes than rotor blades. Compared to a cut-off design, a low-count OGV design is more advantageous with regard to manufacturing costs as well as broadband interaction noise. However, the usually dominant blade passing frequency tone may no longer be cut-off due to the reduced number of stator vanes. This may cause a tonal noise penalty. In order to mitigate this tonal disadvantage, we investigate mechanisms that reduce the noise levels of the blade passing frequency tone. Our intention is to outline and understand the acoustic effects that may provide a benefit for low-count OGV designs. As a long-term goal, we ask the research question: Can low-count OGV designs compete with the noise levels of conventional cut-off designs? As a first step towards answering this question, we put an emphasis on the tonal noise excitation and assess three noise reduction mechanisms for subsonic low-count OGV fans: The mode phase propagation angle (1), the mode cut-on factor (2) and the inverse cut-off of the blade passing frequency tone (3).

There are few studies in the literature regarding the acoustic potential of low-count OGV designs. Dittmar et al. [5,6] examined

different low-count OGV fan stages and compared the noise levels to conventional designs. The results indicate that low-count OGV designs benefit from lower broadband noise and a reduced noise annoyance. Schwaller et al. [7] experimentally investigated different rotor–stator blade count pairings and measured the far-field noise. They confirmed that low-count OGV designs have benefits with regard to broadband noise and identified a reduction of the higher harmonic blade passing frequency tones. Thereupon, Kröger et al. [8] conducted a multidisciplinary optimization of a low-count OGV fan stage. Regarding aerodynamics, they concluded that a reduction from 42 to 14 stator vanes is feasible and even suitable. Regarding acoustics, they observed an increase in the first blade passing frequency tone. To address this noise penalty, Giacché et al. [9] performed an acoustic optimization of a low-count OGV fan stage. The optimized OGV had a modified leading edge profile with non-uniform sweep distribution. They showed that the modification decreases the noise levels of the blade passing frequency tone [9]. Recently, Jaron [4] examined low-count OGV designs regarding their potential to reduce tonal noise and identified that certain blade count pairings benefit from a weaker excitation of the dominant modes. The study indicates that the relative angle between the mode phase propagation angle and the stator leading edge angle is a reason for a lower noise excitation [4]. However, the impact of the mode phase propagation angle on the noise excitation is not fully understood yet. Therefore, we further investigate this effect within the present paper.

To examine the tonal noise reduction mechanisms, we perform a variation of the rotor and stator blade count. The idea is to identify promising blade count pairings that lead to lower noise levels. Casalino et al. [10] described this approach as a "best practice" to decrease "the fan rotor/stator interaction noise". For each blade count pairing we predict the noise levels analytically. For selected blade count pairings we perform Harmonic Balance simulations to validate the analytical prediction. The fan stage for the noise assessment is described in Sec. 2, the analytical fan noise prediction method in Sec. 3 and the numerical method in Sec. 4. The impact of the mode phase propagation angle and the impact of the mode cut-on factor on the noise excitation are assessed in Subsec. 5.1. Afterwards, the relation between the inverse cut-off effect and the rotor tip speed is examined in Subsec. 5.2.

2. Baseline fan stage

For the acoustic analysis, the "Co / Contra Rotating Acoustic Fan Test rig" (CRAFT), operated by the Department of Engine Acoustics of the German Aerospace Center, is used [11]. The CRAFT rig can be equipped either with two counter-rotating rotors or with a co-rotating rotor–stator stage [12]. The latter configuration is shown in Fig. 1. For the acoustic predictions, presented in this paper, the rotor–stator stage is scaled by a factor 2 : 1. The reason is that the thrust level provided by the scaled fan stage would be sufficient to power a small twin-engine aircraft. Thus, the CRAFT rig is representative for a shrouded fan stage of a small airplane, which could be operated in an UAM mission. Table 1 summarizes the design and sideline operating points for the scaled CRAFT rotor–stator stage. The latter is used for the subsequent analysis since it is the loudest operating point of the relevant acoustic noise certification points approach, sideline and cutback.

3. Analytical fan noise prediction method

Different analytical and semi-analytical methods for predicting fan noise exist. Casalino et al. [10] provide a bibliographic overview of such approaches and emphasize that these are essential for the design-to-noise of fan stages. In this paper, the fan noise prediction is performed with the tool "PropNoise" (PN), developed
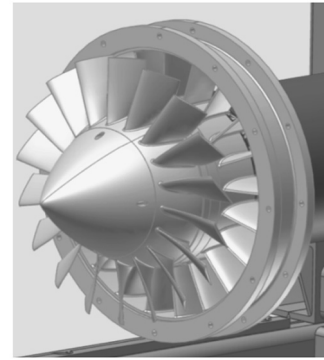

Fig. 1. CRAFT rotor–stator configuration.

Table 1
Design and sideline operating points for the scaled CRAFT rotor–stator stage.

	Design	Sideline
fan diameter [m]	0.908	
pressure ratio	1.039	1.050
mass flow [kg/s]	22.70	24.11
rotational speed [rpm]	2194	2356
rel. rotor tip Mach number	0.31	0.33

by the Department of Engine Acoustics of the German Aerospace Center [13]. Particularly, the noise levels are calculated with the stand-alone module of PropNoise. The stand-alone module provides an aerodynamic preliminary design of the fan stage and a fully analytical noise prediction. The input data are the fan geometry (e.g. diameters, blade count numbers, chord lengths) and the design operating conditions as for example mass flow and rotational speed. The steady and unsteady aerodynamics are calculated at a single meanline position, which is considered as representative for the complete flow. The meanline radius is located at 70% blade span. Subsequently, the aerodynamic solution is extrapolated in radial direction. The data generated in the aerodynamic modules constitute the input for the acoustic module, which relies on a radial-strip approach. That means, the module determines the response of the blade to an aerodynamic excitation for each radial strip as if the problem was two-dimensional. Afterwards, the source term is integrated in radial direction in order to determine the sound pressure amplitude and the sound power propagating within the duct segments [13].

The subsequent acoustic analysis relies on the evaluation of the phase propagation angle ζ_{mn} and the cut-on factor α_{mn} of an acoustic mode of azimuthal and radial order (m, n). In the ray tracing theory, the phase propagation angle describes the propagation of an acoustic ray in a duct. According to [14,15], in absence of swirl, ζ_{mn} is defined as

$$\zeta_{mn}^{\pm} = -\operatorname{sign}(m) \cos^{-1}\left(\frac{-M_x \pm \alpha_{mn}}{1 \mp \alpha_{mn} M_x} \right). \tag{1}$$

In Eq. (1) the superscript $\pm$ indicates the direction of propagation, where $+$ is used for the downstream direction and $-$ for the upstream direction. The phase propagation angle depends on the sign of the azimuthal mode order m, the axial Mach number M_x and the mode cut-on factor α_{mn}. As described in [13,16] and under consideration of a solid body swirl, this factor is given by

$$\alpha_{mn} = \sqrt{1 - (1 - M_x^2)\left(\frac{\sigma_{mn}}{kR - mM_s} \right)^2}. \tag{2}$$

29

In Eq. (2) the variable σ_{mn} is the $(n+1)^{th}$ zero of the first derivative of the radial eigenfunction at the walls, k is the acoustic wave number, R is the duct radius and M_s is the swirl Mach number. At the stator entry, the duct radius is $R = 0.454$ m, the swirl Mach number is $M_s = 0.13$ and the axial Mach number is $M_x = 0.15$. Note that Eq. (1) is only valid for piecewise linear rays. Under consideration of flow swirl, the rays would be curved. Flow swirl is only considered for the calculation of the cut-on factor, as indicated in Eq. (2).

The cut-on factor is a criterion to determine the propagation capability of acoustic modes within a duct [13]. For propagating modes, α_{mn} is a real number and ranges between 0 and 1. Towards the limit of 0, the modes still propagate, but are close to cut-off and for well-propagating modes, α_{mn} tends towards 1. For non-propagating modes (cut-off modes), α_{mn} has an imaginary part which leads to the exponential decay of the acoustic pressure [13,16].

Based on the acoustic pressure of an azimuthal mode m and the in-duct Green's function $\hat{g}_{mn}^{\omega}$ an expression for the modal pressure amplitude can be formulated. According to the derivation which is presented in [13,16], the modal amplitude for the in-duct case and Tyler–Sofrin modes is formulated as

$$A_{mn}^{\pm} = i \cdot B \int_{r}^{R} \hat{g}_{mn}^{\omega} \, e^{-ik_x x_{LE} - im\theta_{LE}} \cdot \sigma \cdot dr_s. \qquad (3)$$

In Eq. (3), B is the number of rotor blades, r is the duct radius at the hub, R is the duct radius at the tip, k_x is the axial wavenumber and x_{LE} and θ_{LE} are the axial and circumferential leading edge positions. The in-duct Green's function $\hat{g}_{mn}^{\omega}$ is given by

$$\hat{g}_{mn}^{\omega} = \frac{i}{4\pi R} \cdot \frac{J_m(k_r r_s) + Q_{mn} Y_m(k_r r_s)}{kR \, \alpha_{mn} \sqrt{F_{mn}}}, \qquad (4)$$

where J_m are the Bessel functions, Y_m are the Neumann functions, k_r is the radial wavenumber, r_s is the radial coordinate at the source position, F_{mn} are normalization factors and the quantity Q_{mn} is equal to zero for hollow ducts [13,17].

In Eq. (3), the quantity σ includes several source terms, i.a. a term for the lift noise component σ_L. This term is given by

$$\sigma_L = i k_n \int_{0}^{c} f_L^{\hat{\omega}} \cdot e^{-ik_l l} dl, \qquad (5)$$

where $f_L^{\hat{\omega}}$ is the chordwise distribution of lift, k_l is the chordwise wavenumber and l is the chordwise position of the noise source on the blades [16]. From Eq. (5) it can be obtained that the lift-generated tonal noise component is affected by the normal wavenumber k_n [13]:

$$k_n = (k - \frac{mM_s}{R}) \sin(\zeta_{mn}^{\pm} - \chi_{LE}) \qquad (6)$$

According to Eq. (6), the relation between the mode phase propagation angle $\zeta_{mn}^{\pm}$ and the stator leading edge angle χ_{LE} influences the normal wavenumber and thus affects the source term σ_L for the lift noise component and its modal amplitude $A_{mn}^{\pm}$.

Following the derivation presented in [16,18], the acoustic modal power under consideration of a solid body swirl is determined from

$$P_{mn}^{\pm} = \frac{1}{1 - \frac{mM_s}{kR}} \pi R^2 \frac{\alpha_{mn}}{\rho_0 a_0} \frac{(1 - M_x^2)^2}{(1 \mp \alpha_{mn} Mx)^2} |A_{mn}^{\pm}|^2, \qquad (7)$$

where ρ_0 is the static density and a_0 is the speed of sound. In the following, the tonal sound power levels at noise generation, i.e. at the stator leading edge, are analyzed.

The tonal wake interaction noise can be classified as unsteady lift-generated noise. The driving physical mechanism for this noise source is a time-dependent variation of the pressure distribution on the blade surface. The pressure variation is caused by the rotor wake which impinges on the stator leading edge. A dipole noise source results from this interaction between the blade profile and the incoming flow, as schematically illustrated in Fig. 2. Hence, the tonal wake interaction noise can be represented by dipoles located at the stator leading edge [19].
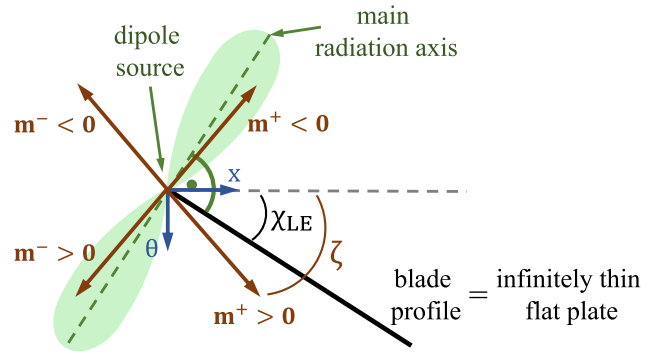

Fig. 2. Relation between mode propagation angle and noise generation at the stator leading edge.

In PropNoise, the blade profiles are modeled as infinite thin flat plates which are staggered at an angle χ relative to the engine axis, where χ_{LE} is the stator stagger angle at the leading edge (see Fig. 2). The main radiation axis of the dipole source is perpendicular to χ_{LE} at the source position. In the subsequent analysis, the mode phase propagation angle ζ_{mn} will be put in relation to the stator stagger angle at the leading edge χ_{LE} in order to evaluate the impact of these quantities on the noise generation. Note that ζ_{mn} and χ_{LE} are defined positive in $-\theta$ direction. In reality, typically twisted stator vanes are used which means that the leading edge angle radially changes. This is considered for the numerical simulations. However, for the analytical noise prediction, untwisted stator vanes are used. Thus, the leading edge angle is treated as constant in radial direction and the approach illustrated in Fig. 2 is valid.

The difference between the stator leading edge angle and the mode phase propagation angle is denoted with Δ and for the subsequent analysis Δ is scaled to the range $[0, 90 \deg]$. Accordingly, Δ can be determined from

$$\Delta = \begin{cases} |\zeta_{mn} - \chi_{LE}|, & \text{if } |\zeta_{mn} - \chi_{LE}| \leq 90 \deg \\ |180 - |\zeta_{mn} - \chi_{LE}||, & \text{if } |\zeta_{mn} - \chi_{LE}| > 90 \deg \end{cases}. \qquad (8)$$

As seen in Eq. (3), Eq. (5) and Eq. (6), if the mode phase propagation angle is exactly congruent to the stator leading edge angle, the acoustic mode will not be excited ($\Delta = 0 \deg$, $\zeta_{mn} = \chi_{LE}$). In that particular case, the phase propagation angle of the acoustic mode is perpendicular to the dipole radiation axis. On the contrary, if the mode phase propagation angle is in line with the dipole radiation axis, the strongest sound excitation occurs. In that particular case, the phase propagation angle of the acoustic mode is perpendicular to the stator leading edge angle ($\Delta = 90 \deg$).

Further, Fig. 2 exemplarily shows the propagation directions of upstream $(-)$ as well as downstream $(+)$ propagating positive and negative azimuthal acoustic modes m. For instance, $m^+ > 0$ is a positive and downstream propagating acoustic azimuthal mode. The sign convention of the azimuthal modes can be determined by applying the curl right hand rule in the direction of the x-axis.

4. Numerical fan noise prediction method

A numerical fan noise prediction is performed for selected rotor–stator combinations. The in-house Navier-Stokes solver "TRACE" [20,21], specifically developed for turbomachinery applications, is applied to numerically predict the unsteady flow field. We use TRACE to perform Harmonic Balance simulations (HB simulations). The HB method applies a Fourier transformation of the Reynolds Averaged Navier Stokes equations (RANS equations) and solves them in the frequency domain for selected frequencies, which are non-linearly coupled [22–24]. The closure of the RANS equation system is achieved with the Menter SST $k - \omega$ turbulence model [25]. For both the rotor blade row and the stator vane row one flow passage with phase-shifted boundary conditions in circumferential direction is modeled. As a consequence, the simulation results only include those flow effects that are circumferentially periodic with the number of rotor blades and stator vanes.

The structured grid has an O-C-H topology around the blades. In spanwise direction, the grid consists of 90 cells, of which 9 cells are placed in the rotor tip gap. In circumferential direction, the grid resolves the smallest considered acoustic wave length with more than 35 cells per wave length. On the airfoil surfaces, the size of the first grid cell resolves the laminar sublayer of the velocity boundary layer ($y^+ < 1$). In total, the computational grid of the rotor–stator stage consists of more than $17 \cdot 10^6$ cells.

Several criteria are used to evaluate the convergence. For instance, the mass flow and pressure are monitored at the inlet and outlet of the computational domain to assess the behavior of these flow quantities as the solution evolves. For the HB simulation an additional acoustic convergence criterion is specified: Monitor plots trace the sound power levels (PWL) of the propagating modes of the first and second blade passing frequencies (BPF1, BPF2). For the converged solution the sound power levels have reached a constant value and the residuals are smaller than 10^{-5}. Compared to the initial solution the residuals have dropped by at least three orders of magnitude.

An extended triple plane pressure mode matching (XTPP) method is applied to extract the acoustics from the simulation [26]. The XTPP approach is based on the method originally developed by Ovenden and Rienstra [27]. The extension of the method enables to better distinguish between convective and acoustic perturbations and leads to an improved prediction of tonal noise [26].

5. Results

Based on the scaled CRAFT geometry, a variation of the rotor and stator blade count is performed using the stand-alone module of PropNoise. The CRAFT rig has 18 rotor blades and 21 stator vanes. This is the initial configuration for the blade count variation. The variation is carried out at constant solidity to achieve a similar aerodynamic blade loading. Thus, the chord length changes between the configurations. For instance, the lower the number of rotor blades or stator vanes the longer the blade or vane chord. The initial configuration is used to determine the chord lengths of all other blade count pairings based on the condition that the solidity is constant. Further, the distance between the rotor trailing edge and stator leading edge remains constant. Hence, the propagation distance of the rotor wake up to the stator leading edge is identical for all configurations.

Fig. 3 shows the analytically predicted sound power levels of the BPF1 tone for different rotor–stator blade count pairings. All low-count OGV configurations are framed in green and the dotted yellow line shows the BPF1 cut-off border. Within the low-count OGV design space, we identified three subareas with lower overall

BPF1 sound power levels. We named these subareas "A", "B" and "C". In Subsec. 5.1 we analyze the acoustic effects that cause blade count pairings in areas "A" and "B" to have lower sound power levels than adjacent blade count pairings. In Subsec. 5.2 we put the focus on the configurations from area "C".
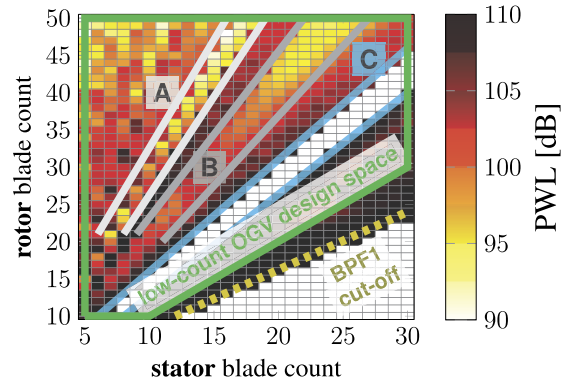
Fig. 3. BPF1 sound power level for different rotor–stator blade count combinations. (For interpretation of the colors in the figure(s), the reader is referred to the web version of this article.)

5.1. Phase propagation angle and cut-on factor

The studies by Guérin et al. [28] and Jaron [4] indicate that the sound power decreases if the phase propagation angle of an acoustic mode is congruent to the stator leading edge angle. To better understand this effect, we examine selected configurations from area "A" in more detail. For this purpose, the number of rotor blades is kept constant and set to $B = 35$. This ensures that the width and depth of the rotor wakes remain identical. The number of stator vanes varies between $V = 11$ and $V = 14$. The configurations with $V = 12$ and $V = 13$ stator vanes belong to area "A". For equidistant blades, the triggered azimuthal mode orders m are a function of the rotor blade count B and stator vane count V: $m = hB - kV$, where $h \in \mathbb{N}_0$ and $k \in \mathbb{Z}$ (Tyler and Sofrin's rule [29]). For each azimuthal mode order m several radial mode orders n may be cut-on. Each mode has a different propagation direction and thus a different phase propagation angle. Therefore, the angle Δ between the stator leading edge angle and the mode phase propagation angle changes. This leads to a weaker or stronger noise excitation of the acoustic modes.

Fig. 4 depicts the analytically predicted upstream and downstream sound power levels of the BPF1 tone. The labels show the values of Δ for the dominant acoustic mode of each configuration. The dominant propagating BPF1 modes are summarized in Table 2. For a specific acoustic mode, Δ does not change in radial direction, since $\chi_{LE} = -33 \deg = const.$ is used for the analytical study. An advantage of the analytical noise prediction is that particular acoustic effects can be examined individually. To specifically assess the impact of the mode phase propagation angle on the noise excitation, we manually manipulated Δ in the PropNoise code. We consider two cases in Fig. 4: 1) A phase propagation angle approximately congruent to the stator leading edge angle ($\Delta = 10 \deg$) and 2) a phase propagation angle perpendicular to the leading edge angle ($\Delta = 90 \deg$). In both cases the phase propagation angle is adjusted for all propagating modes. The reason why $\Delta = 10 \deg$ is applied is that the acoustic modes would not be excited at all if the phase propagation angles were exactly identical with the stator leading edge angle. The dotted green line shows the BPF1 sound power levels for $\Delta = 10 \deg$. The dotted red line shows the sound power levels for $\Delta = 90 \deg$. For the latter case the phase propagation angle is in line with the dipole radiation axis. The maximum sound excitation occurs in the direction of the
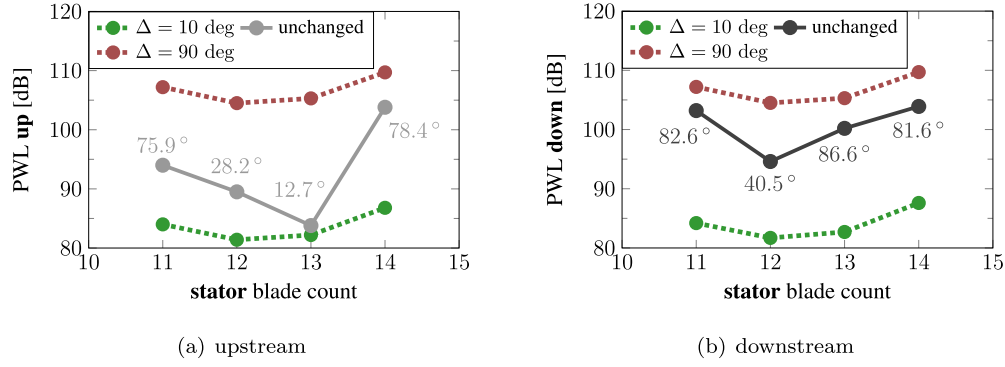
(a) upstream

(b) downstream

Fig. 4. Upstream and downstream sound power levels of the BPF1 for $B = 35$ and different stator vane counts with unchanged, nearly congruent and perpendicular phase propagation angle relative to the stator leading edge angle. For the unchanged case the inscribed labels indicate the values of Δ for the dominant mode.

Table 2
Dominant propagating BPF1 modes for $B = 35$ and varying stator vane count and respective values for α_{mn}, σ_{mn} and Δ.

	upstream				downstream			
	(m, n)	α_{mn}	σ_{mn}	Δ [deg]	(m, n)	α_{mn}	σ_{mn}	Δ [deg]
V11	$(2, 1)$	0.66	8.55	75.9	$(-9, 0)$	0.56	10.65	82.6
V12	$(-1, 0)$	0.994	1.25	28.2	$(-1, 0)$	0.994	1.25	40.5
V13	$(-4, 0)$	0.914	4.95	12.7	$(-4, 1)$	0.603	9.71	86.6
V14	$(7, 0)$	0.62	8.43	78.4	$(-7, 0)$	0.741	8.43	81.6

dipole radiation axis. Consequently, it is reasonable that the highest sound power levels are obtained for $\Delta = 90$ deg.

According to the analytical prediction, the difference of the sound power levels between $\Delta = 90$ deg and $\Delta = 10$ deg is larger than 20 dB. In other words, the manipulation of Δ indicates that for one configuration the sound power level could be more than 20 dB lower, if the phase propagation angles of the propagating modes would be congruent to the stator leading edge angle rather than perpendicular. Thus, the phase propagation angle relative to the stator leading edge has a significant impact on the sound excitation. In particular, the study confirms that acoustic modes having a phase propagation angle congruent to the stator leading edge angle are excited weakly. The results with the actual mode propagation angles, without imposing a fixed value for Δ in the analytical model artificially, are in between the results for $\Delta = 10$ deg and $\Delta = 90$ deg.

The effect may be slightly overestimated in the analytical prediction from PropNoise since the stand-alone module uses flat plates to model the blade profiles [4,13]. In addition, the analytical study is performed with untwisted stator vanes, i.e. the leading edge angle is constant in radial direction. Consequently, for one particular acoustic mode, the difference between the mode phase propagation angle and the stator leading edge angle is also constant. Therefore, we perform a validation of the analytical results using Harmonic Balance simulations. Contrary to the stand-alone module, the HB simulation uses three-dimensional curved blade profiles. Thus, in the HB simulation the leading edge angle radially changes and the dipole sources are distributed along the curved surface. Fig. 5 compares the noise prediction from PropNoise with the numerical results obtained from the HB simulation. The numerical data have a constant offset compared to the prediction from PropNoise. However, the numerical results confirm the analytically predicted trend and verify that also in the numerical simulation the phase propagation angle significantly affects the sound excitation, even though twisted stator vanes are considered.

Besides the stand-alone module, PropNoise offers the option to perform an analytical noise prediction based on RANS simulations [4]. For the RANS-informed analytical noise prediction with PropNoise, all input parameters needed for the acoustics module

are extracted from a steady-state RANS simulation. The RANS simulation uses the same fan geometry and blade profiles as the HB simulation. In Fig. 5 the results obtained from the RANS-informed noise prediction are plotted in yellow. These results also confirm the trend predicted by the stand-alone module and exemplarily verify that the assumption of flat plates leads to a reasonable noise prediction.

The labels inserted in Fig. 5 show the values of Δ. These values are calculated at 70% span. Comparing Fig. 4 with Fig. 5 indicates that the numerically calculated Δ is in good agreement with the analytically predicted value. Regarding the upstream direction, the phase propagation angle is almost congruent to the stator leading edge angle for the configurations B35V12 and B35V13. Note that B35 indicates the number of rotor blades and V13 the number of stator vanes. With regard to B35V13, the dominant Tyler-Sofrin mode is $m = 35 - 3 \cdot 13 = -4$. For this azimuthal mode the phase propagation angle is almost congruent to the stator leading edge angle. Hence, the lowest difference Δ occurs ($\Delta \approx 15$ deg). Due to the impact of the phase propagation angle the dominant mode $m = -4$ is excited weakly, which is one reason why B35V13 has the lowest upstream sound power level. Regarding the downstream direction, the phase propagation angle tends to be oriented almost perpendicularly to the leading edge. The only exception is the configuration B35V12. For this configuration PropNoise and the HB simulation predict $\Delta \approx 40$ deg, which is the reason for the lower downstream sound power level compared to the adjacent configurations. In addition, PropNoise and the HB simulation predict $\Delta \approx 30$ deg for this configuration in the upstream direction. Thus, the configuration with 12 stator vanes provides a good compromise with regard to the phase propagation angle. This is the first reason why the upstream and downstream BPF1 sound power levels of this configuration are comparable or lower than the sound power levels of adjacent blade count pairings.

For all other blade count pairings from area "A", we observe a similar result to that shown in Fig. 4 and Fig. 5. Our interim conclusion for area "A" is that the phase propagation angle of modes propagating upstream is almost congruent to the stator leading edge angle. These modes are excited weakly resulting in a significant tonal noise reduction.
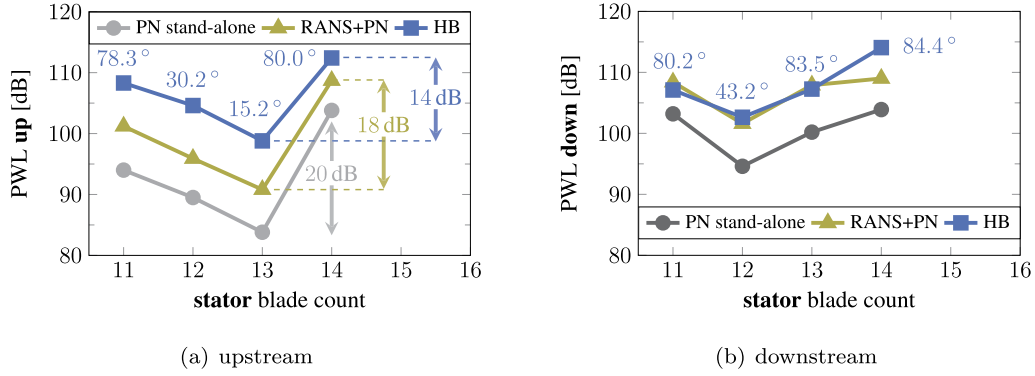
(a) upstream

(b) downstream

Fig. 5. Upstream and downstream sound power levels of the BPF1 for $B = 35$ and different stator vane counts. Labels indicate the values of Δ for the dominant modes.

In area "A", the phase propagation angle particularly impacts the sound power levels of the upstream direction. As an additional effect, the mode cut-on factor α_{mn} is identified to influence the sound power levels of the upstream and the downstream direction. The mode cut-on factor provides the explanation why the overall sound power levels are lower in area "A" compared to adjacent blade count pairings. The importance of α_{mn} for modes propagating in ducts was introduced by Rice [30], who identified this factor as a basic parameter for noise propagation. In the following, we investigate the impact of the cut-on factor on the noise generation.

Fig. 6 plots the relation between the sound power level and the cut-on factor for the dominant mode. The cut-on factor might be different for the upstream and the downstream direction since different azimuthal and radial modes may be dominant and each set of modes has a different α_{mn}. The cut-on factor is calculated using Eq. (2). The data points colored in red show the analytical prediction for the case that the influence of the phase propagation angle is neglected. That means, Δ is again manipulated in the Prop-Noise code and set to $\Delta = 90 \deg$. The results indicate that acoustic modes, which are further away from the cut-off limit ($\alpha \rightarrow 1$), are excited weakly and carry a lower sound power. Close to the cut-off limit ($\alpha \rightarrow 0$), the sound power increases remarkably, which is also shown in [31]. According to the distribution of the red data points, the relation $PWL \sim -10 \log_{10}(\alpha_{mn}) + y_0$ describes the impact of the cut-on factor on the sound power level. This correlation is deduced from the analytical modeling, which predicts that the sound power is inversely proportional to α_{mn} (see Eq. (3), Eq. (4) and Eq. (7)).

The data points colored in light and dark grey show the actual results from PropNoise without the manipulation of the phase propagation angle. These data points exhibit a larger scattering due to the impact of the phase propagation angle. For instance, for the configuration B35V12 the upstream and downstream phase propagation angles of the dominant Tyler-Sofrin mode $m = -1$ are almost congruent to the stator leading edge angle. Therefore, the data point shifts to a lower sound power level while the cut-on factor remains unchanged. The mode $m = -1$ is excited weakly due to the phase propagation angle. By contrast, if $\Delta = 90 \deg$ is applied, the mode phase propagation angle is perpendicular to the leading edge angle. As a result, the sound power level increases and the data point is located close to the red curve. For B35V14 both results, with and without the manipulation of the phase propagation angle, are almost similar. The reason is that for this configuration the phase propagation angles of the dominant azimuthal modes $m = \pm 7$ are perpendicular to the stator leading edge angle in any case.

Taking into account the configurations B35V12 and B35V14, the question arises: Why does the mode $m = -1$ carry a lower sound power than the modes $m = \pm 7$? The answer is the influence of both, the phase propagation angle and the cut-on factor. Besides

the phase propagation angle of the mode $m = -1$, which is almost congruent to the stator leading edge angle, the cut-on factor is close to 1. Both effects lead to a lower sound power level. A cut-on factor close to 1 is the second aspect why the upstream and downstream BPF1 sound power levels of the configuration with 12 stator vanes are comparable or lower than the sound power levels of adjacent blade counts.

(a) upstream
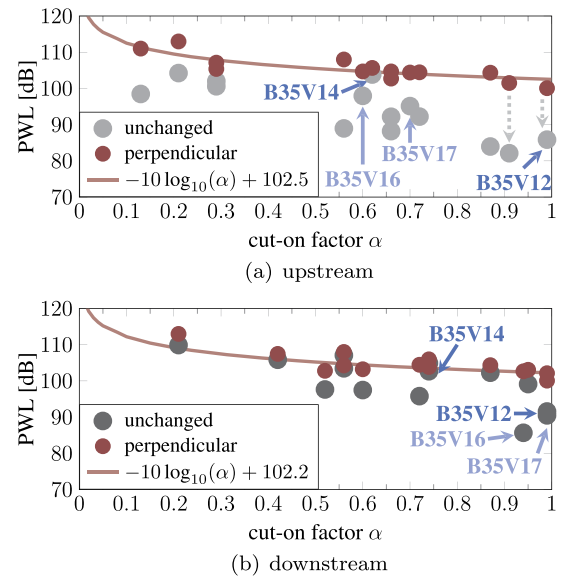
(b) downstream

Fig. 6. Upstream and downstream sound power levels of the BPF1 as a function of the cut-on factor α for $B = 35$ and different stator vane counts.

The interim conclusion formulated earlier can now be extended as follows: The sound power levels of the blade count pairings from area "A" are mainly affected by the impact of the phase propagation angle and the cut-on factor. For these configurations, low azimuthal mode orders are dominantly excited, the upstream phase propagation angles of the dominant modes are almost congruent to the stator leading edge angle and the dominant modes are far away from the cut-off limit. These effects cause that the dominant modes are excited weakly and carry a lower sound power. Thus, the two acoustic phenomena reduce the tonal interaction noise.

In area "B", the explanations are still valid and the same two phenomena impact the sound excitation. Compared to area "A", the difference is: The downstream phase propagation angle is congruent to the leading edge angle but the upstream phase propagation angle tends to be oriented almost perpendicular to the leading edge angle. This can exemplarily be seen in Fig. 6 by comparing

33

the upstream and downstream sound power levels of the configuration B35V16. Upstream, the data point is located close to the red line, which means that the phase propagation angle is almost perpendicular to the leading edge angle. Downstream, the cut-on factor of the dominant mode is close to one and the phase propagation angle is rather congruent to the leading edge angle resulting in a lower noise level.

5.2. Inverse cut-off of the blade passing frequency tone

In this subsection we examine the low-count OGV configurations from area "C". For all blade count pairings from area "C" the BPF1 tone is cut-off. Conventionally, a cut-off design is realized with stator vane counts larger than the rotor blade count (by factor 2 or more). However, if the tip Mach number is low enough, a cut-off design can also be achieved with fewer stator vanes than rotor blades. This is called an "inverse cut-off" and corresponds to area "C". Area "C" is a promising design space compared to the conventional cut-off design space since the stator vane count is reduced significantly. Hence, this region has the potential to decrease the stator-generated broadband noise and still benefit from the cut-off of the blade passing frequency tone. Consequently, the question arises why large high-speed fan stages are not designed with inverse cut-off of the first blade passing frequency tone? Typically, for these fan stages, the rotor tip Mach number is close to one, or higher. However, in this section we will show that the inverse cut-off effect is restricted to smaller tip Mach numbers.

To investigate the formulated question, we analyze the impact of the change of the rotor tip Mach number on the tonal rotor–stator interaction noise. The impact of the tip Mach number is demonstrated by a study on the variation of rotor and stator blade count. This study is performed with the stand-alone module of PropNoise. The fan entry flow Mach number is kept constant at a value of 0.21, which is a typical flight Mach number for small airplanes in cruise condition. In addition, the aerodynamic loading of the rotor and stator blades is kept constant. As a result, the fan pressure ratio and the fan diameter differ if the tip Mach number changes. In particular, the fan diameter scales inversely with the fan pressure ratio, which means that the lowest rotor tip speed corresponds to the lowest fan pressure ratio and the largest fan diameter. For instance, due to the variation of the rotor tip speed the fan diameter at the rotor tip d_{tip} varies between $d_{tip} = 0.91$ m (for $M_{\text{tip}} = 0.33$) and $d_{tip} = 0.80$ m ($M_{\text{tip}} = 0.41$). The rotor tip Mach number is calculated from $M_{\text{tip}} = (N d_{tip} \pi)/a$, where N is the rotational speed and a is the speed of sound at the rotor entry.

Fig. 7 depicts how the sound power levels of the BPF1 tone vary with the rotor and stator blade counts for four different rotor tip Mach numbers. The tip Mach number 0.33 corresponds to a fan pressure ratio of 1.05 and $M_{\text{tip}} = 0.41$ corresponds to a fan pressure ratio of 1.072. These pressure ratios are realistic for low-speed fan stages of small airplanes.

For all blade count configurations from area "C" the acoustic modes of the BPF1 tone are not able to propagate. The BPF1 tone is cut-off following the inverse cut-off principle. If the rotor tip speed is increased above 0.4, the acoustic modes start to propagate, the blade passing frequency tone becomes cut-on and area "C" shrinks until the effect vanishes completely for larger tip Mach numbers. In other words, the smaller the rotor tip Mach number, the wider the inverse cut-off area, which means that additional blade count pairings become cut-off for lower rotor tip speeds. The variation of the rotor tip Mach number leads to two main observations: First, a correlation between the rotor tip speed and the inverse cut-off effect exists. Second, a decrease of the fan pressure ratio and the rotor tip speed make an inverse cut-off design possible and es-
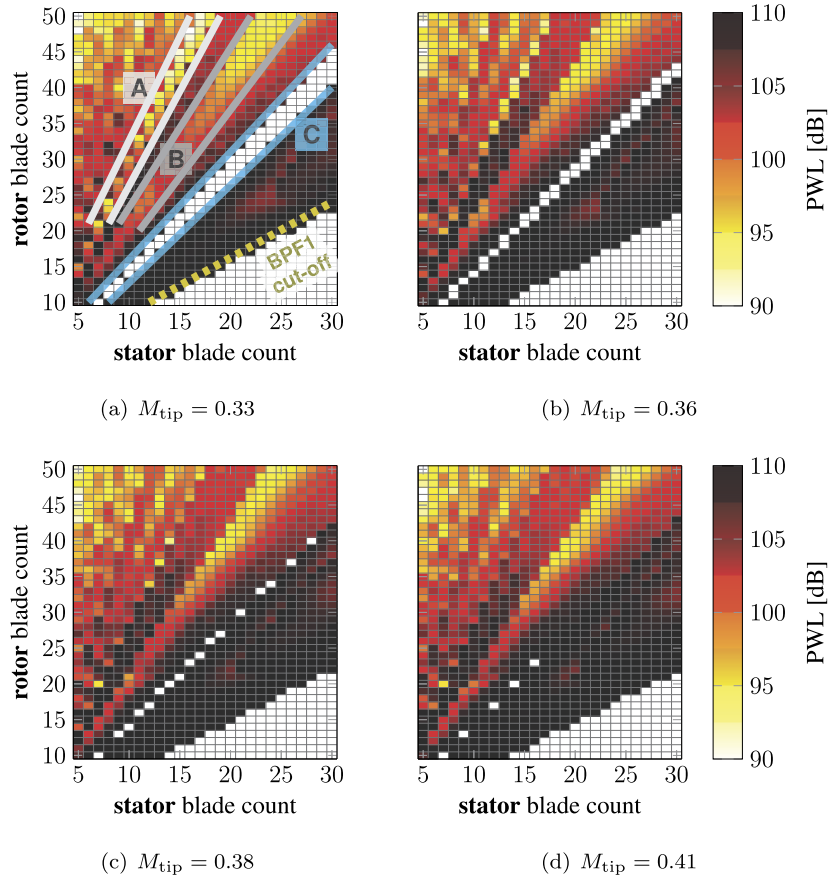

(a) $M_{\text{tip}} = 0.33$ (b) $M_{\text{tip}} = 0.36$ (c) $M_{\text{tip}} = 0.38$ (d) $M_{\text{tip}} = 0.41$

Fig. 7. BPF1 sound power levels for different rotor–stator blade count combinations and four rotor tip speeds.

tablish new options in terms of blade count selection within the low-count OGV design space.

Fig. 7 indicates that the effect might be restricted to small rotor tip speeds. Additionally, a narrow tip Mach number range exists, below which all blade count pairings from area "C" almost simultaneously become cut-off. Thus, an inverse cut-off design is possible if the rotor tip Mach number is lower than a critical Mach number ($M_\text{tip} < M_\text{tip, crit}$). For cut-off modes, the factor α_{mn} is an imaginary number ($\Re(\alpha) = 0$). Therefore, in absence of swirl, Eq. (2) and $\Re(\alpha) = 0$ lead to the relation

$$M_\text{tip, crit} = \sqrt{1 - M_x^2}\, \frac{\sigma_{m0}}{B}. \qquad (9)$$

Equation (9) shows the correlation between the critical tip Mach number and the inverse cut-off effect. In first approximation, the variable σ_{m0} is equal to $|m|$ in hollow ducts. This simplifies the relation to $M_\text{tip, crit} \approx \sqrt{1 - M_x^2}\, |m|/B$. As a result, $M_\text{tip, crit}$ only depends on the axial Mach number M_x and the respective blade count pairing, since the dominant azimuthal mode order m can be expressed as a function of the rotor blade count B and stator vane count V with $m = hB - kV$ (Tyler and Sofrin's rule [29]).

The critical tip Mach number linearly depends on the variable $|m|/B$, which is visualized in Fig. 8(a) for four different axial Mach numbers. The axial Mach number is varied between $M_x = 0.1$ and $M_x = 0.7$ to illustrate the impact of the axial Mach number on $M_\text{tip, crit}$, although the axial Mach number for the CRAFT rotor–stator stage is $M_x = 0.15$. It can be seen that the impact of M_x on $M_\text{tip, crit}$ becomes relevant for high axial Mach numbers. In case $M_x < 0.3$, the impact of the axial Mach number is negligible in good approximation. Consequently, the ratio of the triggered mode order and the rotor blade number $|m|/B$ determines the critical tip Mach number in this case. Fig. 8(b) depicts this ratio for all low-count OGV blade count pairings. For each configuration, the lowest possible BPF1 mode order ($|m| = \min(|1 \cdot B - kV|)$) is used to calculate $|m|/B$. To realize an inverse cut-off design for low-speed fan stages, only the blade count pairings from area "C" are suitable. The reason for this is, as shown in Fig. 8(b), that in

area "C" an inverse cut-off of the BPF1 tone can be achieved for $M_\text{tip} < M_\text{tip, crit} \approx |m|/B \approx 0.38$. The fulfillment of this condition may be possible for fan stages with low pressure ratios and large diameters, e.g. fan stages for UAM airplanes. For all other blade count pairings, which do not belong to area "C", the ratio $|m|/B$ is lower than 0.2. That means, M_tip would have to be lower than 0.2 to achieve an inverse cut-off. This might not be feasible for a fan design since $M_\text{tip} < M_\text{tip, crit} = 0.2$ might be too low for the given thrust requirement. Overall, the approximation of $M_\text{tip, crit}$ confirms the trend shown in Fig. 7. Regarding the preliminary design of low-speed fan stages, the approximation offers a convenient way to estimate for which blade count pairings an inverse cut-off of the BPF1 tone is possible.

In order to exemplarily verify that the inverse cut-off effect depends on the rotor tip speed, we numerically examined the configuration with 18 rotor blades in combination with 11, 12, 13 and 14 stator vanes. Two different rotor tip speeds are considered, $M_\text{tip} = 0.33$ and $M_\text{tip} = 0.38$. The analytical prediction from PropNoise is compared with the results obtained from the Harmonic Balance simulation in Table 3. For $M_\text{tip} = 0.33$ both the analytical and the numerical results predict that the BPF1 modes are not able to propagate if 12 or 13 stator vanes are combined with 18 rotor blades. Thus, the Harmonic Balance simulations confirm that the BPF1 tone is cut-off following the inverse cut-off principle if the rotor tip Mach number is $M_\text{tip} = 0.33$. If the tip Mach number is increased to $M_\text{tip} = 0.38$, the Harmonic Balance simulations also verify that the acoustic modes start to propagate. Hence, the BPF1 tone becomes cut-on for the higher rotor tip speed. Regarding the configuration with 12 stator vanes, the acoustic mode $(m, n) = (-6, 0)$ becomes cut-on and regarding the configuration with 13 stator vanes, $(m, n) = (5, 0)$ becomes cut-on.

As a result, an inverse cut-off design can be realized particularly for low-speed fan stages with low fan pressure ratios and large fan diameters (compared to the size of the aircraft). Thus, an inverse cut-off design using the blade count pairings of area "C" may be promising for fan stages of small airplanes operating in urban areas.

(a) Correlation between $M_\text{tip, crit}$ and $|m|/B$ (b) $|m|/B$ for different blade count pairings
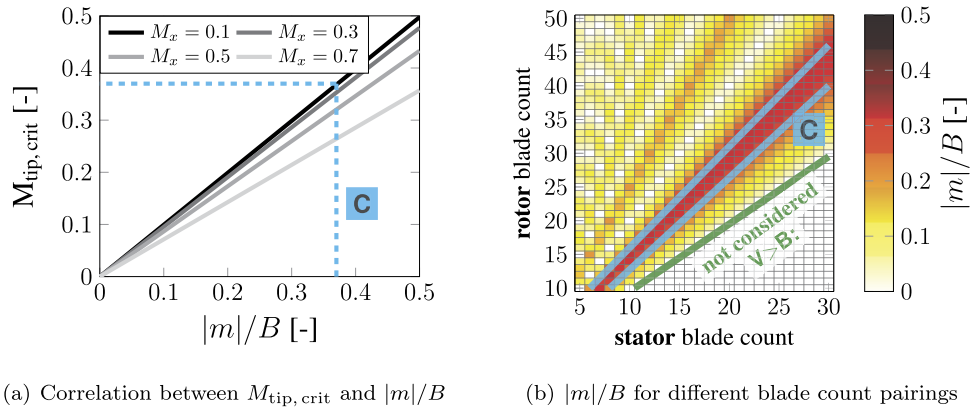
Fig. 8. Approximation of the critical rotor tip Mach number $M_\text{tip, crit}$.

Table 3
BPF1 sound power levels (in [dB]) for 18 rotor blades and varying stator vane count. Comparison between PropNoise and Harmonic Balance simulation for two different rotor tip speeds in order to verify the inverse cut-off effect. Note that "−" indicates that no HB simulation was performed for this configuration.

	V11		V12		V13		V14	
	PN	HB	PN	HB	PN	HB	PN	HB
$M_\text{tip} = 0.33$	112.0	115.2	inverse cut-off		inverse cut-off		116.0	121.0
$M_\text{tip} = 0.38$	112.0	—	113.8	117.3	118.7	123.0	114.8	—

6. Conclusion and discussion

With the noise assessment presented in this paper, we intended to provide a step towards the design-to-noise of low-speed axial fan stages for small airplanes, which may operate in urban areas. Particularly, we focused on fan stages with fewer stator vanes than rotor blades (low-count OGV fan stages). We illustrated promising mechanisms to reduce the blade passing frequency tone. In summary, our analytical and numerical noise assessment led to the following findings:

- We showed that two acoustic parameters dominantly impact the tonal noise excitation of low-count OGV configurations: The mode phase propagation angle and the mode cut-on factor.

- While varying the rotor and stator blade counts, we identified three low-count OGV design spaces, for which the blade passing frequency tone is either strongly reduced or fully suppressed.

- For two identified low-count OGV design spaces, the phase propagation angle of either the upstream or the downstream dominant mode was congruent to the stator leading edge angle. In that case the acoustic mode is excited weakly and the sound power level is low at noise generation. This mechanism was verified by means of unsteady numerical simulations.
In addition, for the blade count pairings of those two design spaces, the triggered acoustic interaction modes were far away from the cut-off limit. Hence, these modes propagate well inside the duct segments. However, the results indicated that modes that are further away from the cut-off limit are excited weakly and carry a lower sound power at their generation. Therefore, regarding the noise excitation, we concluded that certain low-count OGV designs acoustically benefit from a combination of both, the impact of the mode phase propagation angle and the impact of the mode cut-on factor.

- For the blade count pairings of the third low-count OGV design space, we observed a cut-off of the blade passing frequency tone even though the number of stator vanes was lower than the number of rotor blades (inverse cut-off). In particular, the variation of the rotor tip speed indicated that decreasing the tip speed makes an inverse cut-off of the blade passing frequency tone possible. The unsteady numerical simulations confirmed the connection between the rotor tip speed and the inverse cut-off effect. Further, our assessment showed that the effect seems to be restricted to small rotor tip speeds. Thus, the inverse cut-off effect could be a promising tonal noise reduction mechanism for low-speed axial fan stages with low fan pressure ratios.

As a first step towards answering the formulated research question, we focused on the noise excitation and outlined several tonal noise reduction mechanisms for low-count OGV fan stages. The assessment emphasized that specific low-count OGV configurations benefit from a weaker noise excitation, even though the BPF1 tone may be cut-on. Further research should examine the following:

- Although our assessment focused on the first blade passing frequency tone, higher harmonics are also contributing to the fan noise and should be included in subsequent studies.

- Regarding the inverse cut-off effect, the question of the robustness of the cut-off design remains unanswered. In the analytical and the numerical noise prediction an idealized geometry is considered. We assumed that all rotor wakes, which impinge on the stator leading edge, are identical. This is not the case in reality since the rotor blades may vary from another, e.g. due to manufacturing tolerances. Wakes with different width and velocity deficit create new modes that can be cut-on and thus mitigate the inverse cut-off effect.

- We concluded that for certain low-count OGV configurations the resulting interaction modes are far away from the cut-off limit, i.e. these modes propagate efficiently. Therefore, the transmission of sound through the rotor would be an interesting aspect to examine. Philpot [32] states that the blockage of the rotor and the resulting attenuation are larger for acoustic modes that rotate against the rotor rotation.

- Acoustic modes that rotate in the direction of the flow swirl propagate less efficient compared to modes that rotate against the swirl direction [4]. Therefore, for higher swirl Mach numbers, the influence of the flow swirl on the mode propagation would be a further aspect that should be considered to assess the noise reduction potential of low-count OGV designs.

- Another facet of the design-to-noise of fan stages is the noise reduction due to acoustic liner. Regarding the noise propagation, the following question arises: Does an acoustic lining change the observed trends of the blade count variation and can those low-count OGV designs, which benefit from a weaker noise excitation, remain competitive while including the liner damping?

Declaration of competing interest

The authors declare that they have no known competing financial interests or personal relationships that could have appeared to influence the work reported in this paper.

References

[1] W. Neise, L. Enghardt, Technology approach to aero engine noise reduction, Aerosp. Sci. Technol. 7 (5) (2003) 352–363, https://doi.org/10.1016/S1270-9638(03)00027-0.

[2] C.A. Hall, D. Crichton, Engine design studies for a silent aircraft, J. Turbomach. 129 (3) (2006) 479–487, https://doi.org/10.1115/1.2472398.

[3] S.A. Rizzi, D.L. Huff, D.D. Boyd, P. Bent, B.S. Henderson, K.A. Pascioni, D.C. Sargent, D.L. Josephson, M. Marsan, H. He, R. Snider, Urban air mobility noise: Current practice, gaps, and recommendations, NASA/TP-2020-5007433, 2020.

[4] R. Jaron, Aeroakustische auslegung von triebwerksfans mittels multidisziplinärer optimierungen, Dissertation, German Aerospace Center, Institute of Propulsion Technology, Berlin, Germany, 2018, https://doi.org/10.14279/depositonce-7057.

[5] J.H. Dittmar, J.N. Scott, B.R. Leonard, E.G. Stakolich, Effects of long-chord acoustically treated stator vanes on fan noise, NASA Tech. Note, NASA TN D-8062, 1975.

[6] J.H. Dittmar, R.P. Woodward, An evaluation of some alternative approaches for reducing fan tone noise, NASA Tech. Memorandum, NASA-TM-105356, 1992.

[7] P.J.G. Schwaller, M.J. Oliver, E. Eccleston, Farfield measurements and mode analysis of the effects of vane/blade ratio on fan noise, in: AIAA/NASA 9th Aeroacoustics Conference, AIAA-84-2280, 1984, https://doi.org/10.2514/6.1984-2280.

[8] G. Kröger, R. Schnell, N.D. Humphreys, Optimised aerodynamic design of an OGV with reduced blade count for low noise aircraft engines, in: Proc. of ASME Turbo Expo 2012: Power for Land, Sea and Air, 2012, pp. GT2012–GT69459, https://doi.org/10.1115/GT2012-69459.

[9] D. Giacché, T.P. Hynes, S. Baralon, J. Coupland, N. Humphreys, P. Schwaller, Acoustic optimization of ultra-low count bypass outlet guide vanes, in: 19th AIAA/CEAS Aeroacoustics Conference, AIAA 2013-2295, 2013, https://doi.org/10.2514/6.2013-2295.

[10] D. Casalino, F. Diozzi, R. Sannino, A. Paonessa, Aircraft noise reduction technologies: a bibliographic review, Aerosp. Sci. Technol. 12 (1) (2008) 1–17, https://doi.org/10.1016/j.ast.2007.10.004.

[11] U. Tapken, L. Caldas, R. Meyer, M. Behn, L. Klähn, R. Jaron, A. Rudolphi, New test facility to investigate the noise generated by shrouded fans for small aircraft applications, in: DICUAM 2021, 2021.

[12] R. Jaron, A. Moreau, Laufschaufeloptimierung der Rotor-Stator-Stufe für den CRAFT-Prüfstand, Tech. Rep. DLR IB 92517-11/B25, 2011.

[13] A. Moreau, A unified analytical approach for the acoustic conceptual design of fans for modern aero-engines, Dissertation, German Aerospace Center, Institute of Propulsion Technology, Berlin, Germany, 2017, https://doi.org/10.14279/depositonce-5935.

[14] E. Rice, M. Heidmann, T. Sofrin, Modal propagation angles in a cylindrical duct with flow and their relation to sound radiation, in: 17th Aerospace Sciences Meeting, AIAA 79-0183, 1979, https://doi.org/10.2514/6.1979-183.

[15] A. Moreau, S. Guérin, S. Busse, A method based on the ray structure of acoustic modes for predicting the liner performance in annular ducts with flow, in: International Conference on Acoustics NAG/DAGA 2009 Conference Proceedings, 2009, pp. 1248–1251.

[16] A. Moreau, S. Guérin, Similarities of the free-field and in-duct formulations in rotor noise problems, in: 17th AIAA/CEAS Aeroacoustics Conference (32nd AIAA Aeroacoustics Conference), AIAA 2011-2759, 2012, https://doi.org/10.2514/6.2011-2759.

[17] S. Rienstra, B. Tester, An analytic Green's function for a lined circular duct containing uniform mean flow, in: 11th AIAA/CEAS Aeroacoustics Conference, AIAA 2005-3020, 1979, https://doi.org/10.2514/6.2005-3020.

[18] S. Guérin, Farfield radiation of induct-cutoff pressure waves, in: 23rd AIAA/CEAS Aeroacoustics Conference, AIAA 2017-4037, 2017, https://doi.org/10.2514/6.2017-4037.

[19] W.R. Sears, Some aspects of non-stationary airfoil theory and its practical application, J. Aeronaut. Sci. 8 (3) (1941) 104–108, https://doi.org/10.2514/8.10655.

[20] D. Nürnberger, F. Eulitz, S. Schmitt, A. Zachcial, Recent progress in the numerical simulation of unsteady viscous multistage turbomachinery flow, ISOABE 2001-1081, 2001.

[21] H. Yang, D. Nürnberger, H.P. Kersken, Towards excellence in turbomachinery computational fluid dynamics: a hybrid structured-unstructured Reynolds-averaged Navier-Stokes solver, J. Turbomach. 128 (2) (2006) 390–402, https://doi.org/10.1115/1.2162182.

[22] K.C. Hall, K. Ekici, J.P. Thomas, E.H. Dowell, Harmonic balance methods applied to computational fluid dynamics problems, Int. J. Comput. Fluid Dyn. 27 (2) (2013) 52–67, https://doi.org/10.1080/10618562.2012.742512.

[23] C. Frey, G. Ashcroft, H. Kersken, C. Voigt, A harmonic balance technique for multistage turbomachinery applications, in: ASME Turbo Expo 2014: Turbine Technical Conference and Exposition, GT2014-25230, 2014, https://doi.org/10.1115/GT2014-25230.

[24] D. Wang, X. Huang, A complete rotor–stator coupling method for frequency domain analysis of turbomachinery unsteady flow, Aerosp. Sci. Technol. 70 (2017) 367–377, https://doi.org/10.1016/j.ast.2017.08.025.

[25] F.R. Menter, M. Kuntz, R. Langtry, Ten years of industrial experience with the SST turbulence model, Heat Mass Transf. 4 (2003) 625–632.

[26] A. Wohlbrandt, C. Weckmüller, S. Guérin, A robust extension to the triple plane pressure mode matching method by filtering convective perturbations, Int. J. Aeroacoust. 15 (1–2) (2016) 41–58, https://doi.org/10.1177/1475472X16630842.

[27] N.C. Ovenden, S.W. Rienstra, Mode-matching strategies in slowly varying engine ducts, AIAA J. 42 (2016) 1832–1840, https://doi.org/10.1115/GT2014-25230.

[28] S. Guérin, A. Moreau, U. Tapken, Relation between source models and acoustic duct modes, in: 15th AIAA/CEAS Aeroacoustics Conference, AIAA 2013-2295, 2009, https://doi.org/10.2514/6.2009-3364.

[29] J.M. Tyler, T.G. Sofrin, Axial Flow Compressor Noise Studies, SAE International, 1962, https://doi.org/10.4271/620532.

[30] E.J. Rice, Inlet noise suppressor design method based upon the distribution of acoustic power with mode cutoff ratio, Adv. Eng. Sci. 3 (1976) 883–894.

[31] M.V. Lowson, Theoretical studies of compressor noise, NASA Contractor Rep. NASA CR-1287, 1969.

[32] M.G. Philpot, The role of rotor blade blockage in the propagation of fan noise interaction tones, in: AIAA 2nd Aeroacoustics Conference, 1975, https://doi.org/10.2514/6.1975-447.

2.2   Publication II

This article is licensed under a Creative Commons license, CC-BY 4.0,
https://creativecommons.org/licenses/by/4.0/.

Article

Smart Blade Count Selection to Align Modal Propagation Angle with Stator Stagger Angle for Low-Noise Ducted Fan Designs

Stephen Schade * , Robert Jaron, Lukas Klähn and Antoine Moreau

German Aerospace Center, Department of Engine Acoustics, Bismarckstraße 101, 10625 Berlin, Germany
* Correspondence: stephen.schade@dlr.de

Abstract: The rotor–stator interaction noise is a major source of fan noise. Especially for low-speed fan stages, the tonal component is typically a dominant noise source. A challenge is to reduce this tonal noise, as it is typically perceived as unpleasant. Therefore, in this paper, we analytically, numerically and experimentally investigate an acoustic effect to lower the tonal noise excitation. Our study on an existing low-speed fan indicates a reduction in tonal interaction noise of more than 9 dB at the source if the excited acoustic modes propagate parallel to the stator leading edge angle. Moreover, a design-to-low-noise approach is demonstrated in order to apply this effect to two new fan stages with fewer stator than rotor blades. The acoustic design of both fans is determined by an appropriate choice of the rotor and stator blade numbers in order to align the modal propagation angle with the stator stagger angle. The blade geometries are obtained from aerodynamic optimization. Both fans provide similar aerodynamic but opposing acoustic radiation characteristics compared to the baseline fan and a significant tonal noise reduction resulting from the impact of the modal propagation angle on noise excitation. To ensure that this effect can also be applied to other low-speed fans, a design rule is derived and validated.

Keywords: design-to-low-noise; rotor–stator interaction noise; aerodynamic optimization

1. Introduction

Recently, new electrified propulsion systems, for example, with distributed, low-speed fan stages or distributed propellers, are under development to power the next generation of urban and regional aircrafts. The noise emitted, especially that from the engines, is a crucial sound source that can be unpleasant to hear. Therefore, acoustic effects that enable a low-noise design of the propulsion system need to be investigated and understood [1]. In particular, reduction mechanisms should be evaluated that allow for the reduction in noise directly at its source.

In general, the noise emission of fan stages is composed of several sources that can radiate noise at discrete frequencies (tonal noise) and throughout a wide frequency range (broadband noise). Typically, for low-speed fan stages, the rotor–stator interaction noise represents the dominant source [2]. An important challenge is to reduce the tonal component, as it is often perceived as unpleasant [3,4]. Consequently, there is a need to assess noise reduction methods, particularly those that minimize the tonal component of this noise source.

Analytical and numerical studies on low-speed fan stages indicate that the excitation of tonal rotor–stator interaction noise is significantly affected by the propagation angles of the acoustic modes relative to the stator leading edge angle [2,5,6]. In [6], an analytical and numerical acoustic investigation of fan stages with fewer stator than rotor blades is performed. These designs are called low-count outer guide vane (OGV) fans [2,6]. It is shown that, for certain blade count numbers, a tonal advantage is achieved if the propagation angles of the dominantly excited modes are nearly parallel to the stator leading edge angle [2,6]. In recent measurements on a low-speed fan stage, the effect

39

was also confirmed experimentally in design operating conditions [7]. Regarding the transmission of sound through rotor or stator blade rows, a similar effect is known as the "modal condition" [8,9].

The described effect can be achieved if the modal propagation angle is aligned with the stator stagger angle. Thus, the rotor and stator blade numbers need to be chosen appropriately. The reason for this is that the choice of blade numbers determines the excited Tyler and Sofrin mode orders, and the azimuthal mode orders define the modal propagation angles for the respective flow conditions. Consequently, an acoustic advantage is achieved by iterating the blade numbers until the exact acoustic modes that preferably propagate parallel to the stator leading edge angle become dominant. In this paper, it is verified that, depending on the fan design, the effect can reduce the excitation of tonal interaction noise upstream or downstream. The effect is particularly suitable for low-speed fan stages, as only a few acoustic modes are excited.

In the first part of this paper, we verify and validate the impact of the modal propagation angle on tonal noise excitation for a wider range of operating points, including off-design conditions, using analytical, numerical and experimental data. The studies are performed on a low-speed shrouded fan, which is representative of aircraft engines for urban and regional air mobility. The experimental measurements are conducted in DLR's fan test facility, Co-/Contra Rotating Acoustic Fan Test rig (CRAFT) [10].

In the second part of this paper, the noise reduction potential of the described effect is demonstrated on two new low-count OGV fan stages. Reducing the tonal interaction noise is particularly relevant for low-count OGV fans, as these designs may have a tonal disadvantage. Contrary to conventional fan designs, the usually dominant blade-passing frequency tone may no longer be cut off, since fewer stator than rotor blades are used [6]. Due to the described effect, for both low-count OGV fans, the tonal disadvantage is eliminated, as the results indicate a significant tonal noise reduction compared to the baseline fan. However, contrary to the baseline fan, due to an appropriate choice of blade numbers, the tonal noise is not reduced upstream but downstream. Consequently, an opposing noise radiation characteristic is achieved. Thus, this effect not only reduces tonal noise but also specifically influences the radiation direction. Taking into account liners and shielding effects, this can be used to improve certification levels and the psychoacoustic noise impact.

The rotor and stator geometries of both low-count OGV fan stages are designed in a multi-objective aerodynamic optimization. The optimization ensures that all considered fan stages provide similar aerodynamic characteristics. However, opposing acoustic characteristics are achieved due to the modal propagation angles. Therefore, all fans are well suited for acoustic and psychoacoustic investigations.

2. Rotor–Stator Interaction Noise

The rotor–stator interaction (RSI) noise source consists of a broadband and a tonal component. This source results from the aerodynamic flow around the rotor blade and its interaction with the stator leading edge. Particularly, the velocity boundary layers on the suction and pressure sides of the rotor blades lead both to an inhomogeneous velocity distribution (rotor wake) and to an increased turbulence intensity behind the rotor [2]. These flow disturbances interact with the downstream stator vanes and generate the interaction noise.

The broadband component of the RSI noise source occurs due to turbulent fluctuations that interact with the stator leading edge. The tonal component results from the rotor wakes, which periodically impinge on the stator leading edge. Therefore, it can be classified as unsteady lift-generated noise. The tonal noise occurs at discrete blade passing frequencies (BPFs), which are calculated as multiples of the number of rotor blades and the rotational speed.

As visualized in Figure 1, the periodic impingement of rotor wakes on the stator leading edge results in a dipole noise source with its main radiation axis perpendicular to the leading edge angle. The excited azimuthal mode orders m can be determined from

$m = hB - kV$ formulated by Tyler and Sofrin [11]. In this relation, $h \in \mathbb{N}_0$ represents the harmonics of the rotor blade number B, and $k \in \mathbb{Z}$ describes the scattering at the stator vanes V.
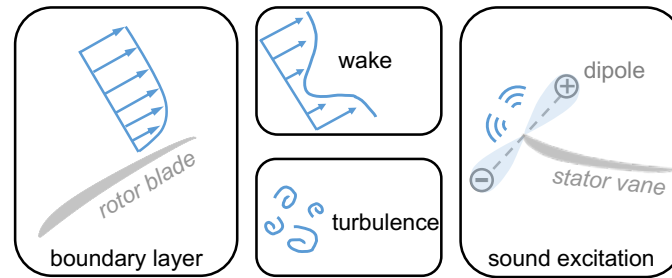

Figure 1. Excitation mechanism of the RSI noise source.

The Impact of the Modal Propagation Angle on Noise Excitation

The propagation directions of acoustic modes with azimuthal order m and radial order n can be described with the modal propagation angle $\zeta_{mn}^{\pm}$ [12,13].

$$\zeta_{mn}^{\pm} = -\text{sign}(m)\cos^{-1}\left(\frac{-M_x \pm \alpha_{mn}}{1 \mp \alpha_{mn} M_x} \right) \tag{1}$$

The formulation in Equation (1) is obtained from Moreau [13] and is equivalent to Equation (27) from Rice [12]. In Equation (1), the upstream propagating modes are indicated by $(-)$ and the downstream propagating modes by $(+)$. The axial Mach number is M_x, and α_{mn} is the cut-on factor. As specified in [13], under consideration of a solid body swirl, the cut-on factor is calculated as

$$\alpha_{mn} = \sqrt{1 - (1 - M_x^2)\left(\frac{\sigma_{mn}}{kR - mM_s} \right)^2}. \tag{2}$$

In Equation (2), σ_{mn} is the $(n+1)^{th}$ zero of the first derivative of the radial eigenfunction at the walls, k is the acoustic wave number and M_s is the swirl Mach number.

The modal propagation angle $\zeta_{mn}^{\pm}$ has a direct impact on the modal sound pressure amplitude $A_{mn}^{\pm}$, since $A_{mn}^{\pm}$ depends on the source term σ, which is a function of the wave number normal to the profile chord k_n, which, in turn, is a function of the modal propagation angle. The expressions used to calculate these quantities are provided in Equations (3)–(5).

As derived in [13],

$$A_{mn}^{\pm} = i \cdot B \int_r^R \hat{g}_{mn}^{\omega} \, e^{-ik_x x_{LE} - im\theta_{LE}} \cdot \sigma(\sigma_L) \cdot dr_s \tag{3}$$

describes the modal sound pressure amplitude within the duct, where r is the hub radius, R is the tip radius, k_x is the axial wave number and x_{LE} and θ_{LE} define the leading edge (LE) position. The definition of the induct Green's function $\hat{g}_{mn}^{\omega}$ can be obtained from [13,14].

The source term σ is composed of different terms for the respective noise-generation mechanisms, where

$$\sigma_L = i\, k_n \int_0^c f_L^{\hat{\omega}} \cdot e^{-ik_l l} dl \tag{4}$$

is the source term for the lift-generated component (e.g., tonal RSI noise) [13]. In Equation (4), $f_L^{\hat{\omega}}$ specifies the chordwise distribution of lift, k_l is the chordwise wave number and l defines the chordwise position of the noise source on the blade. The lift-generated tonal noise component depends on the normal wave number

$$k_n = (k - \frac{mM_s}{R})\sin(\zeta_{mn}^{\pm} - \chi_{LE}), \tag{5}$$

which depends on the modal propagation angle $\zeta_{mn}^{\pm}$ and the stator leading edge angle χ_{LE}.

As indicated in Equations (3)–(5), an acoustic mode (m, n) will not be excited if the modal propagation angle is exactly parallel to the stator leading edge angle ($\zeta_{mn}^{\pm} = \chi_{LE}$). In contrast, the strongest sound excitation occurs if the modal propagation angle is exactly perpendicular to the stator leading edge angle ($\zeta_{mn}^{\pm} \perp \chi_{LE}$). The reason for this is that the modal propagation angle is in line with the dipole radiation axis in this case.

In order to simplify the subsequent analysis, the difference between the modal propagation angle and the stator leading edge angle is scaled to the range $[0, 90\,\text{deg}]$ and specified as

$$\Delta = \begin{cases} |\zeta_{mn} - \chi_{LE}|, & \text{if } |\zeta_{mn} - \chi_{LE}| \leq 90° \\ |180 - |\zeta_{mn} - \chi_{LE}||, & \text{if } |\zeta_{mn} - \chi_{LE}| > 90° \end{cases}. \tag{6}$$

Figure 2 schematically illustrates a dipole noise source at the stator leading edge and visualizes the relation between $\zeta_{mn}^{\pm}$, χ_{LE} and Δ. In order to illustrate the modal propagation angle, the propagation direction of a negative acoustic mode $m < 0$, which propagates upstream $(-)$ and downstream $(+)$, is exemplarily shown. In the sketched example, the modal propagation angle is nearly parallel to the stator leading edge angle upstream (see $m^- < 0$), whereas downstream, the modal propagation angle is nearly perpendicular to the leading edge angle (see $m^+ < 0$). Thus, in this case, a lower noise excitation would be expected upstream.
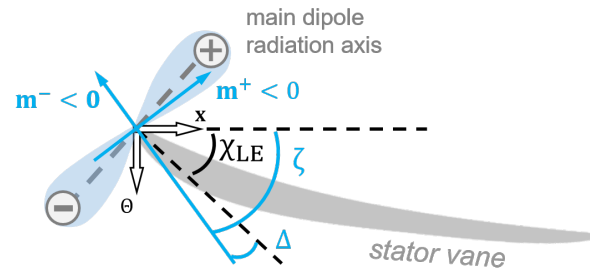
Figure 2. Illustration of a dipole noise source at the stator LE and exemplary visualization of the propagation directions of an acoustic mode $m < 0$.

3. The Baseline Fan Stage

The baseline rotor–stator fan stage is equipped with $B = 18$ rotor blades and $V = 21$ stator vanes. For this blade count combination, the acoustic modes at the first blade passing frequency (BPF1) are cut-on. The fan has a diameter of 0.454 m and is shown in Figure 3a. The stator leading edge angle is $\chi_{LE} = 45$ deg.

(a)

(b)

Figure 3. Baseline fan stage. (**a**) Baseline fan geometry [10]; (**b**) performance map [15].

Table 1 outlines the four considered operating points for the studies in this paper. These operating conditions are also highlighted in the performance map in Figure 3b. At the design point (DP), the rotor–stator stage is operated at 6.98 kg/s with a rotational speed of $4500 \, \text{min}^{-1}$. The resulting pressure ratio is PR = 1.038 and the rotor tip Mach number is $M_{tip} = 0.31$. In addition to the design point, three additional operating points are considered for the acoustic analysis: PR_{max} and $\dot{m}_{\text{max}}$ are located on the 4500 rpm speed line and define the points at maximum pressure ratio and maximum mass flow, respectively. OP_4 is the operating point at zero incidence on the 3375 rpm speed line.
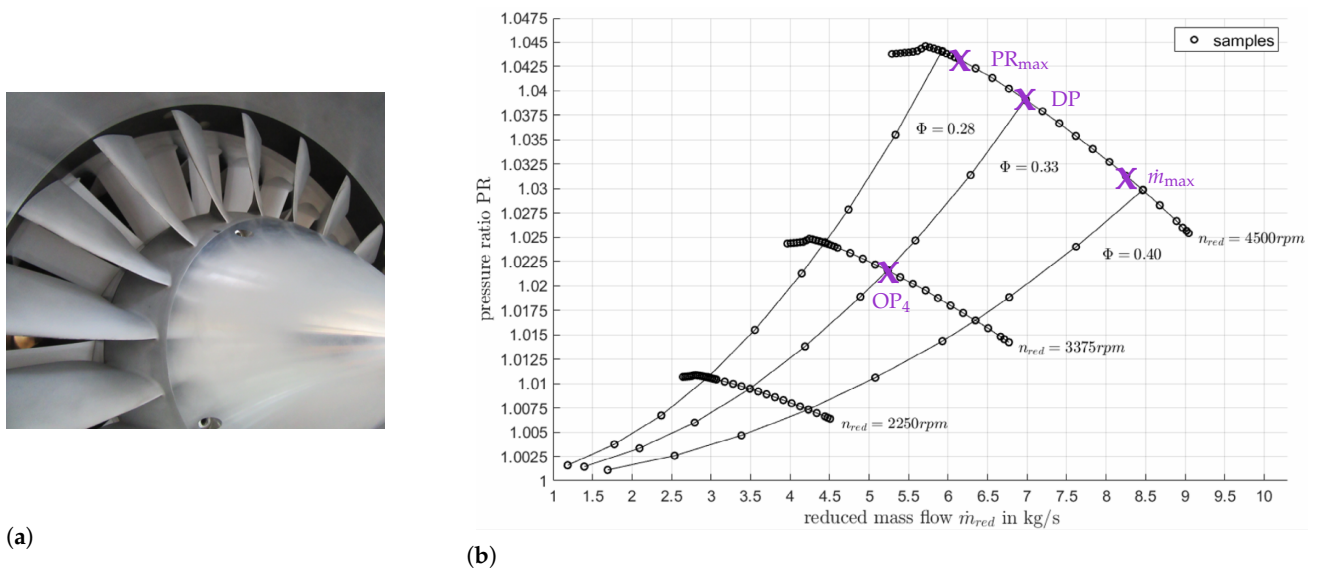
Table 1. Operating conditions for the CRAFT rotor–stator stage. Pressure ratios and Mach numbers are determined from RANS simulations. Mach numbers are flux-averaged values calculated upstream of the stator leading edge.

	N [rpm]	Mass Flow [kg/s]	PR	Axial Ma	Swirl Ma
DP	4500	6.98	1.038	0.165	0.146
PR_{max}	4500	6.10	1.043	0.139	0.158
$\dot{m}_{\text{max}}$	4500	8.30	1.031	0.196	0.130
OP_4	3375	5.21	1.021	0.123	0.109

4. Methods

The subsequent investigation of the tonal noise excitation on low-speed fan stages is based on analytical, numerical and experimental data. The methods used to determine the noise levels are described in Sections 4.1–4.3. In Section 4.4, the aerodynamic optimization procedure is described.

4.1. Analytical Noise Prediction

The analytical fan noise prediction is performed with the in-house tool PropNoise (PN) [2,13]. PropNoise can be used with different operating methods. One option to operate PropNoise is the so-called stand-alone method. This method provides an aerodynamic pre-design of the fan stage and a fully analytical noise prediction following the process visualized in Figure 4.

The stand-alone method uses a meanline approach to calculate the steady and unsteady aerodynamic quantities. The representative streamline for the meanline calculations is at 70% radial blade height. Afterwards, the aerodynamic quantities are extrapolated radially. The radial distributions serve as input for a radial strip approach in order to determine the acoustic source terms. This implies that the response of the blade to an aerodynamic excitation is calculated on each radial strip as if the problem were two-dimensional. Finally, the source term is integrated radially to obtain the induct modal sound pressure amplitude (see Equation (3)). A detailed description of the stand-alone module is outlined in [13].
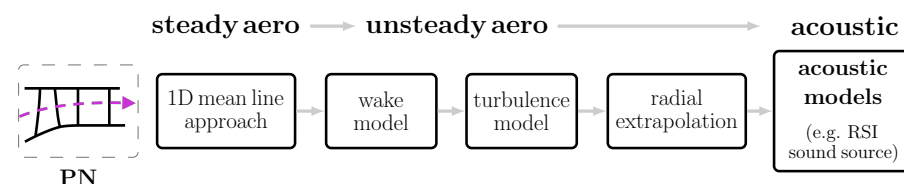
Figure 4. Process chain used for the analytical noise prediction.

4.2. Numerical Noise Prediction

For the numerical fan noise prediction, two methods are used: (1) a RANS-based analytical noise prediction and (2) a fully numerical prediction of fan tonal noise using harmonic balance (HB) simulations. The RANS and HB simulations are processed on a structured grid with O-C-H topology around the blades using the in-house Navier–Stokes solver TRACE [16,17]. The numerical grid is generated with the in-house software

PyMesh [18]. On the rotor and stator blade surfaces, the first grid cell is placed in the laminar sublayer of the velocity boundary layer ($y^+ < 1$). In the spanwise direction, the grid consists of 131 cells, of which 15 cells are placed in the rotor tip clearance. Overall, the grid consists of more than $15 \cdot 10^6$ cells. The outlet is located five axial stator chord lengths downstream of the stator trailing edge, and the inlet is located five axial rotor chord lengths upstream of the rotor leading edge. A single rotor–stator flow passage is modeled, and the closure of the equation system is achieved with the Menter SST k-ω turbulence model. The domain for the numerical simulations is shown in Figure A1, and the grid around the rotor and stator blade is exemplarily visualized in Figure A2.

In addition to the stand-alone method of PropNoise, another method is the RANS-based analytical prediction of fan noise sources [2]. For the RANS-informed noise prediction, the radial distributions of all necessary aerodynamic quantities are extracted from 3D steady-state RANS simulations (see Figure 5). The RANS-based prediction with Prop-Noise uses the same acoustic models as the fully analytical prediction with the stand-alone method. A detailed description of the RANS-based noise prediction is given in [2].
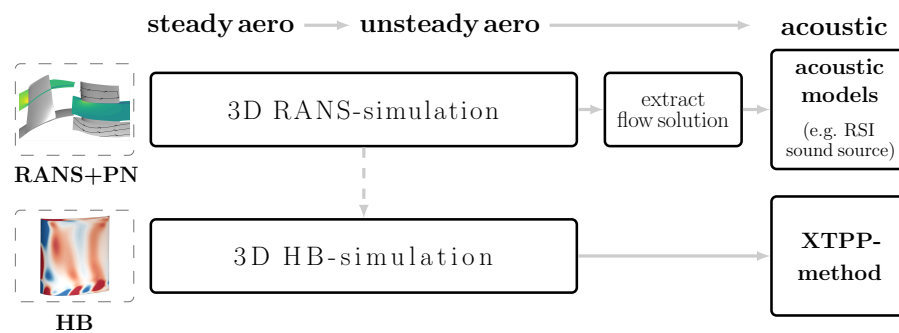
Figure 5. Process chain used for the numerical noise prediction.

The fully numerical calculation of tonal RSI noise relies on unsteady HB simulations. The HB simulations are based on a Fourier transformation of the RANS equations. Selected frequencies, which are non-linearly coupled, are solved in the frequency domain [19–21]. An XTPP method (extended triple plane pressure mode matching method) is used to separate the convective and acoustic flow disturbances and to perform a radial mode analysis [22–24]. With this approach, the tonal sound power levels are extracted from the flow solution.

4.3. Experimental Noise Measurement

The experimental noise measurements are conducted at the CRAFT test facility of the DLR Department of Engine Acoustics [10]. In Figure 6, a lateral sketch of the experimental setup is shown, where (1) is the inflow control device, (2) is a honeycomb grid, (3a) and (3b) are the upstream and downstream microphone arrays, (4) is the rotor, (5) is the stator and (6) is the nozzle.

Figure 6. CRAFT test facility.

The test facility is equipped with a two-shaft system to operate either rotor–stator fan stages, counter-rotating rotor–rotor configurations or an isolated rotor [10]. For the studies presented in this paper, the CRAFT test facility is equipped with the baseline rotor–stator fan stage described in Section 3. The operating point is adjusted using a variable nozzle. The hub radius is $r = 0.139$ m and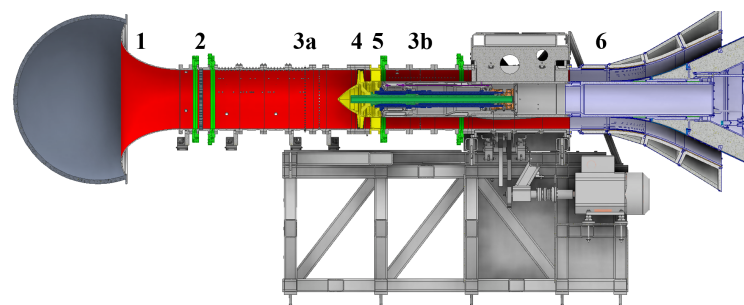 the tip radius is $R = 0.2265$ m. Along the test section, the radii are constant in order to minimize the impact on the propagation of the acoustic modes.

To ensure comparability between the noise prediction and different measurements, the rotational speed and mass flow are normalized to ISA standard conditions ($15\,^{\circ}$C, 101,325 Pa). The upstream and downstream microphone arrays consist of 30 and 22 $1/4''$ G.R.A.S. microphones type 40BP with a pre-amplifier type 26AR, respectively. The microphones are wall-mounted at a distance of 24 mm. To enable a full radial mode analysis, the microphones are mounted in a rotating array, which is rotated to 59 evenly distributed circumferential positions. With this setup, measurements of 10 s are performed. The microphone pattern allows radial mode analyses up to 6 kHz, which includes the first four BPFs at maximum speed. With a synchronously recorded shaft trigger, phase-locked averaging is applied. The resulting spectrum contains only rotor coherent sound field components. The mid-frequencies of this spectrum are integer multiples of $1/8$ of the rotation frequency. The results of the radial mode analysis are the modal sound pressure amplitudes at the first four BPFs [25]. The sound power of every mode is calculated with the formulation given by Morfey [26]. In addition, the inflow control device ensures low turbulent inflow conditions and prevents undesired noise sources, for example, due to vortex structures sucked in from the laboratory. This experimental setup is well suited for comparisons with analytical and numerical predictions as the inflow is almost free from undesired disturbances.

4.4. Aerodynamic Optimization Procedure

Two new, low-count OGV fan stages are designed for the CRAFT test facility with identical operating conditions as the baseline fan. The rotor and stator geometries of the two low-count OGV fan stages are obtained from a multi-objective aerodynamic optimization procedure. The optimization is performed with the in-house software AutoOpti developed in DLR's Fan and Compressor Department [27–29]. As the acoustic design is determined by an appropriate choice of the blade numbers, the optimization should ensure that the aerodynamic characteristics are as similar as possible to the baseline fan. Therefore, aerodynamic efficiency and pressure ratio are the primary criteria for evaluating the optimization results. Similar aerodynamic characteristics ensure the comparability of all three fans for aeroacoustic studies.

The blade numbers of both new fan stages are chosen to reduce the excitation of tonal RSI noise due to the effects resulting from the modal propagation angle. Thus, the blade numbers are determined prior to the optimization process and do not represent a degree of freedom of the optimization. Instead, the 3D geometry of the fan blades is being optimized. Thus, the following parameters defining the shape of the airfoil geometry are chosen as degrees of freedom:

- Metal angles at the leading edge and trailing edge.
- Leading edge and trailing edge radii.
- Shape of the profile at the leading edge.
- Axial airfoil length.
- Profile contours of the pressure and suction side.
- Thickness of the profile.

In order to avoid intersections between the suction side and pressure side, the profile control points of the pressure side are defined at a relative distance to the suction side. This procedure is schematically illustrated in Figure 7.
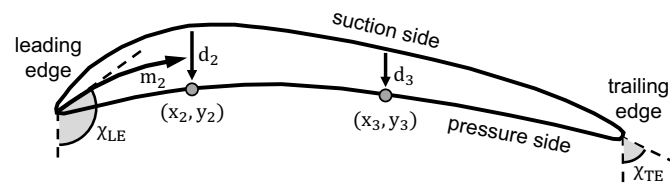
Figure 7. Construction of pressure side with thickness of distributed control points.

The optimization of the above parameters is performed on three radial sections, which are located at 5%, 60% and 95% blade height. In total, 42 degrees of freedom are specified, 14 on each radial section. In addition, the optimization is performed using two operating points. These are the design point and the point on the same speed line at the maximum pressure ratio. The latter is used to ensure a sufficient stability margin.

Table 2 summarizes the objectives and constraints. The optimization is carried out with two objectives: that the efficiency and pressure ratio under the design operating conditions are maximized. Moreover, three constraints are specified. These constraints ensure (1) a wide operating range on the design speed line ($\mathrm{PR_{maxPR}/PR_{DP}} > 1.0031$), (2) a minimum remaining swirl in the flow downstream of the stator ($\theta_\mathrm{out} \in [-3,+3]$) and (3) that the rotor does not impinge on the tip lining ($D < 30\%$).

Table 2. Objectives and constraints for aerodynamic optimization.

Parameter	Range
efficiency: η_{is}	maximize
pressure ratio: $\mathrm{PR_{DP}}$	maximize
$\mathrm{PR_{maxPR}/PR_{DP}}$	>1.0031
radial displacement D	<30% of blade tip gap
outflow angle θ_out [deg]	$[-3,+3]$

As sketched in Figure 8, initially, the optimization process generates randomly distributed configurations within the parameter space, which are subsequently passed through the process chain and evaluated with regard to the objectives and constraints. Based on this evaluation, a Pareto rank is determined for all configurations that successfully pass the process. Afterwards, the configurations are stored in the database according to the Pareto rank.
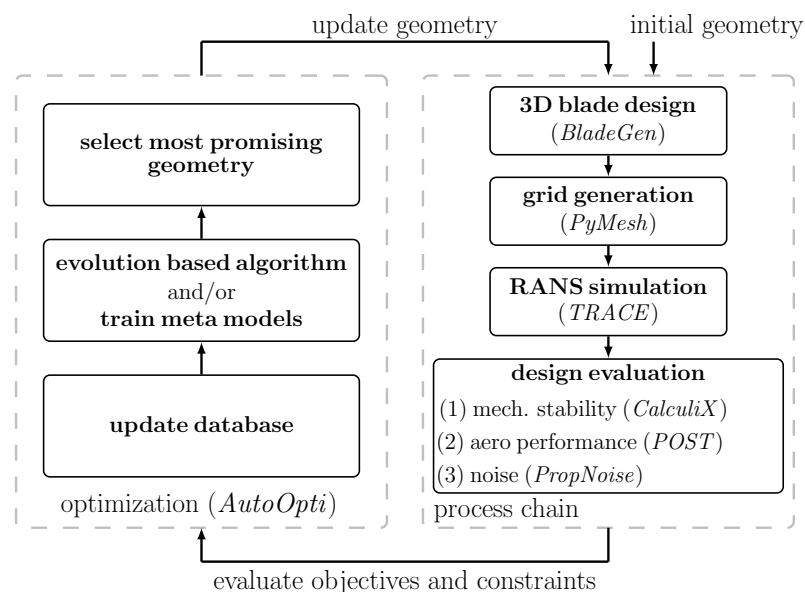

Figure 8. Process chain used for multidisciplinary optimization. Figure adapted from [2].

To generate new configurations, a surrogate model is trained with the updated database. Based on the surrogate model, sub-optimizations are performed using evolution-based algorithms. In the sub-optimizations, new configurations are selected using the volume gain criterion [28]. This criterion ensures that new configurations provide an increase in volume compared to the existing Pareto front [28]. The gradient-enhanced Kriging meta-model, which is explained in detail in [30], is applied as a surrogate model. The Kriging model is used as it offers reliable extrapolation capabilities [30]. This allows us to keep the number of initial configurations small and still make meaningful predictions in those parts of the parameter space for which no configurations have been evaluated yet.

The physical process chain consists of six steps: (1) 3D blade design, (2) grid generation with PyMesh [18], (3) RANS simulation with TRACE [16,17], (4) evaluation of the mechanical stability with CalculiX [31], (5) evaluation of the aerodynamic performance with POST [32] and (6) noise source prediction with PropNoise [2,13]. The grid generation and set-up for the numerical simulations are performed according to the specifications in Section 4.2.

5. Results

In this section, the impact of the modal propagation angle on the excitation of tonal RSI noise is analyzed. First, in Section 5.1, this is investigated analytically and numerically and validated experimentally using the baseline fan stage. Secondly, in Section 5.2, the noise reduction potential resulting from the modal propagation angle is demonstrated on two new fan stages, a low-tone fan and a low-broadband fan. For both fans, the rotor and stator blades are designed for aerodynamic optimization. In Sections 5.2.2 and 5.2.3, the optimization results are outlined and the acoustic noise emission is examined.

5.1. Acoustic Validation Using the Baseline Fan

The current CRAFT baseline fan stage is equipped with an 18-blade rotor and a 21-vane stator. For the subsequent comparison of the RSI noise levels between measurements and prediction, the axial distance between the rotor trailing edge and stator leading edge is 63 mm, measured at the casing. The comparison is performed at the three operating points DP, PR_{max} and $\dot{m}_{max}$ (see Table 1). A detailed description of the pure experimental data can additionally be found in [33].

In Figure 9, the tonal RSI sound power levels are compared between measurements (M), a fully analytical prediction (PN) and a fully numerical prediction (HB). Note that the arrows correspond to the experimental results and indicate the differences between upstream and downstream noise radiation. Figure 9a shows the sound power levels of the dominantly excited BPF1 azimuthal mode $m = -3$, and Figure 9b shows the sound power levels of the dominantly excited BPF2 azimuthal mode $m = -6$. Note that for both $m = -3$ and $m = -6$, only one radial mode, $n = 0$, is excited.

(a)   **(b)**
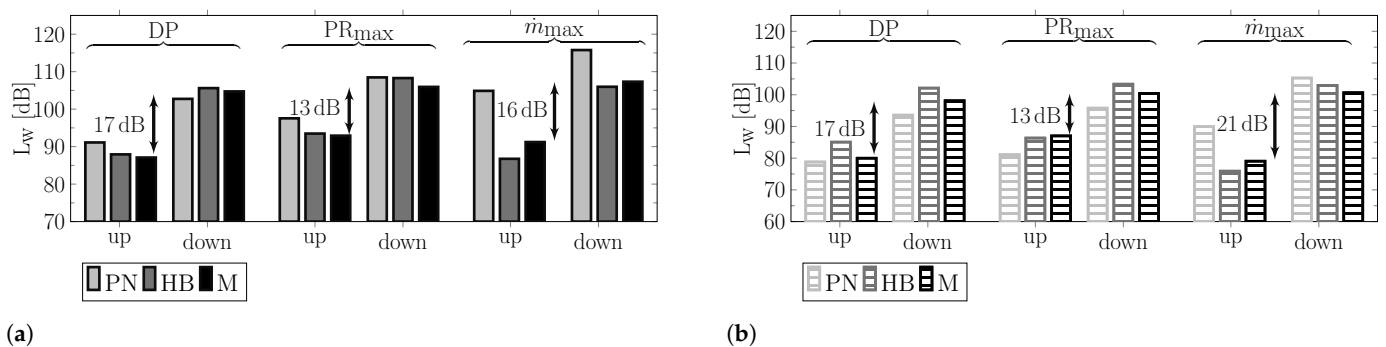
Figure 9. Analytical (PN), numerical (HB) and experimental (M) predictions of tonal RSI noise for the baseline fan, determined for three operating conditions. (**a**) BPF1, $(-3, 0)$; (**b**) BPF2, $(-6, 0)$.

For all considered operating points, the tonal noise emission of the CRAFT baseline fan stage is mainly dominated by BPF1 and BPF2. Moreover, the experimental results indicate a significant difference between the upstream and downstream radiated tonal BPF1 and BPF2 noise levels. Overall, the numerical simulation and analytical noise prediction both accurately reproduce this level difference and provide good agreement with the experimental results. However, for $\dot{m}_{\max}$ operating conditions, the fully analytical prediction provides higher absolute values.

For all operating conditions, the upstream noise radiation of the dominantly excited BPF1 mode $(-3, 0)$ is more than 13 dB lower than that of the downstream. The BPF2 shows an identical radiation characteristic. The noise levels of the dominantly excited mode $(-6, 0)$ are also more than 13 dB lower upstream. The reason for the significantly different noise radiation upstream and downstream can be found in the excitation of the fan tones. For the excitation of modes $(-3, 0)$ and $(-6, 0)$ at the stator leading edge, the scenario schematically illustrated in Figure 2 applies. Upstream, the modal propagation angles are almost parallel to the stator leading edge angle. As a result, the acoustic modes are excited weakly upstream. By contrast, downstream, a stronger noise excitation of the modes $(-3, 0)$ and $(-6, 0)$ occurs, as the propagation angles downstream are almost perpendicular to the stator leading edge angle. This is shown in Table 3, which depicts the difference Δ between the stator leading edge angle and the modal propagation angle obtained from HB simulations for the dominantly excited BPF1 and BPF2 modes at design, $\dot{m}_{\max}$ and $\mathrm{PR}_{\max}$ operating conditions. For all considered operating points and all acoustic modes, upstream, the modal propagation angle is nearly parallel to the stator LE angle ($\Delta < 15$ deg), and downstream, it is nearly perpendicular ($\Delta > 86$ deg). Thus, the upstream noise excitation of the baseline fan stage shows a strong dependence on the modal propagation angle over a wide operating range. This leads to significantly lower sound power levels upstream compared to downstream. Similar values for Δ are obtained from fully analytical predictions and measurements. These values are listed in Table A1 in Appendix B.

Table 3. Difference Δ between stator LE angle and modal propagation angle as well as α_{mn} for BPF1 and BPF2 modes obtained from HB simulations.

		Upstream		Downstream	
Operating Point	**Mode**	α_{mn}	Δ **[deg]**	α_{mn}	Δ **[deg]**
DP	$(-3, 0)$	0.788	13.6	0.755	86.2
	$(-6, 0)$	0.799	14.4	0.767	87.6
$\dot{m}_{\max}$	$(-3, 0)$	0.788	12.7	0.756	87.9
	$(-6, 0)$	0.798	13.5	0.772	89.1
$\mathrm{PR}_{\max}$	$(-3, 0)$	0.792	12.9	0.753	87.4
	$(-6, 0)$	0.801	13.7	0.766	88.6

Figure 10a shows the tonal RSI noise obtained from an HB simulation in design operating conditions. The sound power levels are plotted along the axial position within the flow channel, where location 3a from Figure 6 is at position $x = 0.05$ m and locations 4 and 5 are at position $x = 0.3$ m and $x = 0.45$ m, respectively. The numerical simulation confirms that the difference between the upstream and downstream tonal RSI levels arises from the noise excitation. A difference of more than 10 dB is predicted between upstream and downstream noise levels under design conditions. The numerical data indicate that the transmission of sound through the rotor blade row does not dominantly contribute to the level difference between upstream and downstream. The BPF1 and BPF2 noise levels are reduced by approximately 2 dB due to transmission through the rotor blade row. Figure 10b,c show that these findings are also valid for the two other operating points.

In order to further quantify the impact of the modal propagation angle on tonal noise excitation, a trend study is shown in Figure 11. The results are calculated fully analytically using PropNoise. For the trend study, the propagation angles of all cut-on BPF1 modes

are intentionally manipulated in PropNoise code. The modal propagation angles are continuously varied between $\Delta = 0$ deg and $\Delta = 90$ deg. For $\Delta = 0$ deg, the modal propagation angles are parallel to the stator LE angle, and for the latter case, the modal propagation angles are perpendicular to the LE angle. In Figure 11, the resulting BPF1 sound power levels are plotted over the difference Δ.
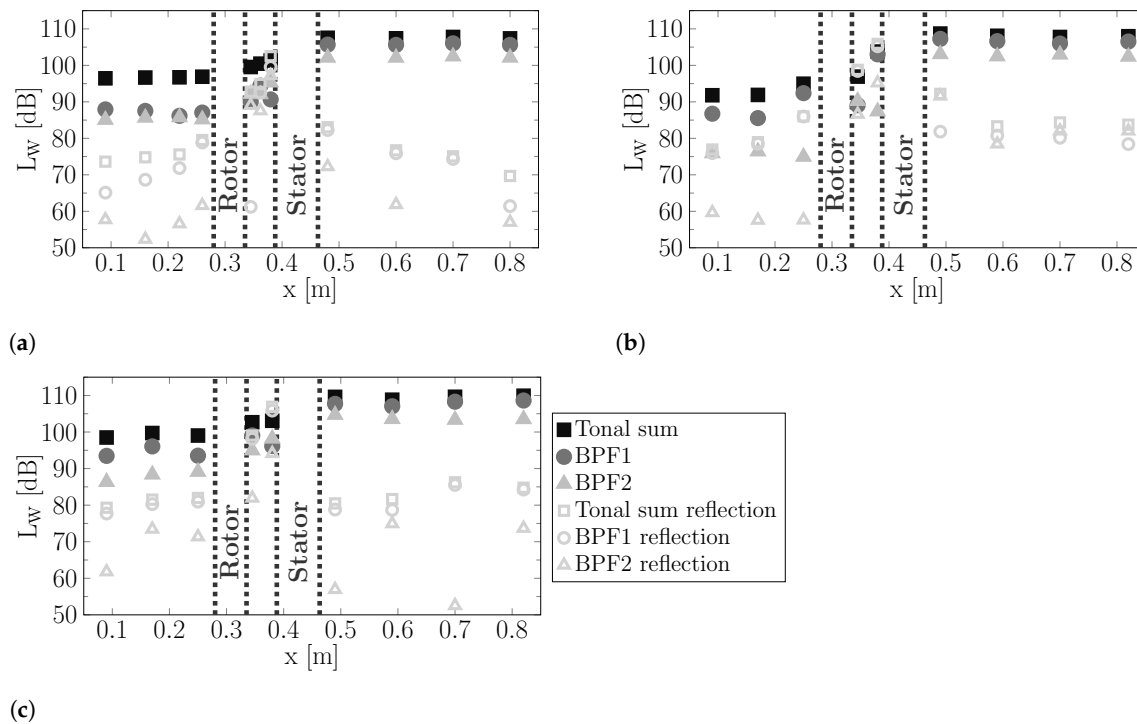

(a)

(b)

(c)

Figure 10. Tonal RSI noise levels for the baseline fan obtained from HB simulations and plotted along the axial position. (**a**) Design operating point; (**b**) $\dot{m}_{\text{max}}$ operating point; (**c**) PR$_{\text{max}}$ operating point.

The triangle and square markers indicate the actual upstream and downstream BPF1 sound power levels of the CRAFT baseline fan without any manipulation. The three curves for the three operating points are vertically shifted and are at a constant offset to each other. The results illustrate that the modal propagation angle strongly influences tonal noise excitation. The difference in sound power level between $\Delta = 0$ deg and $\Delta = 90$ deg is approximately 40 dB, according to the analytical prediction.

Based on the results obtained from the analysis of the modal propagation angle, a design rule for future acoustic designs of low-speed fan stages could be derived. Using Equation (5), it can be deduced that the expected noise level reduction compared to the case $\Delta = 90$ deg can be estimated with the factor

$$20 \log_{10}(\sin(|\Delta|)). \tag{7}$$

Equation (7) shows the correlation between the estimated noise level reduction and the difference Δ between the stator leading edge angle and modal propagation angle. In practice, this means that once the rotor and stator blade numbers and the stagger angles are known, the expected reduction in noise level compared to $\Delta = 90$ deg can be calculated using Equation (7). In Figure 11, this design rule is visualized by the dashed line and plotted for const. $= 100$ dB.

As an intermediate conclusion, the analytical, numerical and experimental data illustrate that the modal propagation angle significantly impacts the excitation of tonal RSI noise for all considered operating points. Also, in off-design conditions, for the baseline fan, the tonal RSI noise is reduced by more than 10 dB upstream compared to downstream, as the modal propagation angle upstream is nearly parallel to the stator leading edge angle.

Thus, a tonal advantage is achieved upstream due to the impact of the modal propagation angle on noise excitation.

The experimental data obtained from the CRAFT test facility and the baseline fan provide, first, a validation of the analytical and numerical results, and second, experimental evidence that the modal propagation angles strongly influence the excitation of tonal RSI noise. Especially for low-speed fan stages, where only a few azimuthal modes are cut-on, tonal RSI noise can be significantly reduced using the described effect. The acoustic benefits can be achieved with an appropriate choice of the rotor and stator blade numbers, since the blade numbers determine the excited Tyler and Sofrin mode orders, and with the azimuthal mode orders, the modal propagation angles are defined, as indicated in Equation (1). In a fan pre-design process, the stator leading edge angle is typically known at an early stage, as it directly results from rotational speed and fan pressure ratio. Consequently, the blade numbers should be iterated until the propagation angles of the dominantly excited modes are preferably parallel to the stator leading edge angle. To demonstrate the impact of the modal propagation angle on noise generation, this design-to-noise process is subsequently applied to select blade numbers for two new, low-count OGV fan stages, which are intended to be operated in the CRAFT test facility.
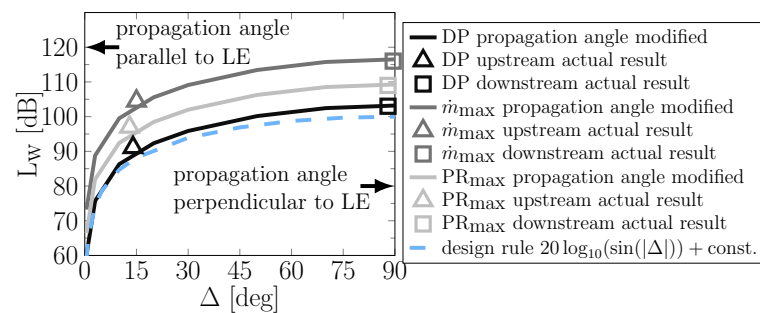

Figure 11. Variation in Δ: BPF1 sound power levels analytically predicted with PN.

5.2. Low-Count OGV Fan Stages

The analyzed noise reduction potential of the effect resulting from the modal propagation angle is demonstrated on two low-noise fan stages with fewer stator than rotor blades. Both new, low-count OGV fans are designed according to the design-to-noise process outlined at the end of Section 5.1. Consequently, in order to apply the described effect to low-count OGV fan stages and to achieve acoustic benefit, the rotor and stator blade numbers have to be chosen appropriately. The blade numbers of both new fans are chosen to achieve a weak tonal noise excitation due to the impact of the modal propagation angle. Thus, the blade numbers should be selected in such a way that the dominant excited modes propagate parallel to the stator leading edge angle. Due to the given flow conditions in the CRAFT test rig, the rotor and stator stagger angles are predefined. Thus, the rotor and stator blade numbers are varied in order to find suitable blade count combinations for which exactly those modes are dominantly excited with the modal propagation angle approximately parallel to the stator stagger angle ($\zeta_{mn}^{\pm} \approx \chi_{LE} = 45\,\text{deg}$).

Achieving an acoustic benefit based on the effect resulting from the modal propagation angle is the primary acoustic design criterion for both new low-count OGV fan stages. In addition to that, additional design criteria are defined that set further requirements regarding the acoustic behavior of the fan stages. This is important as the fans are intended to be used in a process consisting of measurements, virtual flyover simulations, auralizations and listening tests in the future. In order to achieve fundamentally different perceived noise characteristics with the same aerodynamic performance, the fan stages should also differ with regard to the following aspects:

(a)   Different dominant noise radiation direction.
(b)   Different ratio between tonal and broadband noise levels.
(c)   Different base frequency.

5.2.1. Blade Count Selection

In order to assess which blade count combinations satisfy the defined requirements, analytical blade count variations are performed using RANS-based noise prediction with PropNoise (see Figure 12). The baseline fan stage with 18 rotor blades and 21 stator vanes is selected as the initial configuration for the blade count variation. This configuration is framed in purple in Figure 12. The blade count pairing of the baseline fan is chosen such that the acoustic BPF1 modes are cut-on, which results in very high sound power levels and a tonally dominant sound radiation.
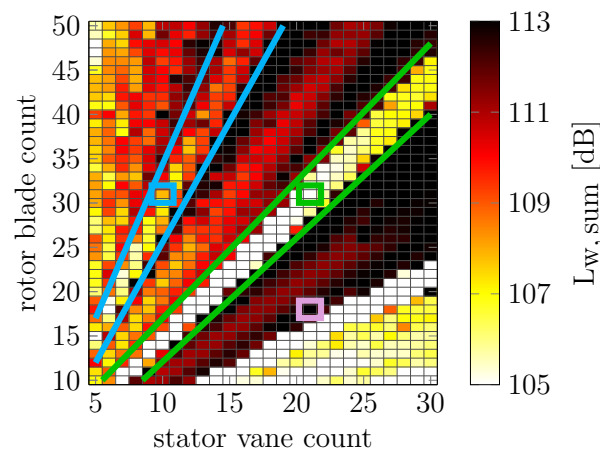

Figure 12. Overall sound power levels for different rotor and stator blade counts calculated with RANS-based noise prediction. For each blade count paring, the overall sound power level is summed over three operating points (DP, PR$_{max}$ and OP$_4$).

Using the baseline fan, a RANS simulation is performed for the three operating points, DP, PR$_{max}$ and OP$_4$ (see Table 1). The aerodynamic flow field is extracted from each RANS simulation and used as input for PropNoise in order to analytically predict the noise levels, following the process visualized in Figure 5. Based on this initial prediction, the blade numbers are subsequently varied using PropNoise, and the noise levels are calculated for the new configurations for each operating point. For the blade count variation, the following assumptions are made:

1. All aerodynamic flow parameters and streamlines remain unchanged. Therefore, RANS simulations are performed only for the initial configuration.
2. The blade's solidity is constant. Thus, the chord length changes between the configurations (e.g., the lower the blade count, the longer the blade chord).

A detailed description of the procedure applied to the RANS-based noise prediction and blade count variation with PropNoise is given in [2,6].

Figure 12 shows the overall sound power levels of the RSI noise source summed over the three operating points as a function of the rotor and stator blade numbers. In [6], a similar blade count variation is performed, and several acoustically promising areas are introduced. These areas are marked in green and blue in Figure 12. For all blade count pairings within the green area, two acoustic effects ensure that lower sound power levels occur. Firstly, the BPF1 tone is inversely cut off. Secondly, an acoustic benefit is achieved due to the effect resulting from the modal propagation angle. Due to these acoustic advantages, the first blade count combination for one of the new fan stages is selected from the green area. This fan stage consists of a 31-blade rotor combined with a 21-vane stator. As the 21-vane stator already exists (stator of the baseline fan), this blade count combination is also a good choice to keep the manufacturing costs low. The B31V21 low-count OGV fan is subsequently named the low-tone fan, and the aeroacoustic results are shown in Section 5.2.2.

For all blade count pairings within the blue area, two acoustic effects also ensure that lower sound power levels occur. Similar to the green area, the impact of the modal propagation angle on noise excitation leads to an acoustic benefit. In addition to that, as the number of stator vanes is reduced compared to configurations in the green area, a reduction in broadband noise is obtained. Due to these acoustic benefits, the second blade count combination for one of the new fan stages is selected from the blue area. This low-count OGV fan also uses the 31-blade rotor, which is combined with a 10-vane stator. The B31V10 fan is subsequently named the low-broadband fan, and the aeroacoustic results are shown in Section 5.2.3.

5.2.2. Low-Tone Fan: Aerodynamic Optimization and Acoustic Evaluation

The low-tone fan is equipped with a new 31-blade rotor and the 21-vane baseline stator. Since the 21-vane stator geometry already exists, only the rotor geometry is optimized using the multi-objective optimization process described in Section 4.4.

Figure 13a shows the generated members of the optimization and the Pareto front between the efficiency and pressure ratio for design operating conditions. The baseline fan stage is marked in purple, and the selected member for the 31-blade rotor is marked in green. The reason for choosing this particular member is that the fan stages should be similar to each other regarding their aerodynamic characteristics. The final geometry of the 31-blade rotor is shown on the left in Figure 13b, and the combination of this rotor with the baseline 21-vane stator is shown on the right.
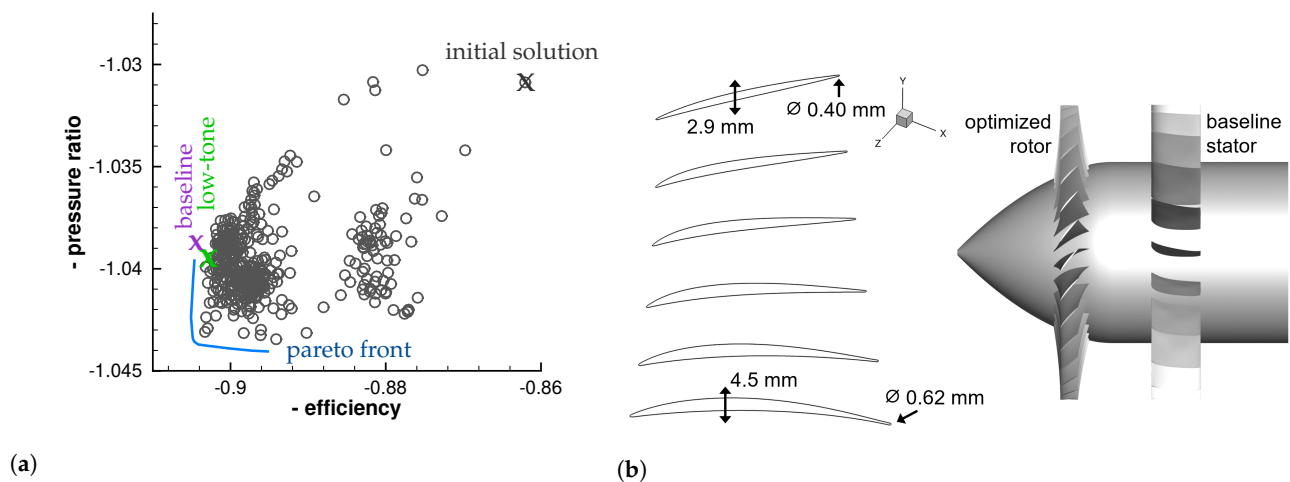

(**a**)   (**b**)

Figure 13. Results of the optimization for the 31-blade rotor. (**a**) Pareto front; (**b**) geometry of the 31-blade rotor.

This B31V21 low-count OGV fan stage is named the low-tone fan since two acoustic effects are used to efficiently reduce the tonal noise component. Firstly, the rotor–stator blade counts are chosen such that the acoustic BPF1 modes are inversely cut off. The inverse cut-off is achieved due to the low rotor tip Mach number, $M_{\text{tip}} = 0.31$. Conventionally, a cut-off design is realized with stator vane counts larger than the rotor blade count. However, in [6], it is verified that a cut-off design can also be achieved with fewer stator than rotor blades on condition that the rotor tip Mach number is low enough. This is called an inverse cut-off. As a design rule to achieve an inverse cut-off, the Mach number should be lower than a critical Mach number [6]. This critical Mach number is defined as $M_{\text{tip,crit}} \approx \sqrt{1 - M_x^2}\,|m|\,/\,B$. For the low-tone fan $M_{\text{tip,crit}}$ is approximately 0.32. Consequently, the inverse cut-off of the BPF1 tone is possible, since $M_{\text{tip}} = 0.31 < M_{\text{tip,crit}} = 0.32$.

Secondly, in addition to the inverse cut-off of the BPF1 tone, the blade numbers of this fan stage are chosen such that the excited BPF2 modes benefit from the impact of the propagation angle upstream. For the BPF2 tone, the acoustic mode $(-1, 1)$ is dominantly

excited. As shown in Table 4, the propagation angle of this mode upstream is nearly parallel to the stator leading edge angle, and downstream it is nearly perpendicular. Therefore, the mode is excited more weakly upstream, leading to lower sound power levels.

Table 4. Difference Δ between stator LE angle and modal propagation angle as well as α_{mn} for the BPF1 and BPF2 modes under design conditions for the low-tone fan stage.

		Upstream		Downstream	
f [Hz]	**(m,n)**	α_{mn}	**Δ [deg]**	α_{mn}	**Δ [deg]**
2325	inverse cut-off	–	–	–	–
4650	$(-1, 1)$	0.91	24.0	0.91	74.8

This is confirmed by the results from the HB simulation, which are shown in Figure 14. The HB simulation is performed under design operating conditions. The results indicate a difference of 5 dB between the upstream and downstream noise excitations, leading to significantly lower noise radiation upstream. In addition to the effect resulting from the propagation angle, the upstream noise radiation also benefits from the transmission of the mode $m = -1$ through the rotor blade row. The reason for this is that the mode $m = -1$ rotates against the rotor's rotation direction. According to Philpot [34], modes rotating against the rotor's rotation are attenuated more efficiently when propagating through a rotor blade row compared to modes rotating in the same direction. In the present case, the HB simulation shows that, due to the transmission through the rotor, the noise levels are attenuated by 3 dB. Adding the 5dB from the noise excitation results in a total difference of 8dB between the upstream and downstream noise radiation.
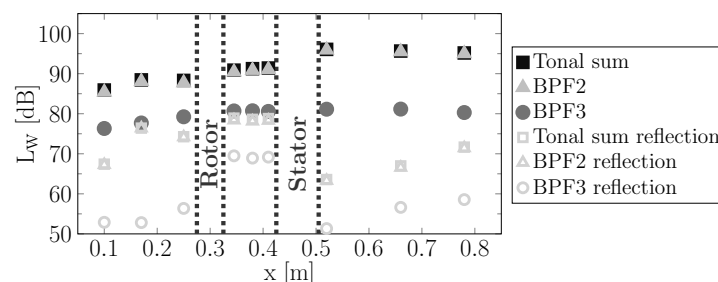

Figure 14. Tonal RSI noise levels under design conditions obtained from an HB simulation and plotted along the axial position for the low-tone fan stage.

Compared to the numerical results of the baseline fan stage presented in Figure 10a, this fan shows lower sound power levels of more than 10 dB in both upstream and downstream directions. Nevertheless, the general tonal noise radiation characteristic is similar to that of the baseline fan: lower tonal sound power levels occur upstream, whereas higher levels are observed downstream.

Figure 15 shows the noise directivity of the low-tone fan at design operating conditions. The noise directivity indicates that, over all radiation angles, the tonal component of the RSI noise has similar levels compared to the broadband component. For radiation angles between 60 deg and 150 deg, the tonal noise levels are even lower than the broadband levels, such that the broadband component is the dominant sound source over a wide range of radiation angles. Consequently, the noise impression of this low-speed fan is mainly characterized by broadband noise, whose energy is spread over a wide range of frequencies, and less by discrete frequencies that create tonal noise. This is particularly interesting for future listening tests, since broadband sounds are often perceived as less annoying.

As an intermediate summary, the noise emission of the low-tone fan is characterized by the following features:

1. The BPF1 tone is inversely cut off.

2. Upstream, the tonal noise excitation at the second BPF benefits from a modal propagation angle that is relatively parallel to the stator LE angle.
3. The dominant tonal noise radiation direction is downstream.
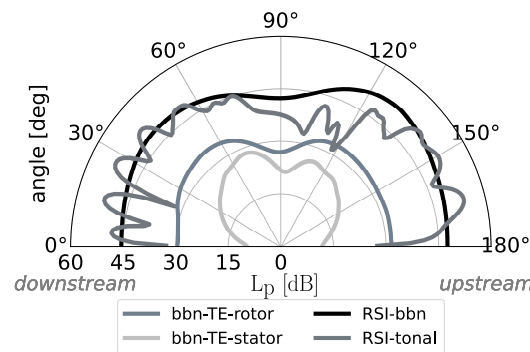4. The tonal RSI noise is lower than the broadband component over a wide range of radiation angles.

Figure 15. Noise directivity at design operating conditions for the low-tone fan stage obtained from RANS-based noise prediction.

For a possible application of this fan design in an urban air mobility airplane (e.g., a small airtaxi with a distributed propulsion system), it should be noted that this fan is equipped with a large amount of rotor and stator blades, which might increase production as well as maintenance costs. Therefore, an additional fan design with a significantly lower stator vane count is investigated in the following subsection.

5.2.3. Low-Broadband Fan: Aerodynamic Optimization and Acoustic Evaluation

The low-broadband fan is equipped with the 31-blade rotor from Section 5.2.2 and a new 10-vane stator. Similar to the 31-blade rotor, the new stator geometry is optimized using the multi-objective optimization process described in Section 4.4.

The generated members of the optimization and the Pareto front between the efficiency and pressure ratio for design operating conditions are shown in Figure 16a. Again, the baseline fan is marked in purple and the low-tone fan in green. The selected member from the optimization for the 10-vane stator is marked in blue. It becomes evident that all three fan stages provide similar efficiencies and pressure ratios for design operating conditions. Thus, the aerodynamic and acoustic comparability of all three fan stages is ensured. In Figure 16b, the geometry of the 21-vane stator is shown in detail, and its combination with the 31-blade rotor is illustrated.

Compared to the baseline fan and the low-tone fan, which both have 21 stator vanes, the number of stator vanes is approximately halved for the low-broadband fan. Due to the reduced number of stator vanes, the broadband noise is reduced significantly, as this noise source scales with the number of stator vanes [2]. As a rule of thumb, the broadband noise is reduced by 3 dB if the number of stator vanes is halved. This is the reason why the B31V10 fan stage is named the low-broadband fan.

In order to reduce not only the broadband noise component but also the tonal component, the rotor–stator blade count of this fan stage is chosen such that the excitation of BPF1 benefits downstream from the impact of the modal propagation angle (see Table 5). Downstream, the propagation angle of the dominantly excited mode $(1, 1)$ is relatively parallel to the stator leading edge angle, resulting in lower noise levels. This is confirmed by the HB simulation performed under design operating conditions and plotted in Figure 17. The numerical results indicate a difference of 7 dB between the inter-stage and the downstream BPF1 noise levels. Consequently, the dominant noise radiation direction is upstream. Compared to the low-tone fan, which primarily emits tonal noise downstream, the low-broadband fan provides an opposing tonal radiation characteristic (see Figures 14 and 17).

Thus, both fan stages are well suited to investigate the impact of the dominant noise radiation direction on noise perception in future psychoacoustic assessments.
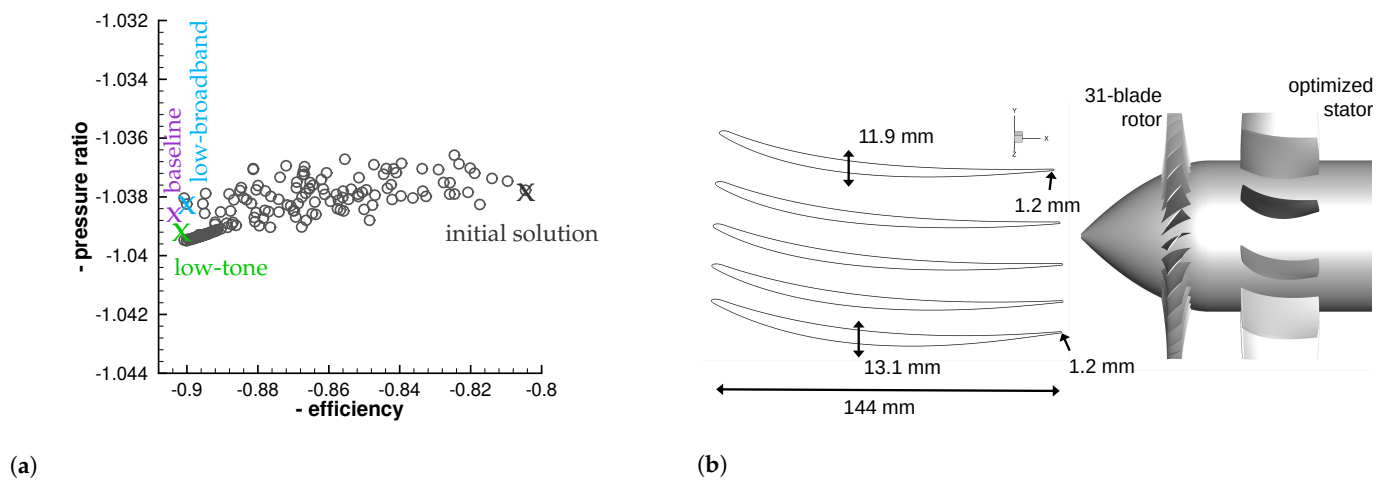

(**a**)   (**b**)

Figure 16. Results of the optimization for the 10-vane stator. (**a**) Generated members. (**b**) Geometry of the 10-vane stator.

Table 5. Difference Δ between stator LE angle and modal propagation angle as well as α_{mn} for the BPF1 and BPF2 modes under design conditions for the low-broadband fan stage.

		Upstream		Downstream	
f [Hz]	**(m,n)**	α_{mn}	Δ **[deg]**	α_{mn}	Δ **[deg]**
2325	(+1, 1)	0.53	86.9	0.53	23.0
2325	(+1, 0)	0.99	49.0	0.53	34.0

In line with our expectations, for the transmission through the rotor blade row, the HB simulation predicts only slight attenuation of the dominantly excited mode $m = +1$ (see gray triangles). This is because the mode $m = +1$ rotates in the rotor rotation direction. As outlined in Section 5.2.2, for the low-tone fan, the mode $m = -1$ is dominantly excited, so opposing transmission behavior is expected. Therefore, both fan stages are well suited to investigate the transmission through the rotor blade row, as $m = -1$ rotates against the rotor rotation direction and $m = +1$ rotates with the rotor rotation.
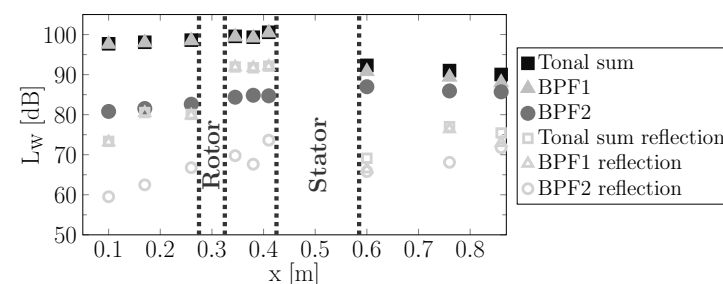
Figure 17. Tonal RSI noise levels under design conditions obtained from an HB simulation and plotted along the axial position for the low-broadband fan stage.

Figure 18 shows the noise directivity of the low-broadband fan at design operating conditions. The radiation characteristic of the tonal RSI noise clearly reflects the impact of the modal propagation angle. Downstream, the tonal noise levels are reduced due to the modal propagation angle, and thus, similar noise levels are observed for the tonal and broadband noise components for radiation angles between 0 deg and 70 deg. Upstream, the tonal noise levels are higher compared to the broadband levels (see radiation angles between 100 deg and 180 deg). Thus, for the low-broadband fan, tonal RSI noise is the

dominant noise source over a wide range of radiation angles. In contrast, for the low-tone fan, it is observed that the broadband component is the dominant source over a wide range of radiation angles. Therefore, due to this opposing noise emission characteristic, both fan stages are well suited to investigate the impact of differences between tonal and broadband noise levels on noise perception.

Figure 18. Noise directivity at design operating conditions for the low-broadband fan stage obtained from RANS-based noise prediction.

As an intermediate summary, the noise emission of the low-broadband fan is characterized by the following features:
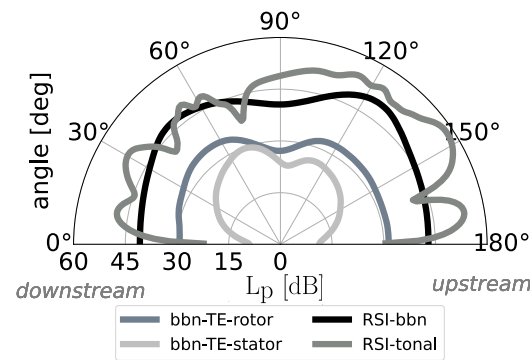
1. The BPF1 tone is cut-on.
2. Downstream, the tonal noise excitation at the first BPF benefits from a modal propagation angle that is relatively parallel to the stator LE angle.
3. The dominant tonal noise radiation direction is upstream.
4. Upstream, the tonal RSI noise is higher than the broadband component, and downstream, similar levels are predicted.

In total, as summarized in Table 6, the baseline, low-tone and low-broadband fan stages are very similar regarding their aerodynamic characteristics. However, as illustrated in Sections 5.1, 5.2.2 and 5.2.3 and as summarized in Table 7, all three fans provide opposing acoustic characteristics. In particular, the fan stages differ with regard to the dominant noise radiation direction and with regard to the ratio between tonal and broadband noise levels.

Table 6. Pressure ratio and efficiency for all three fan stages in design as well as PR_{max} conditions.

OP	Quantity	Baseline	Low-Tone	Low-Broadband
DP	η_{is}	90.4%	90.2%	90.0%
	PR	1.0382	1.0396	1.0382
PR_{max}	η_{is}	90.1%	90.3%	89.0%
	PR	1.0424	1.0430	1.0420

Additionally, compared to the baseline fan, for both new low-count OGV fans, the rotor blade count changes from $B = 18$ to $B = 31$ blades. Thus, as shown in Table 7, the base frequency of the fan tones increases from 1350 Hz to 2325 Hz for the low-broadband fan and to 4650 Hz for the low-tone fan. Despite the same number of rotor blades, the low-tone fan has a higher base frequency than the low-broadband fan, as the first blade passing the frequency tone is inversely cut off. This allows us to investigate the impact of a frequency change on humans' noise perception. Moreover, due to atmospheric absorption, higher frequencies are significantly attenuated during propagation from the noise source to an observer on the ground. This provides an additional advantage for the low-tone fan, as the higher-frequency tonal components are further attenuated while propagating through the atmosphere. All in all, as summarized in Table 7, the fan stages are well suited to assess the acoustic criteria (a)–(c) defined in Section 5.2.

Table 7. Summary of the acoustic characteristics of all three fan stages.

Acoustic Design Criterion	Baseline	Low Broadband	Low Tone
benefit from modal propagation angle	upstream	downstream	upstream
dominant noise radiation direction	downstream	upstream	downstream
ratio between tonal and broadband noise	high	medium	low
base frequency	1350 Hz	2325 Hz	4650 Hz

6. Discussion and Conclusions

Using the CRAFT baseline fan stage, an acoustic effect resulting from the modal propagation angle is experimentally confirmed. This effect has already been investigated analytically as well as numerically, and it is now experimentally verified on the CRAFT baseline fan for a wide range of operating conditions. In good agreement, the experimental data provide validation of the analytical and numerical studies.

The experimental data confirm that the modal propagation angle significantly impacts the excitation of tonal rotor–stator interaction noise at the stator leading edge. In particular, if the propagation direction of the dominantly excited mode is nearly parallel to the stator leading edge angle, an acoustic benefit is achieved. In this case, the acoustic mode is only weakly excited. The experimental data for different operating conditions confirm that the acoustic benefit can be more than 13 dB for individual modes, even in off-design conditions. As a rule of thumb, the expected noise level reduction can be estimated with $20 \log_{10}(\sin(|\Delta|))$, where Δ is the difference between the stator stagger angle and the modal propagation angle. Particularly for low-speed ducted fan stages or ventilators, where only a few azimuthal modes are excited, this effect may efficiently reduce tonal rotor–stator interaction noise. Depending on the design, the effect can be used to reduce the tonal noise component upstream or downstream. Thus, in addition to noise reduction, this also allows us to specifically control the fan's radiation direction, which in turn can be used to improve certification levels and psychoacoustic characteristics, taking into account liners, shielding and flight trajectories.

In a fan pre-design process, acoustic benefits can be achieved with a suitable choice of rotor and stator blade numbers, since the blade numbers define the excited acoustic interaction modes, and with the interaction modes, the propagation angles are defined. In particular, the modes should be excited whose propagation angles are parallel to the stator leading edge angle. Typically, the leading edge angle is known at an early stage in a pre-design process as it directly results from rotational speed and pressure ratio. Therefore, through a smart blade count selection, the excited mode orders can be adjusted in such a way that the resulting modal propagation angle is aligned with the stator stagger angle.

This design-to-noise process is demonstrated at two low-speed fan stages with fewer stator than rotor blades, which are representative of ducted fans in urban air mobility aircraft. The blade numbers are chosen such that for the first fan stage, the dominant modes are excited weakly upstream due to the impact of the modal propagation angle. Thus, the upstream noise levels are reduced. For the second fan stage, the blade numbers are chosen to provide an opposing radiation characteristic. Consequently, the modal propagation angle downstream is nearly parallel to the stator leading edge angle in order to reduce the downstream noise excitation. In total, for both fan stages, the radiated noise levels are approximately 10 dB lower than the baseline fan. The geometry of all rotor and stator blades is obtained from an aerodynamic optimization process.

As these fan stages provide opposing acoustic characteristics, these fans will be used in a future process consisting of measurements at the CRAFT test facility, virtual flyover simulations, auralizations and listing tests in order to evaluate the noise perception.

Abbreviations

The following symbols and abbreviations are used in this manuscript:

Symbols

M_x	axial Mach number	
M_{tip}	tip Mach number	
M_s	swirl Mach number	
m	azimuthal mode order	
n	radial mode order	
h	harmonics of rotor blade number	
k	scattering index	
$\zeta_{mn}^{\pm}$	modal propagation angle	rad
α_{mn}	cut-on factor	
σ_{mn}	derivative of radial eigenfunction	
R	tip radius	m
r	hub radius	m
$A_{mn}^{\pm}$	modal sound pressure amplitude	Pa
$\hat{g}_{mn}^{\omega}$	induct Green's function	
k_x	axial wave number	m^{-1}
k_n	normal wave number	m^{-1}
k_l	chordwise wave number	m^{-1}
x_{LE}	x-coordinate of LE	m
θ_{LE}	circumferential LE coordinate	rad
σ	acoustic source term	
σ_L	acoustic source term lift-noise	
$f_L^{\hat{\omega}}$	chordwise distribution of lift	
l	chordwise position	m
χ_{LE}	leading edge angle	rad
χ_{TE}	trailing edge angle	rad
Δ	difference between χ_{LE} and $\zeta_{mn}^{\pm}$	rad
η_{is}	isentropic efficiency	
$\dot{m}$	mass flow	kg/s
D	rotor radial displacement	m
θ_{out}	stator outflow angle	rad
L_w	sound power level	dB
L_p	sound pressure level	dB

Abbreviations

CRAFT	Co/Counter Rotating Acoustic Fan Test rig
OGV	outer guide vane
LE	leading edge
RSI	rotor–stator interaction
BPF	blade passing frequency
B	number of rotor blades
V	number of stator vanes
OP	operating point
DP	design point
PR$_{max}$	operating point at maximum pressure ratio

$\dot{m}_{max}$	operating point at maximum mass flow
RANS	Reynolds-averaged Navier–Stokes
HB	harmonic balance
PR	pressure ratio
PN	PropNoise
XTPP	extended triple plane pressure
M	measurement
up	upstream
down	downstream
N	rotational speed
bbn	broadband noise
TE	trailing edge

Appendix A

In this section, two additional plots are shown, one illustrating the domain for the numerical simulations (Figure A1) and one depicting an example of the mesh around the rotor and stator blades (Figure A2).
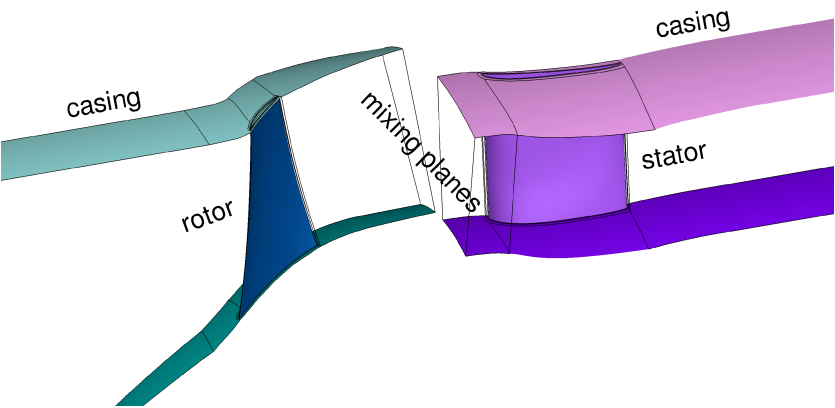
Figure A1. Domain for numerical simulations.
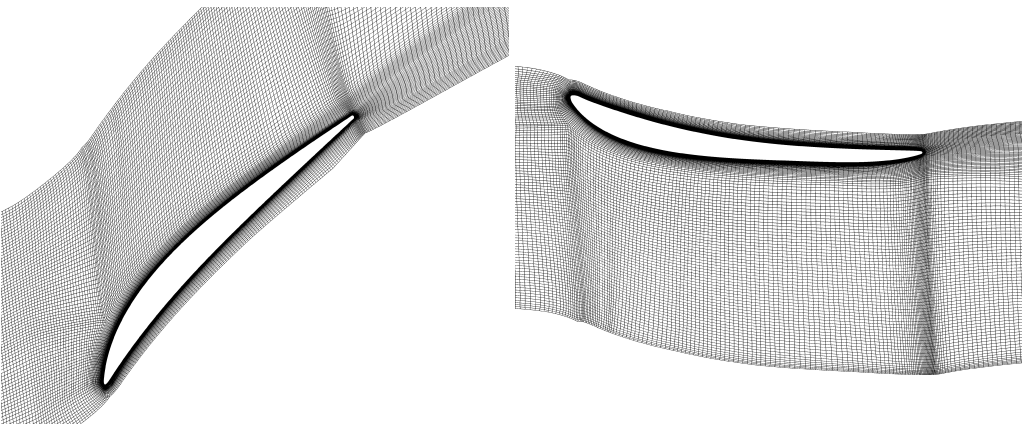
Figure A2. Numerical grid around the rotor (**left**) and stator (**right**).

Appendix B

Table A1 compares the difference Δ between measurements and fully analytical predictions. Since the upstream measurement position is located upstream of the spinner (position 3a in Figure 6), α_{mn} and Δ could not be experimentally determined in the inter-stage area. Therefore, "—" is entered in Table A1 in the corresponding cells.

Table A1. Difference Δ between stator LE angle and modal propagation angle as well as α_{mn} for BPF1 and BPF2 modes obtained from analytical predictions and experiments.

Operating Point	Mode	Method	Upstream		Downstream	
			α_{mn}	Δ [deg]	α_{mn}	Δ [deg]
DP	$(-3,0)$	PN	0.795	13.4	0.795	88.8
		M	—	—	0.760	86.9
	$(-6,0)$	PN	0.805	14.3	0.805	87.7
		M	—	—	0.772	88.1
$\dot{m}_{max}$	$(-3,0)$	PN	0.795	14.4	0.795	89.8
		M	—	—	0.764	88.3
	$(-6,0)$	PN	0.805	15.3	0.805	89.1
		M	—	—	0.776	89.5
PR_{max}	$(-3,0)$	PN	0.796	12.8	0.796	87.8
		M	—	—	0.758	87.8
	$(-6,0)$	PN	0.806	13.6	0.806	86.8
		M	—	—	0.770	89.0

References

1. Rizzi, S.A.; Huff, D.L.; Boyd, D.D.; Bent, P.; Henderson, B.S.; Pascioni, K.A.; Sargent, D.C.; Josephson, D.L.; Marsan, M.; He, H.; et al. *Urban Air Mobility Noise: Current Practice, Gaps, and Recommendations*; NASA/TP-2020-5007433; NASA: Langley Research Center: Hampton, VA, USA, 2020.
2. Jaron, R. Aeroakustische Auslegung von Triebwerksfans mittels multidisziplinärer Optimierungen. Ph.D. Dissertation, German Aerospace Center, Institute of Propulsion Technology, Berlin, Germany, 2018. [CrossRef]
3. Töpken, S.; Verhey, J.L.; Weber, R. Perceptual space, pleasantness and periodicity of multi-tone sounds. *J. Acoust. Soc. Am.* **2015**, *138*, 288–298. [CrossRef] [PubMed]
4. More, S.; Davies, P. Human responses to the tonalness of aircraft noise. *Noise Control Eng. J.* **2010**, *58*, 420–440. [CrossRef]
5. Duncan, P.; Dawson, B. Reduction of interaction tones from axial flow fans by suitable design of rotor configuration. *J. Sound Vib.* **1974**, *33*, 143–154. [CrossRef]
6. Schade, S.; Jaron, R.; Moreau, A.; Guérin, S. Mechanisms to reduce the blade passing frequency tone for subsonic low-count OGV fans. *Aerosp. Sci. Technol.* **2022**, *125*, 107083. [CrossRef]
7. Schade, S.; Klähn, L.; Jaron, R. Analytische, numerische und experimentelle Untersuchung des tonalen Rotor–Stator Interaktionsschalls in einer langsam drehenden, ummantelten Fanstufe. In *DAGA 2023—49. Jahrestagung für Akustik*; Conference Proceedings; DAGA: Hamburg, Germany, 2023; pp. 526–529.
8. Hanson, D. Acoustic reflection and transmission of rotors and stators including mode and frequency scattering. In Proceedings of the 3rd AIAA/CEAS Aeroacoustics Conference, Atlanta, GA, USA, 12–14 May 1997. [CrossRef]
9. Behn, M.; Tapken, U.; Puttkammer, P.; Hagmeijer, R.; Thouault, N. Comparative study of different analytical approaches for modelling the transmission of sound waves through turbomachinery stators. In Proceedings of the 22nd AIAA/CEAS Aeroacoustics Conference, Lyon, France, 30 May–1 June 2016. [CrossRef]
10. Tapken, U.; Caldas, L.; Meyer, R.; Behn, M.; Klähn, L.; Jaron, R.; Rudolphi, A. Fan test rig for detailed investigation of noise generation mechanisms due to inflow disturbances. In Proceedings of the AIAA Aviation 2021 Forum, Virtual Event, 2–6 August 2021. [CrossRef]
11. Tyler, J.M.; Sofrin, T.G. *Axial Flow Compressor Noise Studies*; SAE Technical Papers; SAE International: Warrendale, PA, USA, 1962. [CrossRef]
12. Rice, E.; Heidmann, M.; Sofrin, T. Modal propagation angles in a cylindrical duct with flow and their relation to sound radiation. In Proceedings of the 17th Aerospace Sciences Meeting, New Orleans, LA, USA, 15–17 January 1979. [CrossRef]
13. Moreau, A. A Unified Analytical Approach for the Acoustic Conceptual Design of Fans for Modern Aero-Engines. Ph.D. Dissertation, German Aerospace Center, Institute of Propulsion Technology, Berlin, Germany, 2017. [CrossRef]
14. Rienstra, S.; Tester, B. An Analytic Green's Function for a Lined Circular Duct Containing Uniform Mean Flow. In Proceedings of the 11th AIAA/CEAS Aeroacoustics Conference, Monterey, CA, USA, 23–25 May 2005. [CrossRef]
15. Mosch, B.J. Erweiterung der Steuerung eines Fan-Prüfstands um die Regelung aerodynamischer Betriebsgrößen zur Realisierung dynamischer Fuhrungsgrößenverläufe. Master's Thesis, Technische Universität Berlin, Berlin, Germany, 2023.
16. Nürnberger, D.; Eulitz, F.; Schmitt, S.; Zachcial, A. Recent Progress in the Numerical Simulation of Unsteady Viscous Multistage Turbomachinery Flow. In Proceedings of the ISOABE 2001–1081. Bangalore, India, September 2001.
17. Yang, H.; Nürnberger, D.; Kersken, H.P. Towards Excellence in Turbomachinery Computational Fluid Dynamics: A Hybrid Structured-Unstructured Reynolds-Averaged Navier-Stokes Solver. *J. Turbomach.* **2006**, *128*, 390–402. [CrossRef]
18. Weber, A. *G3DHexa-3D Structured Grids for Multistage/Multipassage Turbomachines and Linear Cascades*; DLR Internal Report DLR-IB-325-03-14; Version 2.0; German Aerospace Center (DLR): Cologne, Germany, 2014.

19. Frey, C.; Ashcroft, G.; Kersken, H.; Voigt, C. A harmonic balance technique for multistage turbomachinery applications. In Proceedings of the ASME Turbo Expo 2014: Turbine Technical Conference and Exposition, Düsseldorf, Germany, 16–20 June 2014. [CrossRef]

20. Hall, K.C.; Ekici, K.; Thomas, J.P.; Dowell, E.H. Harmonic balance methods applied to computational fluid dynamics problems. *Int. J. Comput. Fluid Dyn.* **2013**, *27*, 52–67. [CrossRef]

21. Wang, D.; Huang, X. A complete rotor–stator coupling method for frequency domain analysis of turbomachinery unsteady flow. *Aerosp. Sci. Technol.* **2017**, *70*, 367–377. [CrossRef]

22. Ovenden, N.C.; Rienstra, S.W. Mode-matching strategies in slowly varying engine ducts. *AIAA J.* **2016**, *42*, 1832–1840. [CrossRef]

23. Wohlbrandt, A.; Weckmüller, C.; Guérin, S. A robust extension to the triple plane pressure mode matching method by filtering convective perturbations. *Int. J. Aeroacoustics* **2016**, *15*, 41–58. [CrossRef]

24. Guérin, S. Improvement of the triple-plane pressure mode matching technique and application to harmonic balance simulations. In Proceedings of the 16th International Symposium on Unsteady Aerodynamics Aeroacoustics and Aeroelasticity of Turbomachines ISUAAAT16, Toledo, Spain, 19–23 September 2022.

25. Behn, M.; Pardowitz, B.; Tapken, U. Separation of tonal and broadband noise components by cyclostationary analysis of the modal sound field in a low-speed fan test rig. In Proceedings of the International Conference of Fan Noise, Aerodynamics, Applications and Systems, Darmstadt, Germany, 18–20 April 2018.

26. Morfey, C. Sound transmission and generation in ducts with flow. *J. Sound Vib.* **1971**, *14*, 37–55. [CrossRef]

27. Voß, C.; Aulich, M.; Kaplan, B.; Nicke, E. Automated Multiobjective Optimisation in Axial Compressor Blade Design. Volume 6: Turbomachinery, Parts A and B. In Proceedings of the ASME Turbo Expo 2006: Power for Land, Sea, and Air, Barcelona, Spain, 8–11 May 2006; pp. 1289–1297. [CrossRef]

28. Voß, C.; Aulich, M.; Raitor, T. Metamodel Assisted Aeromechanical Optimization of a Transonic Centrifugal Compressor. In Proceedings of the 15th International Symposium on Transport Phenomena and Dynamics of Rotating Machinery, Honolulu, HI, USA, 24–28 February 2014.

29. Aulich, M.; Voß, C.; Raitor, T. Optimization Strategies demonstrated on a Transonic Centrifugal Compressor. In Proceedings of the 15th International Symposium on Transport Phenomena and Dynamics of Rotating Machinery, Honolulu, HI, USA, 24–28 February 2014.

30. Schmitz, A. Entwicklung eines objektorientierten und parallelisierten Gradient Enhanced Kriging Ersatzmodells. Ph.D. Dissertation, Fernuniversität Hagen, Hagen, Germany, 2013.

31. Dhondt, G. *The Finite Element Method for Three-Dimensional Thermomechanical Applications*; John Wiley & Sons, Ltd.: Hoboken, NJ, USA, 2004. [CrossRef]

32. Frey, C.; Ashcroft, G.; Müller, M.; Wellner, J. Analysis of Turbomachinery Averaging Techniques. Volume 10C: Turbomachinery—Design Methods and CFD Modeling for Turbomachinery; Ducts, Noise, and Component Interactions. In Proceedings of the ASME Turbo Expo 2022: Turbomachinery Technical Conference and Exposition, Rotterdam, The Netherlands, 13–17 June 2022. [CrossRef]

33. Klähn, L.; Caldas, L.; Meyer, R.; Moreau, A.; Tapken, U. Experimental Investigation of Inflow-Distortion-Induced Tonal Noise in a Sub-Sonic Fan Test Rig. In Proceedings of the 29th International Congress on Sound and Vibration, Prague, Czech Republic, 9–13 July 2023.

34. Philpot, M.G. The role of rotor blade blockage in the propagation of fan noise interaction tones. In Proceedings of the AIAA 2nd Aeroacoustics Conference, Hampton, VA, USA, 24–26 March 1975. [CrossRef]

2.3 Publication III

This article is licensed under a Creative Commons license, CC-BY 4.0,
https://creativecommons.org/licenses/by/4.0/.

Psychoacoustic evaluation of different fan designs for an urban air mobility vehicle with distributed propulsion system[a]

Stephen Schade,[1,b] Roberto Merino-Martinez,[2] Antoine Moreau,[1] Susanne Bartels,[3] and Robert Jaron[1]

[1]German Aerospace Center, Institute of Propulsion Technology, 10625 Berlin, Germany

[2]Delft University of Technology, Faculty of Aerospace Engineering, 2629 HS Delft, the Netherlands

[3]German Aerospace Center, Institute of Aerospace Medicine, Linder Höhe, 51147 Köln, Germany

ABSTRACT:

Distributed propulsion systems are developed to power a new generation of aircraft. However, it is not known yet which noise emissions these propulsion systems produce, which psychoacoustic characteristics such systems exhibit, and how the generated noise is perceived. This paper investigates how fans with fewer stator than rotor blades affect the noise perception of a distributed propulsion system intended for an urban air mobility vehicle, which is equipped with 26 low-speed ducted fans. Three fan designs with different tonal to broadband noise ratio and opposite dominant noise radiation directions are examined. An analytical process is applied to determine the noise emission, propagate the sound through the atmosphere, auralize the flyover signals, and calculate psychoacoustic metrics. A validation and comparison with A320 turbofan engines at takeoff is provided. The results indicate that the distributed propulsion system generates noise signatures with complex directional characteristics and high sharpness. By applying tonal noise reduction mechanisms at source, a significant effective perceived noise level reduction is achieved for the considered fan stages with fewer stator than rotor blades. In addition, tonality, loudness and roughness are reduced well above one noticeable difference compared to a baseline fan and similar or even lower values are achieved than with turbofans. © 2025 Author(s). All article content, except where otherwise noted, is licensed under a Creative Commons Attribution (CC BY) license (https://creativecommons.org/licenses/by/4.0/).

https://doi.org/10.1121/10.0036228

(Received 1 November 2024; revised 26 February 2025; accepted 6 March 2025; published online 26 March 2025)

[Editor: Matthew Boucher]   Pages: 2150–2167

I. INTRODUCTION

Distributed propulsion systems represent an advancement in the design of future aircraft, offering new degrees of freedom compared to conventional concepts, for instance, regarding the number and arrangement of the engines on the airplane. These degrees of freedom cause new acoustic and psychoacoustic characteristics that may affect the noise perception. Therefore, there is a demand to investigate the noise emissions generated by distributed propulsion systems along with their psychoacoustic characteristics.

Typically, the acoustic design of fans is based on the assessment of individual sound pressure levels of a single engine. Moreover, the propulsors are commonly optimized considering the sound power levels at the source location (Giacche *et al.*, 2013; Jaron, 2018). This approach is consistent with the noise certification process as for the certification of new aircraft, a single value, the effective perceived noise level (EPNL) (measured in EPNdB), is evaluated. The EPNL is measured at takeoff, approach and flyover and designs with lower cumulative EPNL compared to a

reference value are targeted (EASA, 2023; ICAO, 2017). The evaluation of one cumulative EPNL primarily considers that newly certified aircraft are quieter than the specified reference level, however, the design with the lowest EPNL value may not necessarily be the one with the least annoying aural perception (Merino-Martinez *et al.*, 2024c; Rizzi, 2016; Torija and Clark, 2021). Consequently, newer aircraft may not sound more pleasant, even if they have a lower EPNL than conventional aircraft. Therefore, there is a need to assess the noise perception at an early stage within the design phase of new aircraft. For this purpose, it is necessary to develop fast and flexible models that can be incorporated into the acoustic preliminary design phase.

Human sound perception has been shown to not only depend on purely physical quantities (e.g., sound pressure or sound power level) but to a significant extent also on psychoacoustic characteristics, e.g., sharpness, spectral content and tonality for both conventional turbofan aircraft (Soeta and Kagawa, 2020; Torija *et al.*, 2019) and multicopter drone platforms (Gwak *et al.*, 2020; Merino-Martinez *et al.*, 2024c; Torija and Clark, 2021).

However, due to the specific characteristics of distributed fan concepts compared to conventional turbofan and multicopter drone concepts, the current knowledge about the

---

relation between noise perception and physical as well as psychoacoustic parameters is not easily transferable to distributed fans. In general, there is little knowledge yet on how psychoacoustic parameters of modern urban air mobility (UAM) vehicles influence human perception. Boucher *et al*. (2024a) focused on rotorcraft-based UAM designs and found associations between psychoacoustics and perception partly contradicting prior assumptions (e.g., higher sharpness contributed to a more positive perception). To the best of the authors' knowledge, associations among physical characteristics, psychoacoustics, and perception of UAM vehicles with distributed ducted fans have not been reported yet.

The assessment of noise perception becomes particularly relevant for distributed propulsion systems with a large number of propulsors, as acoustic interaction, modulation, and interference effects influence the noise footprint (Bernardini *et al*., 2020; Guérin and Tormen, 2023; Monteiro *et al*., 2024; Pascioni and Rizzi, 2018; Schade *et al*., 2024b). Sound perception is therefore a key factor for public acceptance of new aircraft concepts with distributed propulsion, which, for instance, are developed for UAM (Rizzi *et al*., 2020). This is confirmed in a telephone survey which addressed the acceptance of airtaxis in Germany, where it was found that noise concerns negatively correlate with acceptance (Eißfeldt and Stolz, 2024).

For these reasons, acoustic effects need to be assessed in order to ensure that new propulsion systems are not only quieter than previous concepts but also sound more pleasant. In addition, there is a need to not only investigate individual noise levels of individual engines but also to consider the propulsion system as a whole, for example, as a combination of distributed fans in order to examine the noise signature and psychoacoustic characteristics of the entire propulsion system.

This paper examines the impact of fan design on the noise perception of a distributed propulsion system for an UAM aircraft. For this purpose, an analytical auralization [the acoustical counterpart of visualization (Vorländer, 2008)] framework, developed in house at the Department of Engine Acoustics, is first extended for distributed propulsion systems and then applied to the vectored thrust system of the UAM vehicle. As part of this tool chain, the fan noise emission is determined using Reynolds-averaged Navier Stokes– (RANS-) informed analytical noise prediction. Afterwards, virtual flyover simulations are performed to propagate the sound to specified microphone positions on the ground. The flyovers are then auralized using binaural noise syntheses. As a final step, based on the time signals, acoustic as well as psychoacoustic metrics are evaluated. Before applying this tool chain to the distributed propulsion system, the calculation of the noise immission and the psychoacoustic metrics is validated with measurement data from an A320 takeoff recorded near Schiphol Amsterdam Airport. Recently, this process has already been used to study the impact of speed fluctuations on the psychoacoustic characteristics of a distributed propulsion system (Schade *et al*., 2024b).

The considered UAM concept airplane is equipped with 26 ducted, low-speed fan stages, where three fan designs are examined: (1) A conventional fan (treated as baseline) with more stator vanes than rotor blades, (2) a low-broadband noise fan (henceforth denoted as *low-broadband*) with fewer stator vanes than rotor blades, and (3) a low-tonal noise fan (henceforth denoted as *low-tone*) also with fewer stator vanes than rotor blades. The fan designs are similar with regard to aerodynamic characteristics, for example, efficiency, pressure ratio, and thrust (Schade *et al*., 2024a). However, the fans provide different characteristics with regard to acoustics, for example, the dominant noise radiation direction and the tonal-to-broadband noise ratio. Due to these characteristics, the fan designs are particularly suitable for investigating acoustic and psychoacoustic effects and evaluating the impact on noise perception.

The manuscript is structured as follows: Section II A describes the design of the UAM concept vehicle. Section II B illustrates the different fan designs, as well as the integration of these fans on the vehicle. The auralization framework is described in Sec. II C. The limitations are outlined in Sec. III. The results are evaluated in Sec. IV, where Sec. IV A shows the validation with the A320 turbofan and Sec. IV B provides the transfer to distributed propulsion. The conclusions are summarized in Sec. V and an outlook is provided in Sec. VI.

II. MATERIAL AND METHODS

A. UAM concept vehicle

An UAM vehicle with distributed and tiltable ducted fans is conceptually designed to enable aeroacoustic studies. The design and sizing of the vehicle architecture are performed using an in-house simulation framework for vehicle and fleet assessments. This framework is first introduced by Shiva Prakasha *et al*. (2022) and is extended by Ratei *et al*. (2023) to derive optimal vehicle designs for different architectures and use cases. The basic tool for the conceptual design and sizing of such UAM vehicles with vertical takeoff and landing (VTOL) capabilities is documented by Ratei (2022).

The top level aircraft requirements, which serve as an input for the design of the tilt-duct vehicle, are derived based on existing aircraft demonstrators and prototypes within the UAM market. In order to estimate the
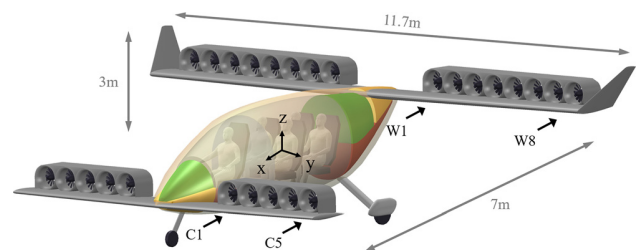

FIG. 1. Tilt-duct vehicle from project VIRLWINT for further high-fidelity disciplinary analysis and acoustic assessment.

J. Acoust. Soc. Am. **157** (3), March 2025

Schade *et al*. 2151

TABLE I. Coordinates of the engine center position relative to the center of gravity of the UAM vehicle. Since the vehicle is symmetrical to the $y = 0\,\mathrm{m}$ plane, only half of the engine positions are listed. C: canard wing; W: main wing.

Engine	x [m]	y [m]	z [m]
C1	2.65	1.2	−0.3
C2	2.65	1.67	−0.3
C3	2.65	2.14	−0.3
C4	2.65	2.61	−0.3
C5	2.65	3.08	−0.3
W1	−3.105	1.2	1.165
W2	−3.105	1.67	1.165
W3	−3.105	2.14	1.165
W4	−3.105	2.61	1.165
W5	−3.105	3.08	1.165
W6	−3.105	3.55	1.165
W7	−3.105	4.02	1.165
W8	−3.105	4.49	1.165

technology readiness level in the vehicle design process, an hypothetical entry into service in the timeframe $2030 - 2035$ is assumed. The vehicle has VTOL capabilities and can carry a payload of up to $450\,\mathrm{kg}$ (four passengers and one pilot on board) over a range of $100\,\mathrm{km}$ at a cruise speed of $200\,\mathrm{km/h}$ while opposed to a headwind of $20\,\mathrm{km/h}$. Additionally, a 20-min loitering reserve is included in the sizing process.

Figure 1 shows the final battery-electric tilt-duct vehicle design including its dimensions and a labeling of the individual fan stages, which are distributed over the canard and the main wings. The corresponding engine center positions are listed in Table I. Based on the thrust provided by the fan stages, their number is determined to ensure that the propulsion system can lift and accelerate the maximum takeoff weight of $2900\,\mathrm{kg}$ vertically during takeoff. As a result, the propulsion system consists of 26 low-speed fan stages, where 10 fans are installed on the canard wing and 16 on the main wing. Each fan has a diameter of $0.45\,\mathrm{m}$.

The design process of the considered tilt-duct vehicle is outlined in more detail by Schade *et al.* (2025).

B. Distributed propulsion system

1. Low-speed ducted fan designs

For the distributed propulsion system of the tilt-duct vehicle, three different rotor-stator fan stages are designed and manufactured. All three fan designs are developed for experimental testing in the CRAFT (Co-/Contra Rotating Acoustic Fan Test) facility (Caldas *et al.*, 2022; Tapken *et al.*, 2021) from DLR. In the CRAFT facility, ducted fan stages with representative conditions (e.g., rotor tip Mach number and fan pressure ratio) for UAM engines can be investigated.

The first fan stage is the baseline fan, which has 18 rotor blades and 21 stator vanes [see Fig. 2(a)]. The blade count pairing of the baseline fan is designed such that the acoustic modes at the first blade passing frequency (BPF) are cut-on. In addition to the baseline fan, two low-count OGV (outer guide vane) fans are designed and manufactured (Schade *et al.*, 2024a). Contrary to conventional fan designs, low-count OGV fans have fewer stator vanes than rotor blades. Schade *et al.* (2024a) outlined the multidisciplinary optimization process to design both low-count OGV fan stages and illustrated that all three fans provide similar aerodynamic but considerably different acoustic characteristics. Thus, these fans are well-suited for acoustic and psychoacoustic comparisons. The first low-count OGV fan stage is equipped with 31 rotor blades and 10 stator vanes [see Fig. 2(b)]. This design is denoted as *low-broadband fan* hereafter. The second low-count OGV fan stage has 31 rotor blades and 21 stator vanes [see Fig. 2(c)]. This fan design is named *low-tone fan* subsequently.

2. Conceptual nozzle design

To theoretically integrate the CRAFT fans on the tilt-duct vehicle and operate them over a wide operating range, a variable nozzle geometry is required. As the tilt-duct vehicle is expected to perform the takeoff and ascending flight phase vertically, the thrust requirements and aerodynamic operating conditions of the fan stage strongly depart from each other at takeoff and during cruise. As a result, a variable-geometry system is necessary to cope with such a
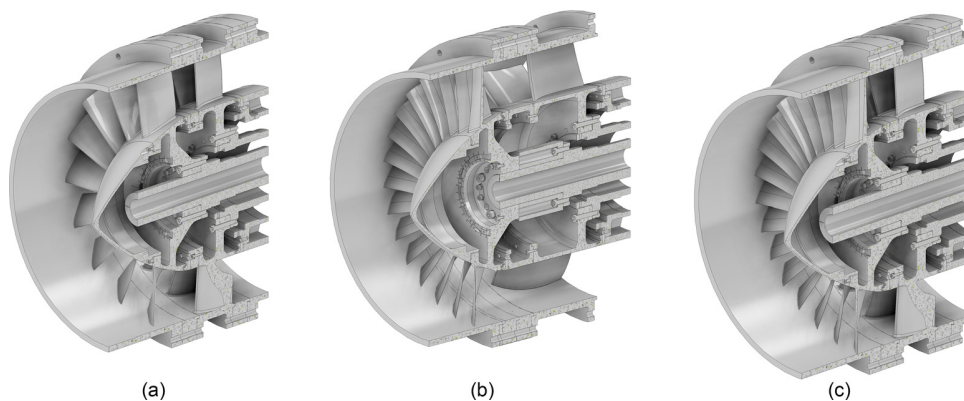

(a)   (b)   (c)

FIG. 2. Geometry of CRAFT baseline (a), low-broadband (b), and low-tone (c) fan stages.

65

TABLE II. Operating conditions and performance of the CRAFT stages when mounted on the tilt-duct vehicle.

	n [rpm]	n_{rel} [%]	$\dot{m}$ [kg/s]	i_{rotor} [deg]	$M_{ax,in}$ [—]	$M_{rel,tip}$ [—]	PR [—]	η_{ise} [%]	SM [—]	altitude [m]	thrust [kN]
Cruise	3375	100	5.25	2	0.11	0.26	1.021	90.0	0.24	1520	2.1
Design	4500	133	6.98	2	0.14	0.31	1.038	90.5	0.24	—	—
Take-off fixed nozzle	8540	253	10.7	6.6	0.22	0.64	1.177	88.0	0.11	1520	30
Take-off VAN +30 %	7995	237	12.3	2	0.25	0.61	1.133	91.5	0.24	1520	30

wide operating range. A variable-area nozzle (VAN) is implemented at the conceptual design level according to the procedure described by Moreau *et al.* (2023b) and the results of the operating point calculations are shown in Table II, where n and n_{rel} define the rotational speed, $\dot{m}$ is the mass flow rate, $M_{ax,in}$ is the inflow Mach number, $M_{rel,tip}$ is the rotor tip Mach number, and PR is the pressure ratio.

The predictions are performed considering the baseline fan stage only. However, the aerodynamics vary slightly between the baseline fan and the two low-count OGV designs, although the differences are small, as examined by Schade *et al.* (2024a), which is sufficiently accurate.

For the fan rotor blades to operate at an acceptable level of flow incidence angle (i_{rotor}, see Table II), the exhaust nozzle must be substantially opened during takeoff. The optimal opening ratio of 30% increased nozzle area was found according to the procedure by Moreau *et al.* (2023b), which provides the best fan isentropic efficiency (η_{ise}, see Table II) and a sufficient stability margin (SM) (see Table II) for the fan stage to operate safely away from its aerodynamic stall line. As shown in the aerodynamic performance map of the stage in Fig. 3, operating takeoff with an opened nozzle shifts the point onto the line of fan peak efficiency.

It should be noted at this point that the large excursion in mass flow and axial Mach number by a factor 2 or more from takeoff to cruise conditions (see Table II), requires a very careful design of the fan intake geometry in order to avoid flow separation at the intake lip, spillage drag, and additional inflow distortion noise. The design of the intake is not, however, considered within the scope of the present preliminary study.
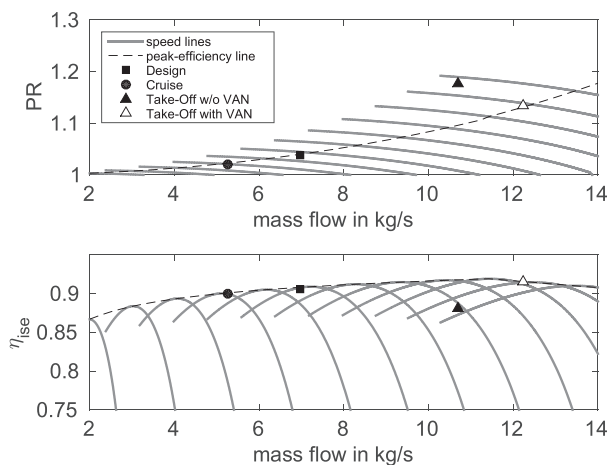
FIG. 3. Fan performance map of the CRAFT stages and position of the relevant operating points. Top: fan pressure ratio (PR), bottom: fan isentropic efficiency (η_{ise}).

C. Auralization framework

The auralization process consists of four steps which are visualized in Fig. 4. First, as described in Sec. II C 1, the noise emission is predicted using the tool PropNoise (Propulsion Noise) (Moreau, 2017). Second, the noise immission is determined using virtual, acoustic flyover simulations performed with the tool VIOLIN (Virtual acoustic flyover simulation) (Dang, 2022). This is outlined in Sec. II C 2. Third, as summarized in Sec. II C 3, a binaural noise synthesis is applied to transfer the acoustic results into stereo audio files using the tool CORAL (Aircraft engine noise auralization) (Moreau *et al.*, 2023a). Finally, a sound quality assessment, as described in Sec. II C 4, is applied which is conducted with the open-source toolbox SQAT (Greco *et al.*, 2024).

1. RANS-informed analytical noise prediction

For the present study, all acoustic sources are predicted using PropNoise (Moreau, 2017). PropNoise can either be applied as a stand-alone program or coupled with an external flow solver. The latter is used for the present study. For this purpose, PropNoise is coupled with the in-house flow solver TRACE (Yang *et al.*, 2006) in order to provide RANS-informed analytical noise predictions (Jaron, 2018). 3D steady-state RANS simulations are performed for each fan design (baseline, low-broadband and low-tone as visualized in Fig. 2) and both operating points (Cruise and Design from Table II). TRACE solves the compressible Navier-Stokes equations on a structured numerical grid using a multi-block approach. Regarding the numerical setup, an isolated fan with uniform inflow conditions is considered and the flow domain is a single rotor–stator passage with periodic boundary conditions. The Menter SST k-ω
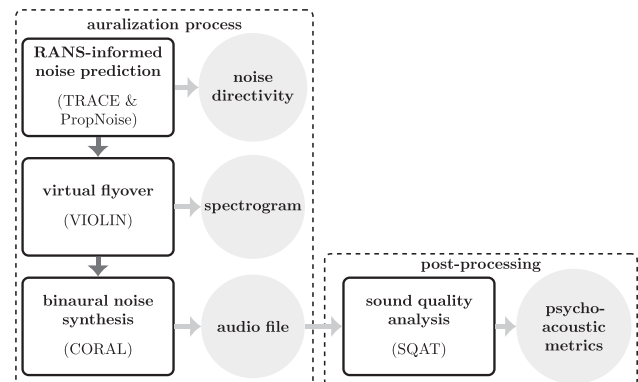
FIG. 4. Auralization process and post-processing.

J. Acoust. Soc. Am. **157** (3), March 2025

Schade *et al.*   2153

66

turbulence model is applied since earlier studies showed that this model provides the best results with regard to the aerodynamic flow solution and analytical noise prediction than other turbulence models (Jaron, 2018). Regarding the numerical grid, an O-C-H topology is used around the blade/vane, where the first cell is placed in the laminar sublayer. Further details regarding the numerical setup and gird as well as the aerodynamic flow solutions for the three fan designs can be obtained from Schade *et al.* (2024a).

The aerodynamic flow variables required to reconstruct the aerodynamic excitation that leads to noise generation are exported from the RANS simulations as radial distributions. These radial distributions are extracted along streamlines and are used as an input for PropNoise to determine the noise source generation and propagation analytically. PropNoise provides a frequency-formulation of all fan noise sources, whereby in this study only rotor–stator interaction noise is considered. The extracted radial distributions of aerodynamic flow variables provide the input for a radial strip approach to calculate the acoustic source terms. Based on the in-duct Green's function $\hat{g}_{mn}^{\omega}$, the modal sound pressure amplitude is determined from a radial integration of the acoustic source terms. For tonal noise, the complex modal sound pressure amplitudes are determined from

$$p_{mn}^{\pm} = i \cdot V \int_{r}^{R} \hat{g}_{mn}^{\omega} \, e^{-ik_x x_{LE} - im\theta_{LE}} \cdot \sigma_L \cdot dr_s \qquad (1)$$

and for broadband noise, the deterministic quantity to consider is the expectation value of the squared modal sound pressure magnitude, which is obtained from

$$\langle |p_{mn}^{\pm}|^2 \rangle = V \int_{r}^{R} |\hat{g}_{mn}^{\omega}| \cdot \langle |\sigma_L|^2 \rangle \cdot l \cdot dr_s, \qquad (2)$$

where $+$ is the downstream and $-$ the upstream direction, V is the number of stator vanes, r is the hub and R the tip radius, k_x denotes the axial wave number, x_{LE} and θ_{LE} specify the leading edge position, σ_L denotes the source term for the lift-generated component, and l is the turbulence correlation length in radial direction (Moreau, 2017). Subsequently, the sound is propagated upstream and downstream through the duct segments of the fan stage and radiated from the entry and exit planes. The noise radiation results are then saved as directivity patterns on a hemisphere with a defined radius. A detailed description of the acoustic models used in PropNoise can be obtained from Moreau (2017) and the coupling between PropNoise and an external flow solver is described by Jaron (2018). Jaron (2018) also validated the RANS-informed noise prediction method for several fan stages using experimental and numerical results.

2. Virtual acoustic flyover simulation

The modal directivity patterns obtained from PropNoise serve as an input for the in-house tool VIOLIN. Using VIOLIN a virtual flyover simulation is performed and the
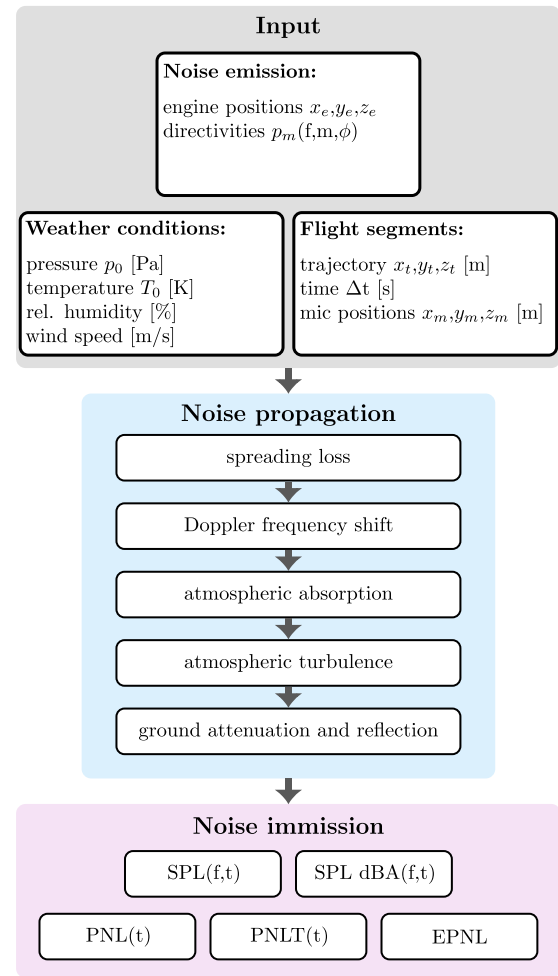
FIG. 5. Process chain for the virtual acoustic flyover simulation with VIOLIN.

noise is propagated through the atmosphere to one or several observer positions on the ground.

VIOLIN provides a frequency-domain formulation to determine the noise immission and accounts for the Doppler frequency shift, the atmospheric absorption (ISO 9613-1, 1993), the impact of atmospheric turbulence on amplitude as well as phase relations (Prescher *et al.*, 2024; Rietdijk *et al.*, 2017) and the attenuation as well as reflection of the sound waves on the ground (Arbeitsgruppe Novellierung der AzB, 2007; Hornikx, 2016). Figure 5 schematically illustrates this analytical process and Moreau *et al.* (2023a) provide an overview of the auralization process.

In order to account for distributed propulsion systems, VIOLIN is extended to consider multiple, distributed engines at arbitrary positions. The engine positions are defined relative to the center position of the airplane using *xyz*-coordinates specified in the airplane reference frame (see Table I).

An individual PropNoise calculation is assigned to each engine in each sub-segment of the flyover. Thus, individual RANS-informed analytical noise predictions (see Sec.

67
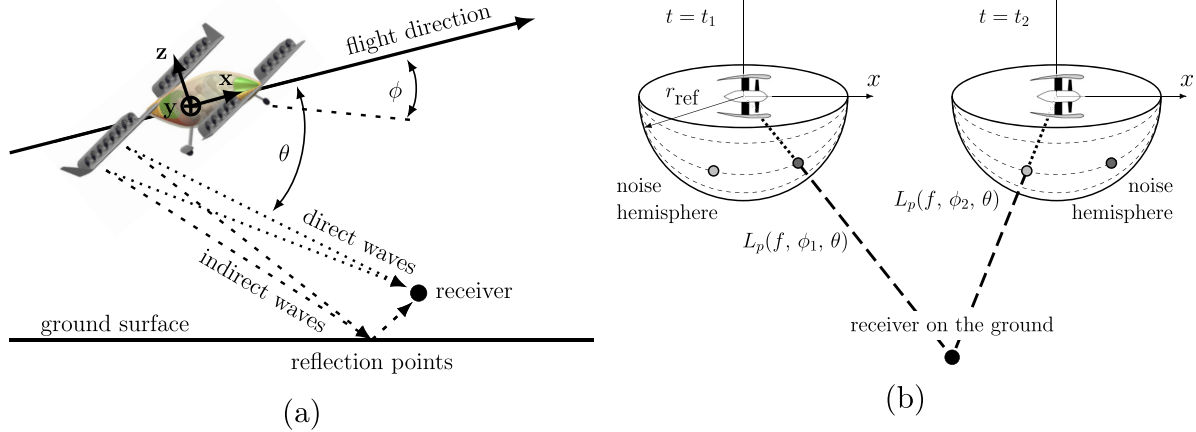
FIG. 6. Polar and lateral angles as a function of flyover time.

II C 1) are performed in advance for each engine. The present study uses steady engine operating conditions. This means that the operation point of each engine does not change during flyover. Consequently, 26 PropNoise calculations are performed (one for each engine) and assigned to the distributed propulsion system. For tonal noise sources, complex pressure amplitudes are assigned [see Eq. (1)] and for broadband sources, absolute squared amplitudes are considered [see Eq. (2)], whereby these are imported as narrow-band power spectral densities with logarithmic frequency distribution. As an initial step, the broadband values are converted to complex pressure amplitudes using $p_{mn}^{\pm} = \sqrt{\langle |p_{mn}^{\pm}|^2 \rangle} \cdot e^{-i \cdot 0}$. This is done only for broadband sources, as for tonal sources, complex pressure amplitudes are directly obtained from PropNoise.

PropNoise determines the noise directivities radiated to a hemisphere of specified radius r_{ref} in the far field for each noise source. To provide the pressure amplitudes at arbitrary receiver distances and positions, a distance correction is implemented in VIOLIN (denoted as spreading loss in Fig. 5). Thereby it is assumed that the tonal/broadband amplitudes are inversely proportional to the propagation distance. Afterwards, the polar and lateral emission angles (ϕ and θ) are calculated for each engine at each time step [see Fig. 6(a)]. Using an interpolation method the respective tonal/broadband amplitudes are extracted from the noise hemispheres based on the calculated emission angles at each time step [see Fig. 6(b)]. With the extracted amplitudes the direct and indirect sound waves are propagated through the atmosphere to the receiver position on the ground considering the mentioned noise propagation effects (see blue box in Fig. 5). For the superposition of the direct and indirect sound waves, a phase relation is included for both tonal and broadband sources. Depending on the travel distance difference Δr between the direct and indirect sound waves, the complex amplitudes of the indirect waves are obtained from $p_{\text{indirect}} = p_{mn}^{\pm} e^{-i2\pi[f_{\text{Doppler}}/c]\Delta r}$, where f_{Doppler} are the Doppler-shifted frequencies and c is the speed of sound. At the

reflection point, the assumption is made that the ground is an acoustically hard surface. In addition to interferences resulting from the travel distance difference, no further interferences are calculated for broadband sources, as this source is assumed to be uncorrelated.

For tonal noise sources, the noise propagation may be strongly affected by interferences. Tonal sources are assumed fully correlated in VIOLIN and their linear superposition is carried out according to the method by Guérin and Tormen (2023). Thus, the complex tonal noise directivity $D_m(f, r_{\text{ref}}, \phi)$ obtained from PropNoise is modified as follows:

$$p_m(f, \phi, \theta) = D_m(f, r_{\text{ref}}, \phi)\, e^{im\theta}, \tag{3}$$

where θ is the lateral emission angle, r_{ref} is the specified reference radius for noise radiation in PropNoise, and m is the vector containing the azimuthal modes according to the Tyler and Sofrin relation (Tyler and Sofrin, 1962). With $m = hB - kV$ and $hB = f/n$, Eq. (3) can be reformulated as

$$p_m(f, \phi, \theta) = D_m(f, r_{\text{ref}}, \phi)\, e^{i(m-f/n)(\theta-\Delta\theta_{\text{stat}})}\; e^{i((f/n)(\theta-\Delta\theta_{\text{rot}}))}, \tag{4}$$

where f is the blade passing frequency vector and n is the rotational speed. This formulation is implemented in VIOLIN as it allows considering the following effects: First, the rotation direction of individual propulsors can be changed by inverting the sign of the azimuthal mode vector m. Thus, counter-rotating configurations can also be considered. Second, the term $(\theta - \Delta\theta_{\text{stat}})$ and the term $(\theta - \Delta\theta_{\text{rot}})$ can be used to modify, respectively, the clocking position of the stator and rotor compared to the reference position from PropNoise. Thereby $\Delta\theta_{\text{stat}}$ describes the angle difference for the stator and $\Delta\theta_{\text{rot}}$ the angle difference for the rotor. For the present study, $\Delta\theta_{\text{rot}}$ is randomized once between the 26 fan stages, and one identical random distribution is applied to all flyover cases. Regarding the stator clocking positions, $\Delta\theta_{\text{stat}} = 0$ is applied to all fan stages. This is reasonable, as the position of the stator vanes can be controlled by design,

J. Acoust. Soc. Am. **157** (3), March 2025
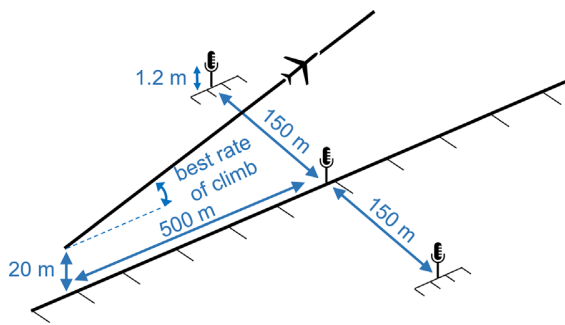
Schade *et al.* 2155

68

FIG. 7. Take-off reference procedure according to EASA specifications for VTOL aircraft (EASA, 2023).

unlike those of the rotor blades that may vary from flight to flight. The trajectory segment for the virtual flyover simulation is selected according to the EASA specifications for VTOL aircraft powered by tilting rotors (EASA, 2023). The takeoff reference procedure, as visualized in Fig. 7, is selected to compare the three fan designs. The flight Mach number is $M_{\text{take-off}} = 0.18$ and the rate of climb is $\alpha_{\text{climb}} = 6°$. Moreover, the flyover is performed for a simulation time of $t = 21$ s and the time discretization is $\Delta t = 0.015$ s. In accordance with the EASA specifications (EASA, 2023), the atmospheric pressure is $101, 325$ Pa, the ambient air temperature is $25 °C$ and the relative humidity is 70%.

Design conditions are assigned to each engine as listed in Table II. According to the findings from Schade et al. (2024b), a fixed random distribution of rotational speed deviations within the range $±1$ % is applied to the distributed engines. Therefore, prior to calculating the noise emission with PropNoise, a speed variation within the range of $±1$ % relative to the nominal speed is randomly determined for each engine. These speed variations are interpreted as a constant deviation from the nominal rotational speed. Thus, one PropNoise calculation is performed for each engine using the determined rotational speed. Afterwards, for the flyover simulation, each PropNoise calculation is assigned to the corresponding engine. Thereby it is assumed that the speed deviations are static and thus do not change during flyover. Since these deviations are very small, tonal noise is still assumed to be correlated. The impact of different sets of speed deviations, which are applied to the 26 ducted fans, on the noise immission results and the sound quality analysis is assessed in Schade et al. (2024b).

As an output from VIOLIN, for tonal noise sources, the spectrograms are provided as complex pressure amplitudes, whereas for broadband noise sources the output spectrograms do not include phase information.

3. Binaural noise synthesis

The spectrograms obtained from VIOLIN are the input for the in-house auralization tool CORAL (Moreau et al., 2023a). Using CORAL, a binaural noise synthesis is applied to transform the spectrograms into time signals for the right and left ear. Since tonal noise sources are assumed as correlated whereas broadband sources are considered

uncorrelated, CORAL processed these noise sources separately. Tonal sources are synthesized using an additive process and broadband sources using a subtractive process involving the filtering of a white noise signal, as described by Moreau et al. (2023a). Head related impulse responses (HRIRs) are used to transfer the monaural time series into stereo signals. The HRIRs represent transfer functions that contain all binaural and spectral characteristics resulting from the interaction of a head with an incoming sound wave. As the primary goal in CORAL is to achieve plausible and realistic binaural auralizations and not to reproduce the exact response of a specific head, no individual HRIRs are measured or simulated, but artificial head HRIRs are used. For this, a far-field data set, measured by Bernschütz (2013), is considered. Based on the relative position between the UAM vehicle and the observer, the two matching HRIRs of the left and right ear are selected from the data set. As a result, a binaural audio signal is generated that represents the sound of a UAM vehicle moving in space. The audio file is stored in Waveform Audio file format (.wav file).

4. Sound quality analysis

Sound quality metrics (SQMs) describe the subjective perception of sound by human hearing, unlike the L_p metric, which quantifies the purely physical magnitude of sound based on pressure fluctuations. Previous studies (Merino-Martinez et al., 2021; Merino-Martinez et al., 2022) showed that these metrics better capture the auditory behavior of the human ear compared to conventional sound metrics typically employed in noise evaluations. The five most commonly used SQMs (Greco et al., 2023b; Merino-Martinez et al., 2024a) are as follows.

- Loudness (N): Subjective perception of sound magnitude corresponding to the overall sound intensity (ISO 532–1, 2017).
- Tonality (K): Measurement of the perceived strength of unmasked tonal energy within a complex sound (Aures, 1985).
- Sharpness (S): Representation of the high-frequency sound content. In general, frequencies higher than 3 kHz are perceived as sharper (von Bismark, 1974).
- Roughness (R): Hearing sensation caused by sounds with modulation frequencies between 15 and 300 Hz (Daniel and Webber, 1997).
- Fluctuation strength (FS): Assessment of slow fluctuations in loudness with modulation frequencies up to 20 Hz, with maximum sensitivity for modulation frequencies around 4 Hz (Osses Vecchi et al., 2017).

These five SQMs were calculated for each audio recording and their 5% percentile values were considered (hence the "5" subindex henceforth), representing the value of each SQM exceeded 5% of the total recording time. These 5% percentile values were then combined into global psychoacoustic annoyance (PA) metric following the model outlined by Di et al. (2016). All SQMs, the PA metric, and

conventional sound metrics (e.g., equivalent A-weighted sound pressure level $L_{p,A,eq}$ and EPNL) were calculated using the open-source MATLAB toolbox SQAT (Sound Quality Analysis Toolbox) v1.1 (Greco *et al.*, 2024). The GitHub repository of the toolbox can be found in Greco *et al.* (2023a).

III. LIMITATIONS

- Analytically determined noise directivities are used as an input for the flyover simulation. In order to improve the results, measured directivities should also be considered as an input in future studies.
- Installation effects such as boundary layer ingestion or noise shielding are neglected although, according to the vehicle design, the fan stages are located on the wings.
- As take-off trajectories are used, it is assumed that the engines are the dominant noise sources. To determine the noise emission of the ducted fans of the UAM vehicle, broadband and tonal rotor–stator interaction noise as well as trailing edge noise are considered. Airframe, background, and other engine noise sources are neglected.
- Since only one sub-segment of the take-off flight phase is simulated, steady engine operating conditions are applied, although the vehicle is accelerating during take-off.
- Vehicle and wing angle of attack changes are not accounted for.
- Liners are not included.
- With regard to the three examined fan designs, only the noise emission levels of the baseline design are validated with measurement data yet (Schade *et al.*, 2024a). The validations of the noise levels of the low-broadband noise and low-tonal noise designs are not included in this study as the respective measurement campaign is not accomplished yet.
- The psychoacoustic annoyance model by Di *et al.* (2016) applied here is already an improved model of the original model developed by Fastl and Zwicker (2007) based on synthetic sounds but also data from listening tests with technical sounds, e.g., car noise, air conditioner or factory noise. However, it remains open to what extent this model is also valid for new sounds from UAM vehicles. For a more accurate evaluation on the perceptual differences between the three fan designs, psychoacoustic listening experiments are recommended.

IV. RESULTS AND DISCUSSION

A. Validation of the auralization framework

In order to provide a qualitative and quantitative validation of the analytical auralization framework (see Fig. 4), a virtual flyover of two turbofan engines is compared with an experimental acoustic measurement of an Airbus A320 take-off recorded near Schiphol Amsterdam Airport, in the Netherlands. The aircraft was equipped with two IAE V2527-A5 turbofan engines.
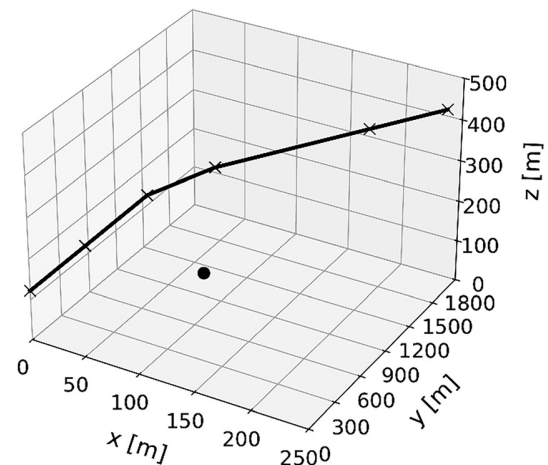
FIG. 8. Flight trajectory and microphone position (denoted as a black dot) for the Airbus A320 takeoff.

For the validation of the auralization framework, the following additional assumptions and limitations apply.

- The noise immission and the sound quality metrics are compared between analytical prediction and measurement for a single A320 take-off at a single microphone. Thereby it is neglected that differences can also occur with regard to the noise levels at source. These data are not part of the flyover measurement so that a comparison was not possible.
- Regarding the operating conditions, a retrofit is performed based on the experimental measurement data for an equivalent Airbus A320-like engine with similar design parameters. Thereby, the rotational speed is reconstructed from the number of blades and the frequency of the BPF in the measurement. Mass flow, blade angle, and nozzle area are selected so that the aerodynamic operating point of the engine is plausible (e.g., small incidence on fan blades).
- The following noise sources are considered: fan buzz-saw noise, jet noise and fan broadband noise. Fan tonal noise is neglected due to two main reasons: Firstly, the BPF tone is cut-off due to the larger amount of stator vanes than rotor blades. Secondly, for the measurement case, the second harmonic of the BPF is efficiently attenuated by a liner since it is not visible in the spectrogram [see Fig. 9(a)]. However, the BPF2 would be cut-on in the simulation and dominantly contribute to the noise radiation as it was out of scope for this work to include a realistic liner geometry. Consequently, to ensure comparability between measurement and prediction, the fan tones were neglected altogether.
- For the atmospheric conditions, an ambient air temperature of $290\,\mathrm{K}$, a pressure of $102\,710\,\mathrm{Pa}$, a relative humidity of 45% and a wind speed of $u_x = u_y - 1.2\,\mathrm{m/s}$ are applied. These data are in accordance with the respective measurement day.

The microphone employed is a PUI Audio POM-2735P-R analog condenser microphone with a sensitivity of $-35 \pm 2\,\mathrm{dB}$ (ref. $1\,\mathrm{V/Pa}$) and a frequency range of $20\,\mathrm{Hz}$ to

J. Acoust. Soc. Am. **157** (3), March 2025

Schade *et al.*   2157

70

FIG. 9. Comparison between the measured (a) and simulated (b) spectrograms of the Airbus A320 takeoff. Color scheme specifically developed for the visualization of noise emission and immission according to Weninger (2015).

25 kHz. The sampling frequency employed is 50 kHz. The microphone was positioned at a small lateral offset to the flight pat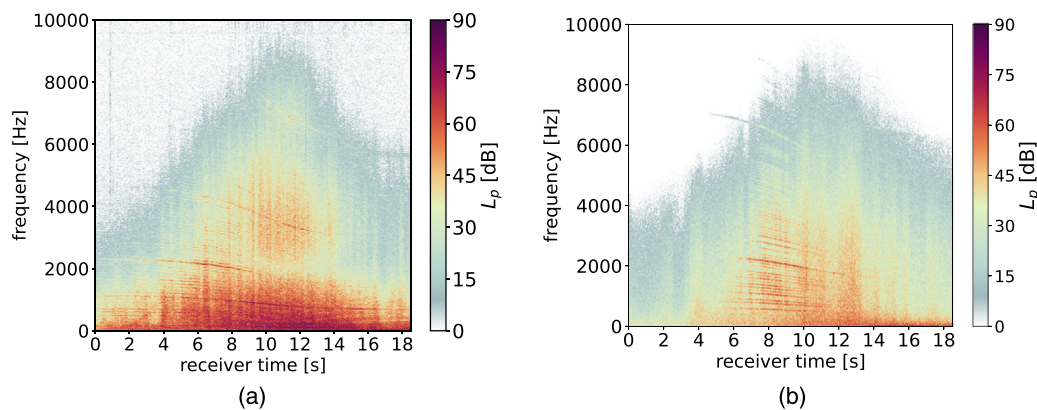h. To mitigate ground reflections, the microphone is placed directly on the ground and placed over a 15-mm layer of acoustic-absorbing foam. Figure 8 depicts the Airbus A320 takeoff flight path estimated from the Automatic Dependent Surveillance-Broadcast (ADS-B) data collected from OpenSky's database (OpenSky, 2025). At the moment of the closest distance to the microphone (equivalent to overhead), the aircraft's altitude was 121.92 m. More information about the experimental setup can be found in Merino-Martinez et al. (2024b).

Figure 9 presents the comparison between the measured and simulated spectrograms of the Airbus A320 takeoff. Overall, a good qualitative agreement is achieved and the overall shape of the spectrogram is reproduced from the virtual flyover simulation. The characteristic shape is mainly affected by atmospheric absorption and atmospheric turbulence, which are both well-predicted compared to the measurement case. The impact of atmospheric attenuation is evident in the lower noise levels at high frequencies and the impact of atmospheric turbulence is visible as vertical interference stripes.

The different noise sources can be identified in specific sections of the spectrogram. Buzz-saw noise is visible between 5 and 10 s and is observed as a low-frequency tone and several of its harmonics. To predict buzz-saw noise a random variation of fan rotor stagger angles within the range $\pm 0.3°$ is applied. Compared to the measurement data, the frequencies of the buzz-saw tones agree well, however, the noise levels are slightly overestimated. This is reflected in higher sound pressure amplitudes [see Fig. 10(a) at $7\,\mathrm{s} < t < 10\,\mathrm{s}$] and higher $L_p(t)$ as well as PNL(t) values [see Fig. 10(b) at $7\,\mathrm{s} < t < 10\,\mathrm{s}$].

For both measurement and prediction, jet noise is particularly visible in the spectrograms within the low-frequency range after the microphone is passed. Whereas in the measured spectrogram jet noise is the dominant source within the time range between 10 and 12 s, in the predicted spectrogram jet noise occurs over a larger time interval (see 10–18 s). This is again reflected in the time signals, where for the measurement case the highest amplitudes occur at 12 s, and for the prediction almost equal amplitudes are observed between 10 and 18 s [see Figs. 10(a) and 10(b)]. Regarding low-frequency noise, it should be noted that the measured data has background noise (typically dominant at very low frequencies) that is not included in the simulated case.

Figure 11 shows the comparison between measurement and prediction for the SQMs calculated using SQAT (see Sec. II C 4). The "just noticeable differences" (JND) are plotted as an error bar from the measurement case. The
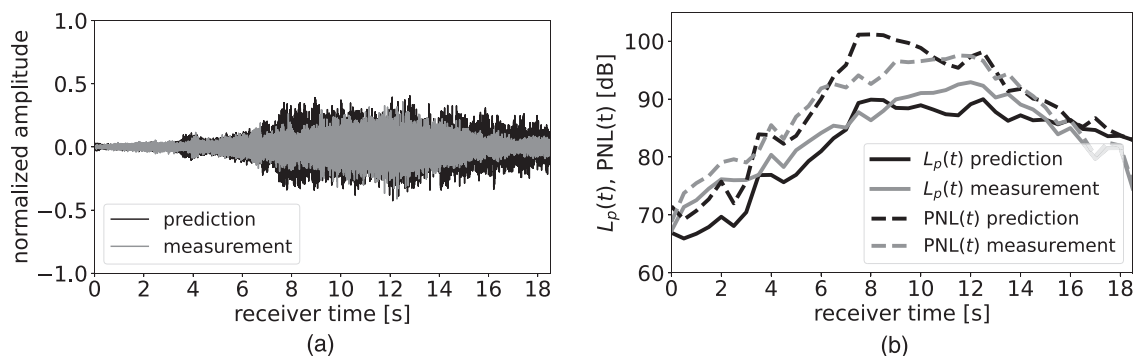

FIG. 10. Comparison between the measured and simulated time signals (a) and the sound pressure levels as well as perceived noise levels (b) of the Airbus A320 takeoff.

2158   J. Acoust. Soc. Am. **157** (3), March 2025
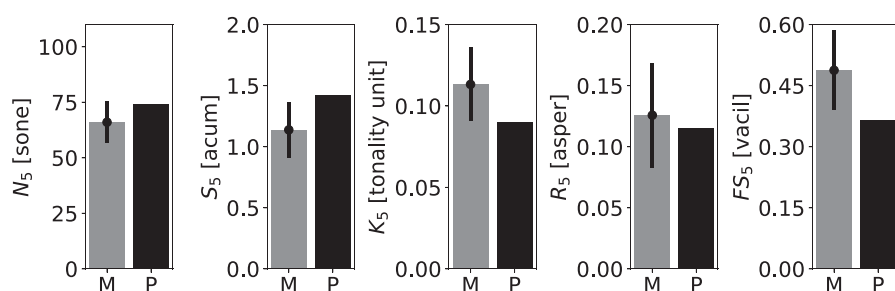
Schade *et al.*

FIG. 11. Comparison of the SQMs between measurement and prediction of the Airbus A320 takeoff. M: measurement; P: prediction. For the measurement case, the error bars refer to the just noticeable differences (JND), where each error bar is plotted as $\pm$ JND.

underlying hypothesis for the JNDs is that sounds differing by more than one JND are detected as different, so that ΔJND values can be obtained for each SQM as suggested by Osses *et al.* (2023). Considering that background noise and airframe noise are not included in the prediction, differences are within an acceptable range. The largest differences occur for the tonality metric. This was expected as fan tonal noise was neglected for the simulation, as aforementioned. However, this assumption is only valid for the BPF tone and its second harmonic since in the measured spectrogram the fourth harmonic of the fan BPF is visible at $t = 12$ s and $f = 7000$ Hz, while this fan tone was excluded from the simulation. In addition, for the measurement, the buzz-saw tones occur over a longer time interval compared to the prediction. Consequently, for these two reasons, the measured spectrogram consists of a slightly higher tonal energy than the prediction, and, hence, the higher tonality value is obtained. The binaural audio file of the synthesized flyover is available in Mm. 1.

Mm. 1. Binaural audio file of the synthesized flyover of the turbofan engines at takeoff. File of type "wav."

B. Distributed propulsion system with ducted fans

1. Noise emission

The noise emission describes the noise that occurs at the noise source. In this section, noise emissions of the individual fans are examined first and, subsequently, the distributed propulsion system consisting of 26 ducted fans is analyzed. Figure 12 depicts the tonal and broadband frequency spectra of the three considered fan stages at design operating conditions. The broadband spectra are presented as one-third-octave bands.

Regarding the baseline fan, the frequency spectrum is dominated by the first BPF tone occurring at 1350 Hz and its second (2700 Hz) and third (4050 Hz) harmonics. All three fan tones provide significantly higher sound power levels than the broadband levels, therefore, the overall noise emission is dominated by tonal noise for this fan. For the low-broadband fan, the first BPF tone is raised to 2325 Hz since the number of rotor blades is increased from 18 to 31. The first BPF tone is still dominant although its sound power level is reduced by 11 dB compared to the first BPF of the baseline fan. In addition, the broadband noise levels are evenly reduced across the entire frequency range compared

to baseline and low-tone fans. The reduced broadband levels result from the lower number of stator vanes which is decreased from 21 to 10. The reason is that the broadband noise source is directly proportional to the number of stator vanes (Moreau, 2017; Nallasamy *et al.*, 2002). As a rule of thumb, the overall broadband noise levels decrease by approximately 3 dB if the number of stator vanes is halved (Jaron, 2018), which is valid for this fan design in good approximation.

For the low-tone fan, the first BPF tone is (inverse) cut-off (Schade *et al.*, 2024a; Schade *et al.*, 2022). The second BPF tone at 4650 Hz has similar noise levels compared to the broadband levels, and the third BPF tone is masked by broadband noise. As a result, for this fan, the overall noise emission is dominated by broadband noise, whereas for the baseline and the low-broadband fan the overall noise emission is dominated by tonal noise.

Figures 13 and 14 show the broadband and tonal noise directivities for the distributed propulsion system of the tilt-duct vehicle. The 26 fan stages are operated at design conditions. The noise levels are shown on a hemisphere with a radius of 100 m. The axial angle ϕ and the lateral angle θ are discretized using 180 points in each direction and $\phi = 180°$ indicates the upstream direction and $\phi = 0°$ is the downstream direction. It should be noted that the pictogram of the vehicle is enlarged for a better illustration.

The broadband noise source is modeled as constant in the lateral direction. Therefore, the broadband noise directivities are plotted in xz-plane and a stripe-shaped pattern is obtained (see Fig. 13). In addition, the overall shape of the broadband directivity is independent of the fan design. The directivity is characterized by two noise radiation maxima:
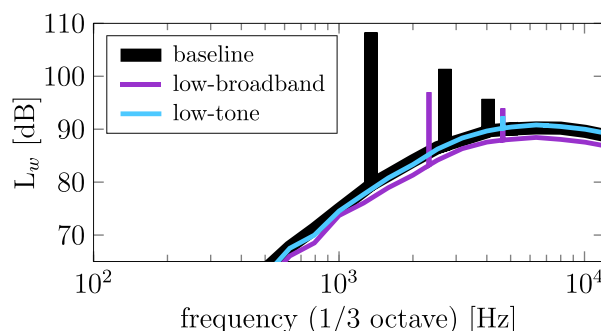

FIG. 12. Sound power spectra of the three considered fan stages at design conditions, $\theta = 90°$ and a reference distance of 100 m.

J. Acoust. Soc. Am. **157** (3), March 2025

72

Schade *et al.*   2159

FIG. 13. Broadband noise directivities in the xz-plane at design conditions for the distributed propulsion system equipped with the baseline fan (a), low-broadband fan (b), and low-tone fan (c). Color scheme according to Weninger (2015).

A global maximum upstream at $\phi = 135°$ and an additional maximum downstream at $\phi = 45°$. The position of these maxima agree well with the expected result from the analytical modeling (Heidmann, 1975). For the low-broadband fan, the noise levels are evenly reduced over all radiation angles compared to the baseline and low-tone fan stages.

The tonal noise directivities are plotted in xy-plane and a strong dependence on the axial as well as the lateral angle is obtained (see Fig. 14). Overall, for tonal noise, directivities with complex interference patterns are obtained. The directivities are mainly characterized by "granulated" structures. In order to understand the formation of these structures, in a preliminary study, not shown here, the influence of the number of fan stages on the directivity was investigated. It was observed that the tonal noise directivity becomes more complex as the number of fans increases and that the granulated pattern is strongly impacted by the amount of fan stages. By increasing the number of fan

stages continuously from 2 to 26 it was observed that the tonal radiation pattern gradually "converges" to a complex interference pattern. Once a certain number of fan stages is reached (in our case more than 16), the interference pattern only slightly changed if additional fan stages are added to the distributed propulsion system. Thus, the system starts to behave like one distributed noise source rather than several individual and independent point sources. As a reference, for an individual baseline, low-broadband and low-tone fan, the tonal and broadband noise directivities can be obtained from Schade et al. (2025). Two additional effects also impact the interference pattern: First, due to the three-dimensional distribution of the fan stages, the Doppler shifted frequencies slightly deviate from each other leading to additional interference and modulation effects. Second, in order to provide a realistic, non-perfect tolerance between the operating conditions of the fan stages, one identical random distribution of speed deviations within the range of
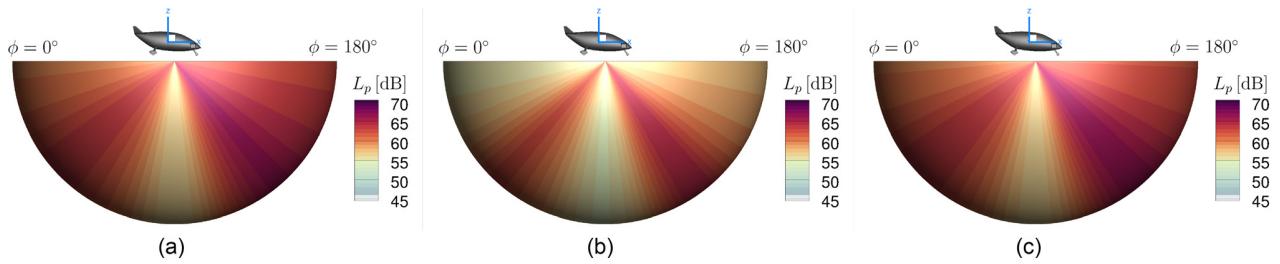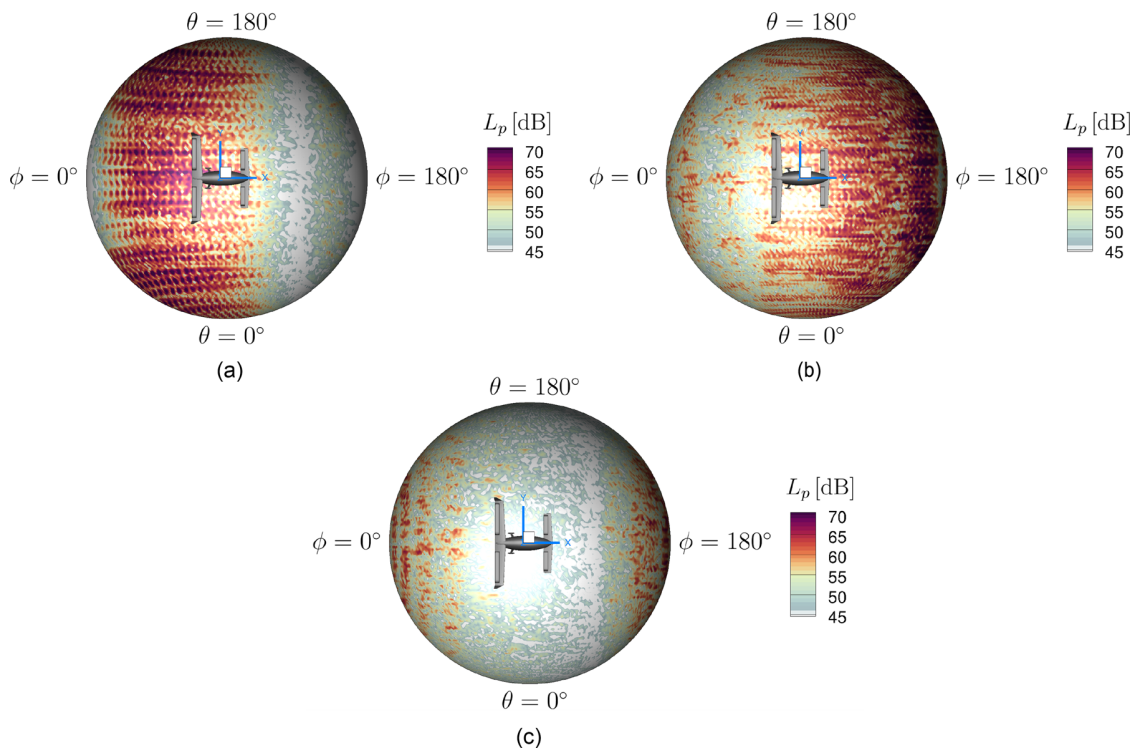

FIG. 14. Tonal noise directivities (sum over all frequencies) in the xy-plane at design conditions for the distributed propulsion system equipped with the baseline fan (a), low-broadband fan (b), and low-tone fan (c). Color scheme according to Weninger (2015).

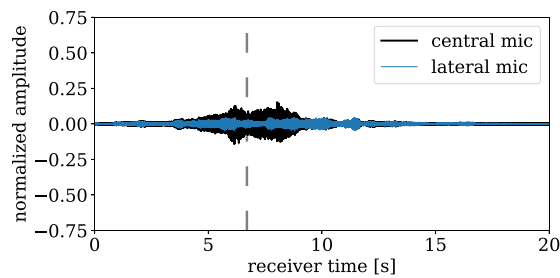2160   J. Acoust. Soc. Am. 157 (3), March 2025   Schade et al.

73

FIG. 15. Broadband time signal for the distributed propulsion system equipped with the baseline fan at the takeoff. The dashed vertical line denotes the time overhead. A value of 1.0 is equivalent to 94 dB.

± 1 % is applied. The choice of the interval is based on the findings from Schade *et al.* (2024b).

If the distributed propulsion system is equipped with the baseline fan, the dominant tonal noise radiation direction is downstream and the peak radiation angle is $\phi = 50°$. By contrast, if the low-broadband fan is used, the dominant tonal noise radiation direction changes to upstream with two peak radiation angles at $\phi = 135°$ and $\phi = 165°$. If the low-tone fan is used, the tonal noise radiation of the distributed propulsion system is significantly reduced over a wide range of radiation angles. However, tonal noise is still radiated upstream and downstream with peak radiation angles at $\phi = 30°$ and $\phi = 170°$. The dominant noise radiation angles of the distributed propulsion system correspond well with the peak radiation angles of the individual fan stages, which are analyzed by Schade *et al.* (2025).

Overall, irrespective of the fan design, the tonal noise directivities of the distributed propulsion systems show a stronger dependence on the axial than the lateral direction. For instance, when using the baseline fan, a lateral stripe

with almost constant tonal noise levels becomes visible at $\phi = 130°$, and tonal noise increases abruptly for axial angles $\phi < 100°$ independently of the lateral angle [see Fig. 14(a)]. This can be explained as only a few azimuthal modes are cut-on for tonal noise which are radiated into the far field.

As an intermediate conclusion, the noise emissions of the distributed propulsion systems are characterized by different tonal to broadband noise ratios and opposite dominant tonal noise radiation directions depending on the choice of the fan design. Thus, a strong dependence of the noise directivities on the axial and lateral emission angles is observed which is additionally intensified by complex acoustic interference patterns.

2. Noise immission

This section describes the noise exposure of the distributed propulsion systems at different microphone positions after propagating from the noise sources through the atmosphere (=noise immission) starting with the examination of broadband and tonal times signals. Spectral patterns are reported via spectrograms in a second step.

Figure 15 shows the broadband time signals at the central and lateral microphones for the distributed propulsion system equipped with the baseline fan. As the characteristic shapes of the broadband time signals of the three propulsion systems are very similar, they are exemplary shown for the baseline design. The only difference between the fan designs is a uniform reduction in sound pressure amplitudes for the low-broadband fan as already visualized in Fig. 13.

Overall, the broadband noise directivity is reflected in the time signal as again two maxima are observed, one before the microphone is passed at $t = 6$ s and one after the microphone is passed at $t = 8$ s. These maxima

(a)

(b)

(c)
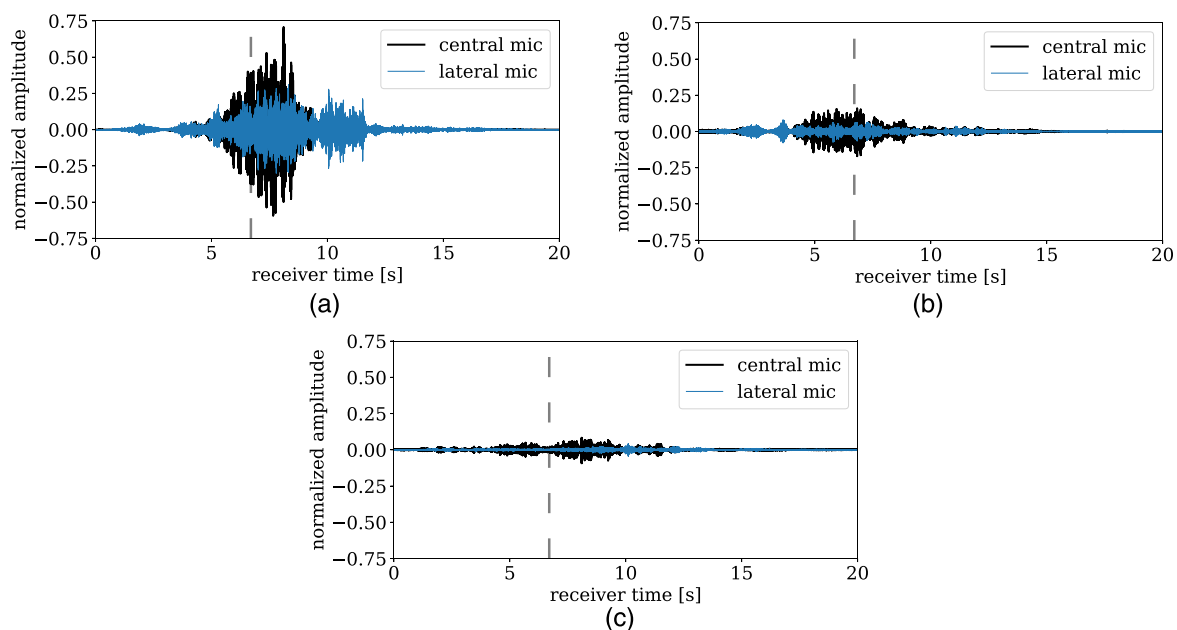
FIG. 16. Tonal time signal for the distributed propulsion system equipped with the baseline fan (a), low-broadband fan (b), and low-tone fan (c) at the takeoff. The dashed vertical line denotes the time overhead. A value of 1.0 is equivalent to 94 dB.

J. Acoust. Soc. Am. **157** (3), March 2025

Schade *et al.*   2161

74
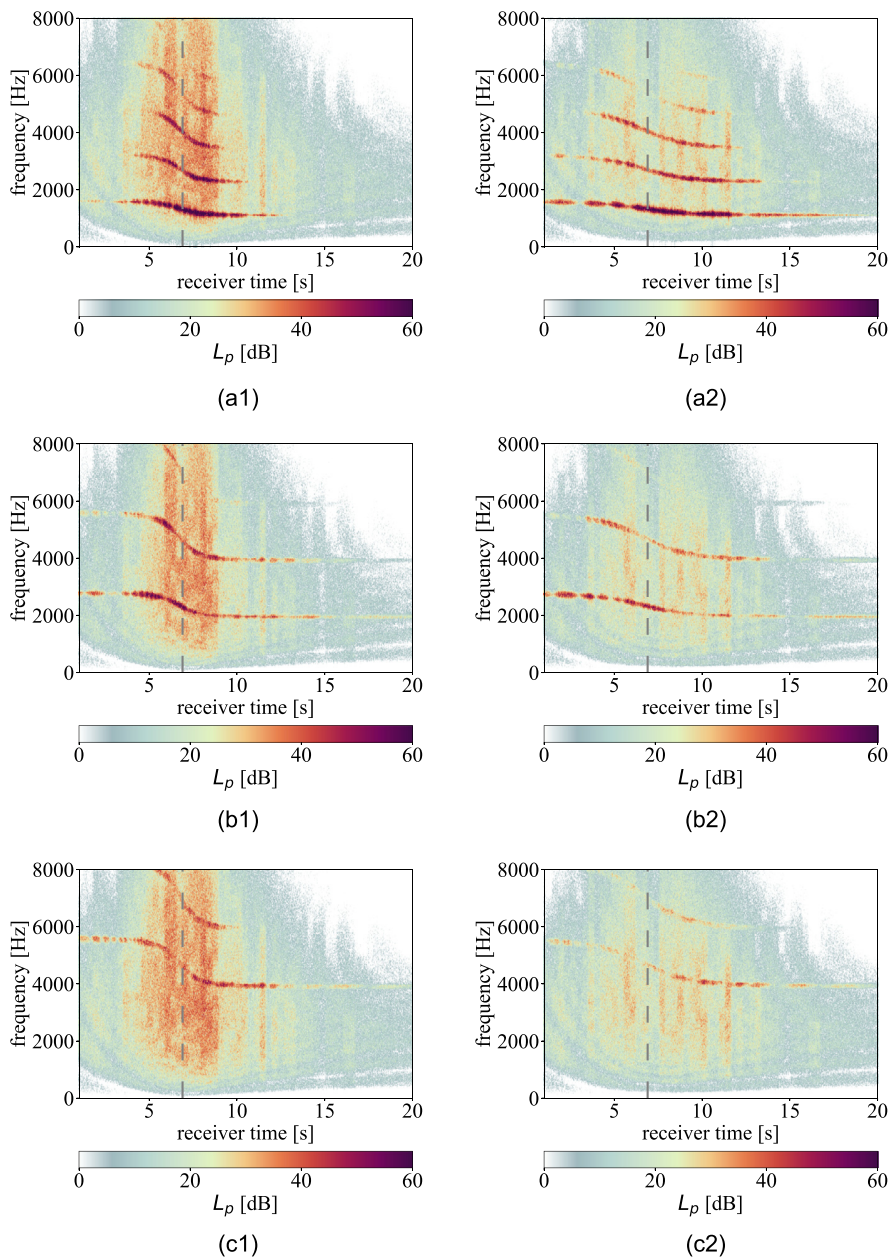
FIG. 17. (Color online) Spectrograms at the central (1) and lateral (2) microphones for the distributed propulsion system equipped with the baseline fan (a), low-broadband fan (b), and low-tone fan (c) at the takeoff. Color scheme according to Weninger (2015).

correspond to the radiation angles $\phi = 135°$ and $\phi = 45°$ [see Fig. 13(a)]. The broadband noise reaches a minimum at $t = 6.5\,s$ which is the time when the microphone is reached indicated by the dashed line. This is equivalent with $\phi = 90°$ in Fig. 13(a).

The tonal time signals for the three propulsion systems are plotted at the central and lateral microphone in Fig. 16, where the dashed line indicates the time when the microphone is reached. Again, the tonal noise directivities are reflected in the time signals. If the distributed propulsion system is equipped with the baseline fan, the highest tonal sound pressure amplitudes occur after the microphone is passed. Meanwhile, for the low-broadband fan, an opposite tonal time characteristic is observed. For the low-tone

design, the tonal sound pressure amplitudes are considerably lower than the broadband amplitudes over all times.

In order to assess not only temporal structures but also spectral patterns, Fig. 17 compares the monaural spectrograms between the different propulsion systems at the central and lateral microphones. The monaural spectrograms are provided to simplify the visualization, although the audio files are binaural (see Mm. 2, Mm. 3, and Mm. 4). The dashed vertical lines indicate the time overhead.

The spectrograms reflect the examined noise radiation characteristics of the three distributed propulsion systems. If the reference fan is used, the BPF tone and its harmonics are clearly visible and broadband noise is masked by the fan tones during all times of the flyover. If the low-broadband

2162   J. Acoust. Soc. Am. **157** (3), March 2025   Schade *et al.*

75

TABLE III. Maximum tone-corrected perceived noise levels (PNLT$_{max}$) and effective perceived noise levels (EPNL) relative to the distributed propulsion system equipped with the baseline fan.

Fan design	ΔPNLT$_{max}$ [dB]		ΔEPNL [dB]	
	Central	Lateral	Central	Lateral
Low-broadband	−8.2	−6.5	−7.0	−8.5
Low-tone	−13.0	−12.2	−11.7	−13.0

fan is used, the BPF tones are shifted to higher frequencies due to the increase in rotor blade count from 18 to 31. For the low-tone fan, the fan tones are shifted to even higher frequencies since the BPF tone is inverse cut-off, so that only the second and third harmonic are visible in the spectrogram. Overall, the tonal noise content is remarkably reduced resulting in a rather broadband-dominated noise immission, although, especially at the central microphone, the second blade passing frequency tone remains visible in the spectrogram [see 4000–5500 Hz in Fig. 17(c1)].

Comparing the central and lateral microphone positions, the main differences are the lower absolute noise levels at the lateral position, which are on the one hand due to the longer propagation distances leading to increased atmospheric absorption and spreading losses, and on the other hand due to the impact of the noise directivities, which show a stronger dependence on the axial direction than the lateral one (as visualized in Fig. 14).

For the acoustic certification of future aircraft with vertical takeoff and landing capabilities, as the considered UAM vehicle presented in Fig. 1, a new standard is currently under development (EASA, 2023). As suggested by EASA (2023), the noise evaluation metric is the effective

perceived noise level (EPNL) which is based on the tone-corrected perceived noise level (PNLT(t)). The maximum PNLT values and EPNL are shown in Table III for the low-broadband and low-tone fan. The differences relative to the values of the baseline fan are given. For both fan designs, PNLT$_{max}$ and EPNL are remarkably reduced at the central and the lateral microphone positions. The EPNL is more than 7 dB lower if the distributed propulsion system is equipped with the low-broadband fan, and for the low-tone fan, an EPNL reduction of more than 11.7 dB is achieved.

3. Sound quality analysis

The values of the SQMs (as 5% percentiles) introduced in Sec. II C 4 are depicted in Fig. 18 for the three fan designs and both the central and lateral microphones. The presented values correspond to the takeoff procedure (see Table II, Fig. 7, and Sec. II C 2). In addition, a similar analysis is also performed for a horizontal flyover trajectory based on the EASA specifications (EASA, 2023). For the horizontal flyover the same specifications and limitations apply as for the takeoff procedure as listed in Sec. II C 2, however, Cruise operating conditions are considered as listed in Table II. Since similar trends are observed for the horizontal flyover as for the takeoff procedure, these results are not shown here for the sake of brevity.

For comparison purposes, the results for the SQM of sharpness, tonality, roughness, and fluctuation strength [Figs. 18(b)–18(e)] also include the experimental values of the Airbus A320 turbofan aircraft measured during takeoff from Fig. 11. The metrics of loudness and PA were not included in this comparison since they were considerably higher for the turbofan aircraft. For comparison with the turbofan case, it should be noted that different trajectories are
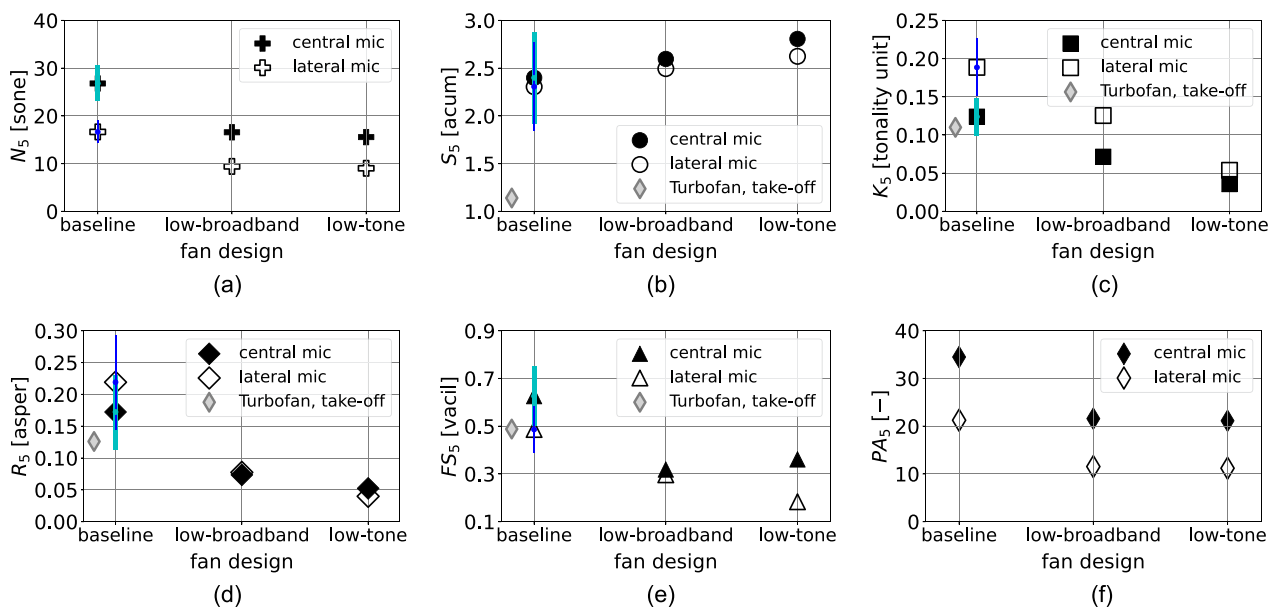
FIG. 18. Sound quality metrics [(a) loudness; (b) sharpness; (c) tonality; (d) roughness; (e) fluctuation strength] and psychoacoustic annoyance values (e) for each fan design and for the takeoff procedure. The values for the central and the lateral microphones are included. For the turbofan, the results from the measurements are re-plotted (see Fig. 11). For the baseline fan, the error bars refer to the JNDs, where each error bar is plotted as ± JND.

76

used, despite both being realistic takeoff trajectories (see Figs. 7 and 8).

In terms of loudness [Fig. 18(a)] both the low-broadband and low-tone fan designs achieve a reduction of roughly 40% in both microphone locations. Since loudness is the dominant SQM influencing the perceived noise annoyance (Greco *et al.*, 2023b), such a considerable reduction is expected to be perceived positively in practice. In comparison with the Airbus A320 takeoff validation case (Fig. 11), the UAM vehicle shows loudness values between two and three times lower for the central microphone, and even lower for the lateral microphone.

On the other hand, the sharpness values [Fig. 18(b)] experience an increase from roughly 2.4 acum for the baseline case to 2.6 and 2.8 acum for the low-broadband and low-tone cases, respectively. This is explained by the higher values of the BPF for the latter cases compared to the baseline, see Fig. 17. This is particularly relevant for the low-tone fan since the first BPF is (inverse) cut-off and only higher-frequency harmonics are present, hence, the acoustic energy is more distributed towards higher frequencies. In comparison, the turbofan aircraft presents a considerably lower sharpness value of 1.15 acum.

Regarding tonality [Fig. 18(c)], both the low-broadband and low-tone fan designs provide a considerable reduction with respect to the baseline. This is especially the case for the low-tone fan design, as expected, which offers a reduction in tonality of more than 70%, whereas the low-broadband fan design presents a lesser reduction of approximately 40%. It should be noticed that the tonality values at the lateral microphone (denoted as white markers) are consistently higher than those at the central microphone. This is explained by the relatively higher prominence of the tones for the lateral microphone shown in the spectrograms of Fig. 17, due to the noise radiation directivity patterns observed in Figs. 13 and 14. In contrast, the measured A320 takeoff procedure presents a tonality value (around 0.11 t.u.) similar to the baseline fan design case. It is interesting to note that the distributed propulsion system equipped with the baseline fan and the turbofan generate similar tonality values at takeoff conditions. On the one hand, for the baseline fan, the relatively high tonality value results from the blade passing frequency tone and its second, third and fourth harmonic which are the dominant tonal frequencies and which are well visible in the spectrogram (see Fig. 17). On the other hand, for the turbofan, the BPF tones and its harmonics are either cut-off or damped by a liner and are therefore not visible in the spectrogram [see Fig. 9(a)]. Thus, the buzz-saw tones, which are the dominant tonal frequencies for the turbofan, are responsible for the relatively high tonality value.

The two proposed fan designs also reduce the roughness metric compared to the baseline case [Fig. 18(d)]. Once again, the low-tone fan design has higher reductions (between 70% and 80% compared to the baseline) than the low-broadband one (between 55% and 65% compared to the baseline) for both microphone positions. With a roughness value of about 0.13 asper, the turbofan aircraft shows again

comparable values to the baseline fan design case. A similar behavior is observed for fluctuation strength [Fig. 18(e)] but with relatively smaller reductions: between 40% and 50% for the low-broadband design and between 42% and 62% for the low-tone one. The Airbus A320 takeoff presents again comparable values to the baseline fan design in terms of fluctuation strength, with a value of approximately 0.5 vacil. It should be noted that, since both metrics are based on amplitude modulations, the values of roughness and fluctuation strength are relatively sensitive to the rotational speed fluctuations within the fans, as discussed in Schade *et al.* (2024b).

Last, to classify the order of magnitude of a relevant change for each SQM, the JNDs are plotted in Fig. 18 as error bars showing the ±JNDs. The JNDs indicate that the two low-count OGV fan stages (low-broadband and low-tone) offer reductions for all considered metrics well above one noticeable difference, despite a slight increase in sharpness which is, however, deemed as non-relevant since it is below one noticeable difference. The global psychoacoustic annoyance (PA) metric is evaluated for the three fan designs and the two microphone locations in Fig. 18(f). In this case, the decreases in PA obtained by the low-broadband and the low-tone fan designs with respect to the baseline case are virtually the same, with reductions of approximately 38% and 47% for the central and the lateral microphone, respectively. Despite the differences in sharpness, tonality, roughness, and fluctuation strength, the psychoacoustic annoyance model employed is strongly based on loudness (Di *et al.*, 2016; Merino-Martinez *et al.*, 2022), and since this metric is comparable in both fan designs [see Fig. 18(a)], the global PA values end up being very similar.

Comparing the reduction in PA from Fig. 18(f) with the reduction in PNLTm and EPNL from Table III, it is noticeable that the low-tone fan design leads to a considerable reduction in PNLT$_{max}$ and EPNL compared to the low-broadband design at both microphones, whereas this is not reflected in the PA values, since both fans have almost identical PA values, as described above. Consequently, although a reduction of EPNL is observed, no reduction of PA between low-tone design and low-broadband design is determined. This confirms the initial hypothesis that propulsion designs with lower EPNL do not necessarily result in lower annoyance. However, the validity of the PA model formulated by Di *et al.* (2016) should be further examined in future listening tests.

Mm. 2. Binaural audio file of the distributed propulsion system equipped with the baseline fan at the central microphone of the takeoff procedure.

Mm. 3. Binaural audio file of the distributed propulsion system equipped with the low-broadband fan at the central microphone of the takeoff procedure.

Mm. 4. Binaural audio file of the distributed propulsion system equipped with the low-tone fan at the central microphone of the takeoff procedure.

77

V. SUMMARY AND CONCLUSION

In this paper, the acoustic characteristics of a distributed propulsion system of an urban air mobility vehicle were investigated. The considered propulsion system consists of 26 low-speed, ducted fan stages, where three acoustically different fan designs are examined: a baseline design, a low-broadband noise design, and a low-tonal noise design. The noise emissions of the distributed fan stages were predicted analytically, propagated through the atmosphere to a central and a lateral microphone using virtual flyover simulations and were auralized to obtain the audio recordings. To examine the perception of human hearing, several sound quality metrics were calculated. A validation of the auralization framework was provided based on measurement data from an A320 takeoff.

It was found that the distributed propulsion systems generate noise directivities with complex interference patterns showing a strong dependence on the axial and lateral angles. Compared to the distributed propulsion system equipped with the baseline fan, the low-broadband noise design achieves reductions of more than 6 dB for the maximum tone-corrected and effective perceived noise levels ($PNLT_{max}$ and EPNL) at both microphones, whereas the low-tonal noise design achieves an even higher reduction of more than 11 dB. In addition, compared to the baseline design, the low-broadband and low-tonal noise designs reach a notable decrease in loudness, tonality, roughness, fluctuation strength, and, globally, psychoacoustic annoyance which is predicted by a model from Di *et al.* (2016). However, the reduction in $PNLT_{max}$ and EPNL for the low-tonal noise design compared to the low-broadband noise design is not reflected in the psychoacoustic annoyance metric as both designs achieve similar values for psychoacoustic annoyance. Moreover, both fan designs showed higher levels of sharpness compared to the baseline design due to their relatively stronger high-frequency noise content.

Regarding the comparison with the A320 turbofan engines, comparable or even lower values of tonality, roughness and fluctuation strength are achieved for the low-broadband noise and low-tonal noise fan designs, whereas sharpness is notably increased for all distributed propulsion systems.

VI. OUTLOOK

The installation of the fans on the wings should be addressed in future studies and the impact of boundary layer ingestion (BLI) on the psychoacoustic characteristics of the propulsion system should be examined. The impact of BLI will affect all fan designs particularly the low-tone fan, as the tonal noise emission of this fan benefits from the inverse cut-off of the blade passing frequency tone. This acoustic effect could be neutralized by BLI as additional acoustic modes and noise sources will be excited (Quaroni *et al.*, 2024). This may result in stronger tonal noise radiation, which in turn may change the psychoacoustic characteristics of the propulsion system.

The fan noise emission, examined in Sec. IV B 1, is calculated using an analytical noise prediction method. These results will be validated in future measurements conducted at CRAFT test facility. The measurements are already scheduled within the project VIRLWINT. As part of the measurement campaign, an inflow distortion representative for the boundary layer on the wing is designed to assess the impact of BLI on tonal noise emission for all considered fan designs. In addition to validating the noise emission, the measurement data also allows one to perform the auralization process chain not only with analytical input as in this paper, but also based on measured noise directivities so that the results can be compared and validated. Furthermore, airframe noise, neglected for this study, will be included in future auralizations as part of the ongoing DLR project *LUFT 2030*.

Regarding the distributed low-tone fans, the tonal noise levels are lower than the broadband levels for almost all radiation angles (see Sec. IV B 1), leading to lower sound pressure amplitudes at both microphones compared to the broadband amplitudes (see Sec. IV B 2) and to the lowest tonality and loudness values (see Sec. IV B 3). This offers the potential to design a liner not for a specific tonal frequency but for a wider frequency range to increase the acoustic attenuation of broadband noise, as for example examined by Sutliff *et al.* (2021).

To confirm the results obtained from the sound quality analysis and obtain new insights on the perceptual differences of the fan designs, psychoacoustic listening experiments with human subjects are of high interest and are planned for the near future. The low-broadband and low-tone fan designs are particularly suited for listening experiments as the loudness and psychoacoustic annoyance values are comparable between both designs, whereas other SQMs like roughness tonality or fluctuations strength are different. Therefore, such a psychoacoustic study would provide insights on the relative role of other SQMs while having similar loudness levels, as suggested by Boucher *et al.* (2024b).

AUTHOR DECLARATIONS
Conflict of Interest

The authors state that they have no conflicts to disclose.

J. Acoust. Soc. Am. **157** (3), March 2025

Schade *et al.* 2165

78

DATA AVAILABILITY

The data that support the findings of this study are available from the corresponding author upon request.

Arbeitsgruppe Novellierung der AzB (**2007**). *Anleitung Zur Berechnung Von Lärmschutzbereichen (AzB)* [*Instructions for Calculation of Noise Protection Areas (AzB)*] (Umweltbundesamt, Dessau-Roßôlau, Saxony-Anhalt).

Aures, W. (**1985**). "Berechnungsverfahren für den sensorischen Wohlklang beliebiger Schallsignale" ("Calculation method for the sensory euphony of arbitrary sound signals"), Acta Acust. united Acust. **59**(2), 130–141.

Bernardini, G., Centracchio, F., Gennaretti, M., Iemma, U., Pasquali, C., Poggi, C., Rossetti, M., and Serafini, J. (**2020**). "Numerical characterisation of the aeroacoustic signature of propeller arrays for distributed electric propulsion," Appl. Sci. **10**(8), 2643.

Bernschütz, B. (**2013**). "A spherical far field HRIR/HRTF compilation of the Neumann KU 100," in *Proceedings of the 39th DAGA*, pp. 592–595.

Boucher, M. A., Christian, A. W., Krishnamurthy, S., Tracy, T., Begault, D. R., Shepherd, K., and Rizzi, S. A. (**2024b**). "Toward a psychoacoustic annoyance model for urban air mobility vehicle noise," technical report No. NASA TM–20240003202, ntrs.nasa.gov/api/citations/20240003202/downloads/NASA-TM-20240003202June.pdf (Last viewed October 2, 2024).

Boucher, M., Rafaelof, M., Begault, D., Christian, A., Krishnamurthy, S., and Rizzi, S. (**2024a**). "A psychoacoustic test for urban air mobility vehicle sound quality," SAE Int. J. Adv. Curr. Prac. Mobility **6**(2), 972–985.

Caldas, L., Kruck, S., Klähn, L., Rudolphi, A., Meyer, R., Enghardt, L., and Tapken, U. (**2022**). "Construction and assessment of an inflow-control-device for a low-speed aeroacoustic fan rig," AIAA J. **60**, 5299–5312.

Dang, M. (**2022**). "Usability and maintainability of the software tools violin and coral," Bachelor thesis, Baden-Württemberg Cooperative State University, Stuttgart, Baden-Württemberg, Germany.

Daniel, P., and Webber, R. (**1997**). "Psychoacoustical roughness: Implementation of an optimized model," Acust. Acta Acust. **83**, 113–123.

Di, G.-Q., Chen, X.-W., Song, K., Zhou, B., and Pei, C.-M. (**2016**). "Improvement of Zwicker's psychoacoustic annoyance model aiming at tonal noises," Appl. Acoust. **105**, 164–170.

EASA (**2023**). "Environmental protection technical specifications applicable to VTOL-capable aircraft powered by tilting rotors," consultation paper No. 1.

Eißfeldt, H., and Stolz, M. (**2024**). "Public perception of air taxis in Germany: Anticipated risks, benefits, and noise sensitivity," Proc. Mtg. Acoust. **54**(1), 040004.

Fastl, H., and Zwicker, E. (**2007**). *Psychoacoustics—Facts and Models*, 3rd ed. (Springer-Verlag, Berlin).

Giacche, D., Hynes, T. P., Baralon, S., Coupland, J., Humphreys, N., and Schwaller, P. (**2013**). "Acoustic optimization of ultra-low count bypass outlet guide vanes," in *19th AIAA/CEAS Aeroacoustics Conference*.

Greco, G. F., Merino-Martinez, R., and Osses, A. (**2023a**). "SQAT: A sound quality analysis toolbox for MATLAB," available at github.com/ggre-cow/sqat (Last viewed May **3**, 2023).

Greco, G. F., Merino-Martinez, R., and Osses, A. (**2024**). "SQAT: A sound quality analysis toolbox for MATLAB (version v1.1)," available at http://dx.doi.org/10.5281/zenodo.10580337 (Last viewed May 20;, 2024).

Greco, G. F., Merino-Martinez, R., Osses, A., and Langer, S. C. (**2023b**). "SQAT: A MATLAB-based toolbox for quantitative sound quality analysis," in *52nd International Congress and Exposition on Noise Control Engineering* (August 20–23) [International Institute of Noise Control Engineering (I-INCE), Chiba, Greater Tokyo, Japan].

Guérin, S., and Tormen, D. (**2023**). "A contribution to the investigation of acoustic interferences in aircraft distributed propulsion," CEAS Aeronaut. J. **14**, 965–982.

Gwak, D. Y., Han, D., and Lee, S. (**2020**). "Sound quality factors influencing annoyance from hovering UAV," J. Sound Vib. **489**, 115651.

Heidmann, M. F. (**1975**). "Interim prediction method for fan and compressor source noise," NASA technical memorandum X-71763, available at ntrs.nasa.gov/citations/19750017876 (Last viewed October 2, 2024).

Hornikx, M. (**2016**). "Ten questions concerning computational urban acoustics," Build. Environ. **106**, 409–421.

ICAO (**2017**). "Annex 16 to the convention on international civil aviation, environmental protection," in *Aircraft Noise*, 8th ed. (International Civil Aviation Organization, Montréal, Canada), Vol. 1.

ISO 532-1 (**2017**). "Acoustics—Method for calculating loudness—Zwicker method" (International Organization for Standardization, Geneva, Switzerland).

ISO 9613-1 (**1993**). "Attenuation of sound during propagation outdoors, Part 1: Calculation of the absorption of sound by the atmosphere" (International Organization for Standardization, Geneva, Switzerland).

Jaron, R. (**2018**). "Aeroakustische auslegung von triebwerksfans mittels multidisziplinärer optimierungen" ("Aeroacoustic design of engine fans by means of multidisciplinary optimizations"), Dissertation, Technical University of Berlin, Berlin, Germany.

Merino-Martinez, R., Ben-Gida, H., and Snellen, M. (**2024a**). "Psychoacoustic evaluation of an optimized low-noise drone propeller design," in *30th International Congress on Sound and Vibration (ICSV)*, Amsterdam, The Netherlands (July 8–11).

Merino-Martinez, R., Besnea, I, von den Hoff, B., and Snellen, M. (**2024b**). "Psychoacoustic analysis of the noise emissions from the Airbus A320 aircraft family and its nose landing gear system," in *30th AIAA/CEAS Aeroacoustics Conference*, AIAA paper 2024–3398, Rome, Italy (June 4–7).

Merino-Martinez, R., Pieren, R., and Schäffer, B. (**2021**). "Holistic approach to wind turbine noise: From blade trailing–edge modifications to annoyance estimation," Renew. Sustain. Energy Rev. **148**(111285), 111285.

Merino-Martinez, R., Pieren, R., Schäffer, B., and Simons, D. G. (**2022**). "Psychoacoustic model for predicting wind turbine noise annoyance," in *The 24th International Congress on Acoustics (ICA)*, Gyeongju, South Korea (October 24–28), www.researchgate.net/publication/364996997_Psychoacoustic_model_for_predicting_wind_turbine_noise_annoyance (Last viewed October 21, 2024).

Merino-Martinez, R., Yupa-Villanueva, R. M., von den Hoff, B., and Pockelé, J. S. (**2024c**). "Human response to the flyover noise of different drones recorded in field measurements," in *3rd Quiet Drones Conference*, Manchester, UK (September 8–11).

Monteiro, F. d N., Merino-Martinez, R., and Lima Pereira, L. T. (**2024**). "Psychoacoustic evaluation of an array of distributed propellers under synchrophasing operation," in *30th AIAA/CEAS Aeroacoustics Conference*, AIAA paper 2024–3321, Rome, Italy (June 4–7).

Moreau, A. (**2017**). "A unified analytical approach for the acoustic conceptual design of fans for modern aero-engines," Dissertation, Technical University of Berlin, Berlin, Germany.

Moreau, A., Prescher, A., Schade, S., Dang, M., Jaron, R., and Guérin, S. (**2023a**). "A framework to simulate and to auralize the sound emitted by aircraft engines," in *InterNoise Conference 2023*.

Moreau, A., Schnell, R., and Mennicken, M. (**2023b**). "Acoustic preliminary design of a low-noise fan stage considering a variable-area nozzle and variable-pitch rotor blades," CEAS Aeronaut. J. **14**, 325–341.

Nallasamy, M., Envia, E., Thorp, S., and Shabbir, A. (**2002**). "Fan noise source diagnostic test—Computation of rotor wake turbulence noise," in *8th AIAA/CEAS Aeroacoustics Conference & Exhibit*.

OpenSky (**2025**). https://opensky-network.org/ (Last viewed September 2021).

Osses, A., Greco, G. F., and Merino-Martinez, R. (**2023**). "Considerations for the perceptual evaluation of steady-state and time-varying sounds using psychoacoustic metrics," in *10th Convention of the European Acoustics Association (Forum Acusticum)*, Torino, Italy (September 11–15).

Osses Vecchi, A., García León, R., and Kohlrausch, A. (**2017**). "Modelling the sensation of fluctuation strength," Proc. Mtgs. Acoust. **28**(1), 050005.

Pascioni, K., and Rizzi, S. A. (**2018**). "Tonal noise prediction of a distributed propulsion unmanned aerial vehicle," in *2018 AIAA/CEAS Aeroacoustics Conference*.

Prescher, A., Moreau, A., and Schade, S. (**2024**). "Model extension of random atmospheric inhomogeneities during sound propagation for engine noise auralization," CEAS Aeronaut. J. **15**, 1111–1125.

Quaroni, L. N., Merino-Martinez, R., Monteiro, F. d N., and Kumar, S. S. (**2024**). "Collective blade pitch angle effect on grid turbulence ingestion noise by an isolated propeller," in *30th AIAA/CEAS Aeroacoustics Conference*, AIAA paper 2024–3209, Rome, Italy (June 4–7).

2166   J. Acoust. Soc. Am. **157** (3), March 2025

Schade *et al.*

79

Ratei, P. (**2022**). "Development of a vertical take-off and landing aircraft design tool for the application in a system of systems simulation framework," Master thesis, Hamburg University of Applied Sciences, Haw, Hamburg, available at elib.dlr.de/186947/ (Last viewed September 18, 2024).

Ratei, P., Naeem, N., and Prakasha, P. S. (**2023**). "Development of an urban air mobility vehicle family concept by system of systems aircraft design and assessment," J. Phys. Conf. Ser. **2526**(1), 012043.

Rietdijk, F., Forssén, J., and Heutschi, K. (**2017**). "Generating sequences of acoustic scintillations," Acta Acust. united Acust. **103**(2), 331–338.

Rizzi, S. A. (**2016**). "Toward reduced aircraft community noise impact via a perception-influenced design approach," in *Inter-Noise 2016*, available at ntrs.nasa.gov/citations/20160011152 (Last viewed September 18, 2024).

Rizzi, S. A., Huff, D. L., Boyd, D. D., Bent, P., Henderson, B. S., Pascioni, K. A., Sargent, D. C., Josephson, D. L., Marsan, M., He, H., and Snider, R. (**2020**). "Urban air mobility noise: Current practice, gaps, and recommendations," NASA/TP-2020-5007433.

Schade, S., Jaron, R., Klähn, L., and Moreau, A. (**2024a**). "Smart blade count selection to align modal propagation angle with stator stagger angle for low-noise ducted fan designs," Aerospace **11**(4), 259.

Schade, S., Jaron, R., Moreau, A., and Guérin, S. (**2022**). "Mechanisms to reduce the blade passing frequency tone for subsonic low-count OGV fans," Aerosp. Sci. Technol. **125**, 107083.

Schade, S., Ludowicy, J., Ratei, P., Hepperle, M., Stürmer, A., Rossignol, K.-S., de Graaf, S., and Geyer, T. F. (**2025**). "Conceptual design of electrically-powered urban air mobility vehicles for aeroacoustic studies," CEAS Aeronaut. J. (in press).

Schade, S., Merino-Martinez, R., Ratei, P., Bartels, S., Jaron, R., and Moreau, A. (**2024b**). "Initial study on the impact of speed fluctuations on the psychoacoustic characteristics of a distributed propulsion system with ducted fans," in *30th AIAA/CEAS Aeroacoustics Conference*.

Shiva Prakasha, P., Naeem, N., Ratei, P., and Nagel, B. (**2022**). "Aircraft architecture and fleet assessment framework for urban air mobility using a system of systems approach," Aerosp. Sci. Technol. **125**, 107072.

Soeta, Y., and Kagawa, H. (**2020**). "Three dimensional psychological evaluation of aircraft noise and prediction by physical parameters," Build. Environ. **167**, 106445.

Sutliff, D. L., Nark, D. M., and Jones, M. G. (**2021**). "Multi-degree-of-freedom liner development: Concept to flight test," Int. J. Aeroacoust. **20**(5-7), 792–825.

Tapken, U., Caldas, L., Meyer, R., Behn, M., Klähn, L., Jaron, R., and Rudolphi, A. (**2021**). "Fan test rig for detailed investigation of noise generation mechanisms due to inflow disturbances," in *AIAA Aviation 2021 Forum*.

Torija, A. J., and Clark, C. (**2021**). "A psychoacoustic approach to building knowledge about human response to noise of unmanned aerial vehicles," Int. J. Environ. Res. Public Health **18**(2), 682.

Torija, A. J., Roberts, S., Woodward, R., Flindell, I. H., McKenzie, A. R., and Self, R. H. (**2019**). "On the assessment of subjective response to tonal content of contemporary aircraft noise," Appl. Acoust. **146**, 190–203.

Tyler, J. M., and Sofrin, T. G. (**1962**). "Axial flow compressor noise studies," SAE Technical Paper 620532.

von Bismark, G. (**1974**). "Sharpness as an attribute of the timbre of steady sounds," Acta Acust. united Acust. **30**(3), 159–172.

Vorländer, M. (**2008**). *Auralization—Fundamentals of Acoustics, Modelling, Simulation, Algorithms and Acoustic Virtual Reality*, 1st ed. (Springer, Berlin).

Weninger, B. (**2015**). "A color scheme for the presentation of sound immission in maps: Requirements and principles for design," in *EuroNoise 2015*, available at https://www.conforg.fr/euronoise2015/proceedings/data/articles/000069.pdf (Last viewed September 12, 2024), pp. 439–444.

Yang, H., Nuernberger, D., and Kersken, H.-P. (**2006**). "Toward excellence in turbomachinery computational fluid dynamics: A hybrid structured-unstructured Reynolds-averaged Navier-Stokes solver," J. Turbomach. **128**(2), 390–402.

J. Acoust. Soc. Am. **157** (3), March 2025

Schade *et al.* 2167

80

Chapter 3

Discussion

The objective of this section is to integrate the results of the three publications into the context of the research question. Therefore, the practical application of the investigated tonal noise reduction mechanisms for distributed propulsion systems is reviewed in Sec. 3.1, the robustness of the acoustic effects is discussed in Sec. 3.2, uncertainties regarding the virtual flyover method are evaluated in Sec. 3.3 and the sound quality characteristics are discussed in Sec. 3.4.

3.1 Application of the noise reduction effects

For the design of low-count OGV fan stages for future propulsion systems of air-taxis, this work contributes the formulation of generally valid design rules, which allow to transfer the investigated tonal noise reduction mechanisms to low-speed, low-count OGV fan stages. To apply the investigated tonal noise reduction mechanisms, blade count variations are required. Within the low-count OGV design space, both the inverse cut-off condition and the impact of the modal propagation angle occur for certain blade count combinations distributed along diagonal stripes in the noise generation results (see Fig. 3 from publication I in Sec. 2.1). This is consistent with the results from Moreau *et al.* [60] investigating the inverse cut-off condition for a ventilator and the results from Jaron [40] investigating the impact of the modal propagation angle on noise generation for an UHBR fan.

Regarding the inverse cut-off condition, for blade count combinations within these stripes, a cut-off is achieved for the blade passing frequency tone although the stator vane count is lower than the rotor blade count provided that the rotor

tip Mach number is low enough. Thus, this effect is restricted to low-speed fans.

Regarding the modal propagation angle, the excited modes found in the diagonal strips correspond to those whose propagation angle is aligned with the stator leading edge angle. In this case, the modal propagation angle is perpendicular to the dipole radiation axis leading to a tonal noise reduction. To apply this mechanism to low-speed fan stages, an iterative process is proposed. Provided that the flow conditions within the fan stage and the rotor geometry are predefined, the stator leading edge angle is predefined as well and serves as an input parameter for the iteration. The rotor and stator blade counts should be adjusted iteratively until a combination is identified, for which the propagation angle of the dominantly excited acoustic mode is aligned with the stator leading edge angle as closely as possible. A drawback of this method is that it is unlikely to achieve a perfect match, as the leading edge angle is set and the modal propagation angle can only be varied discretely using the blade count combination. An alternative approach is to reverse this procedure. Instead of defining the stator leading edge angle first, the rotor and stator blade counts could be selected first, which would in turn impose the modal propagation angle. In this case, the flow conditions should be varied until the stator leading edge angle is aligned with the modal propagation angle. From an acoustic perspective, this approach might be better suited, as the leading edge angle can be changed gradually until a very close match is realized between both angles. Since it was found that the expected noise reduction in good agreement follows the curve $20 \log_{10}(\sin(|\text{angle difference}|))$, with a close match between both angles (angle difference $\to 0$), high noise reductions are theoretically achievable ($\log_{10}(\sin(0)) \to -\infty$) (see Fig. 11 from publication II in Sec. 2.2). From an aerodynamic perspective, higher incidence angles may result and thus, the latter approach might be rather unusual for a fan design, as the fan performance is typically sized first. This illustrates the compromise that needs to be found between aerodynamics and acoustics.

Although the investigated acoustic effects considerably reduce the tonal noise levels at source, for the design of aircraft engines, additional noise reduction measures are commonly used, as for example acoustic liners, maximizing the rotor–stator distance (within a feasible installation space) as well as introducing swept and / or leaned stator vanes. While these measures are initially neglected in this work, further noise level reductions are expected in combination with the invest-

igated tonal noise reduction mechanisms.

For instance, sweeping the stator leading edge reduces the rotor–stator interaction noise since a swept leading edge (1) may lead to destructive radial interferences due to a variation of the radial phase distribution, (2) increases the axial distance between rotor trailing edge and stator leading edge and (3) reduces the component of the inflow velocity normal to the vane leading edge, which determines the strength of the acoustic excitation by a gust [29, 33]. Preliminary analytical studies with PropNoise showed that the expected reduction in broadband noise follows the curve $30 \log(\cos(\text{sweep angle}))$, which is consistent with the results from Hanson [38]. For stator lean, tonal noise decreases with lean angles in the direction of rotor rotation [28]. Similar to sweep, destructive interferences resulting from a variation of the radial phase distribution are the dominant reduction mechanism.

Moreover, if the tonal noise excitation is eliminated at source (e.g. low-tone fan), liners could be designed for an attenuation within a wider frequency range rather than the attenuation of a discrete tonal frequency [49, 80, 42]. However, for more compact fan stages, which are developed for small aircraft, the question arises whether the available space allows the integration of liners. The reason is that the smaller the fan stage and thus the nacelle can be designed, the lower is the induced drag. This further emphasizes the usefulness of investigating effects reducing the tonal noise levels at the source.

3.2   Robustness of the noise reduction effects

The results show that both the inverse cut-off effect and the impact of the modal propagation angle on noise generation can reduce the tonal noise excitation for low-speed, low-count OGV fans. Theoretically, high noise reductions are achievable.

In practice, the noise reduction potential of both effects may primarily be weaken since the modal content is richer than that found in the simulation. Two aspects are identified for the excitation of additional acoustic modes besides the Tyler & Sofrin modes. The first reason are manufacturing uncertainties. On the one hand, the rotor blades may slightly vary from each other due to non-ideal manufacturing. Smaller deviations in the rotor geometry and the blade surface can lead to non-uniform wakes in circumferential direction and thus the excitation of additional modes. On the other hand, the stator leading edge angles may deviate

from the nominal value as a result of manufacturing uncertainties. This changes the difference between the modal propagation angle and the stator leading edge angle, which has a direct impact on the expected noise reduction. However, this is classified as a secondary effect as deviations of the stator leading edge angle from its nominal value are typically small. For instance, assuming that the difference between the leading edge angle and the the modal propagation angle is 5°, a deviation of the leading edge angle of 1° would lower the theoretically expected noise reduction by about 2 dB, according to the design rule, which is plotted in Fig. 11 from publication II in Sec. 2.2.

The second reason for the excitation of additional modes are effects from inflow distortions, such as boundary layer ingestion [48, 17]. Although for the considered tilt-duct vehicle the fans are installed above the wing, the influence of boundary layer ingestion on tonal noise generation is neglected. The reason is that the distance between the wing leading edge and the fan inlet is relatively short (several centimeters). For horizontal flight, the assumption is made that the boundary layer developing upstream of the fan inlet is very small and is therefore negligible. During hover and the transition phase, the inflow may be strongly disturbed, meaning that the two noise reduction measures discussed in this work are not very effective. Klähn *et al.* [45, 47] experimentally investigated the impact of boundary layer ingestion on tonal noise using the baseline fan stage that was also used in the present work. Based on three inflow distortion profiles, the authors observe a reduction of tonal noise levels at the Tyler & Sofrin modes but a stronger excitation at neighboring modes for small to moderate distortions [45]. Due to the stronger excitation of neighboring modes, an increase in overall sound power is obtained. Bearing struts could be another reason why additional modes are excited, which then eliminate the (inverse) cut-off effect, as encountered in the experimental results from Moreau *et al.* [61].

Especially, the tonal noise reduction due to the impact of the modal propagation angle is sensitive to the excitation of additional modes. The reason is that this effect can most efficiently be realized provided that only few tonal modes are excited, which is typically the case for low-speed fans. Thus, low-speed fans are a potential area of application for this effect. If only a few tonal modes are excited, the design procedure could be specifically tuned to the propagation angles of these modes. By contrast, if several modes equally contribute to noise generation, it

may no longer be possible to align all resulting modal propagation angles with the stator leading edge angle. Although Jaron [40] observed this effect for an UHBR fan indicating that no inherent restriction to low-speed fans exists, its practical relevance may primarily be associated with such fans.

Regarding the inverse cut-off condition, the limiting rotor tip Mach number can be estimated from $M_{\text{tip, crit}} \approx \sqrt{1 - M_x^2} \, |m|/B$. However, particularly for distributed propulsion systems, uncertainties such as rotational speed deviations may introduce dynamic changes in the rotor tip Mach number [73]. Especially, if the distributed propulsion system also serves as a flight control system. In this case, individual propulsion units may operate at individual rotational speeds resulting in a distribution of rotor tip Mach numbers, which may considerably deviate from the nominal tip Mach number. Similarly, if the propulsion units are each driven by an individual motor, the motors may not run perfectly synchronized during operation due to uncertainties in the control system. This may lead to smaller rotational speed deviations. The impact of rotor tip Mach number variations can be evaluated with results plotted in Fig. 7 from publication I in Sec. 2.1. With increasing rotor tip Mach number ($M_{\text{tip}} \to M_{\text{tip, crit}}$), the diagonal stripes become successively narrower, as the acoustic interaction modes are cut-on for more and more blade count combinations. For tip Mach numbers close to the limiting Mach number $M_{\text{tip, crit}}$, the excited tonal modes are cut-on but are close to cut-off limit, resulting in a strong excitation of these modes [57, 81]. For distributed propulsion systems, this means that when rotor tip Mach numbers larger than $M_{\text{tip, crit}}$ occur during operation, the inverse cut-off effect is eliminated, which in turn would lead to higher noise levels and a rather tonal noise radiation. Another challenge for VTOL aircraft is that, as shown in Tab. 2 from publication III in Sec. 2.3, the operating conditions remarkably differ between cruise and vertical take-off. The vertical take-off is operated at higher rotational speeds than the cruise flight in order to generate sufficient thrust for the vertical climb. This makes an inverse cut-off design at take-off operating conditions practically impossible, since $M_{\text{tip}} > M_{\text{tip, crit}}$ is expected.

3.3 Uncertainties of the virtual flyover method

The acoustic and psychoacoustic evaluation in this work relies on an analytical process based on virtual flyover simulations and sound syntheses. One key advantage of this approach is its short turnaround time of a few minutes, enabling psychoacoustic investigations within the fan pre-design process. Since the accuracy of the results obtained from this method largely depends on the input quantities, a substantial uncertainty arises from the analytically calculated noise directivities. Although the analytical noise emission results obtained from PropNoise are already validated using different fan engines [94, 40], it is known that the broadband interaction noise levels are underestimated at low frequencies [34]. A change in broadband noise may possibly modify the noise signature and thus also the aural impression. Since tonal noise reduction mechanisms are evaluated in this work, the processing of the tonal prediction results plays a decisive role. It is known that the phase relation of tonal noise sources substantially impacts the directivities of distributed propulsion systems [35]. Therefore, the complex sound pressure amplitudes of all tonal sources are processed within each step of the virtual flyover simulation to account for interferences between the sound fields emitted from individual propulsion units. Nevertheless, the accuracy of the determined aural impression remains uncertain since the noise signatures from UAM propulsion systems are still largely unknown and no benchmark case with measured noise directivities exists for a realistic distributed propulsion system. In addition, a challenge is to validate the individual modeling steps of the flyover simulation and auralization. For this purpose, a comparison with microphone data obtained from a measured flyover with turbofan engines is provided. A drawback is that the comparison is restricted to one measured flyover event due to the lack of further data at take-off conditions. In addition, inaccuracies in the source prediction contribute to the overall difference. The reason for this limitation is the difficulty of comparing noise emissions between measurements and prediction, as the flyover measurements only provide data at the microphones and not at the noise source.

3.4 Impact on sound quality characteristics

The psychoacoustic assessment in this study is restricted to the evaluation of sound quality metrics. Although the sound quality metrics are currently widely applied to assess drone and distributed propulsion noise, open research questions are whether one or several metrics exist that reflect the subjective preferences of test persons and, in particular, whether the annoyance metric, which was originally not developed for this type of noise, can also be applied to such noise signals [10].

The baseline and the low-broadband fan designs demonstrate that an opposite dominant tonal noise radiation direction can be achieved due to the impact of the modal propagation angle on noise excitation. For the noise perception, this means that tonal noise can be better heard before or after the vehicle passes the observer depending on the dominant tonal noise radiation direction. To the best of the author's knowledge, the impact of the dominant tonal noise radiation direction on noise perception has not been investigated yet for a distributed propulsion system. This is a new research question that goes beyond the scope of this work and can be addressed in future listening experiments.

Combining both investigated noise reduction mechanisms leads to a reduction in tonality well above one noticeable difference (low-tone fan). This is relevant for the listening impression as experiments with human subjects showed that a sensitivity of human hearing to tonality exists across a wide range of applications, where annoyance increases with higher tonality values and vice versa. For aircraft noise, this has been verified by More and Davies [56], for noise in working environments by Landström *et al.* [52], for indoor air-conditioning noise by Jeon *et al.* [41] and for noise from building mechanical systems by Lee [53].

All examined distributed propulsion systems show noise signatures with high sharpness values (see Fig. 18 from publication III in Sec. 2.3). A rise by a factor of 2 is observed compared to turbofan engines. Besides high-frequency tonal noise content, especially for the baseline and low broadband fans, the maximum broadband levels are reached at $5\,\text{kHz}$ for all fan designs (see Figs. 12 and 17 from publication III in Sec. 2.3). Thus, a high proportion of acoustic energy exists at frequencies well above $3\,\text{kHz}$, which are perceived as sharper [87]. Based on sharpness, the noise signatures from the distributed propulsion systems studied in this work appear to be similar to hovering drones. The results obtained by

Gwak *et al.* [36] indicate that noise signals from hovering drones lead to sharpness values above 2 acum, which are comparable to the sharpness values from the distributed propulsion system (see Fig. 18 from publication III in Sec. 2.3 and Tab. 3 from [36]). The current research results are partly contradictory with regard to the effect of sharpness on human noise perception. Whereas Gwak *et al.* [36] conclude that drone sounds with higher sharpness lead to an increase in annoyance, Wang *et al.* [89] and Boucher *et al.* [11] found that the annoyance decreases with increasing sharpness. However, all sounds tested in the study conducted by Wang *et al.* [89] had relatively low sharpness values (< 1 acum) compared to drone noise, where values above 1 acum are expected.

The hypothesis is formulated that the obtained noise signatures with high sharpness values produce a rather "hissing" aural impression, in contrast to turbofan engines where the low-frequency jet noise may produce a rather "humming" noise perception. Nevertheless, since the analytical calculation of noise directivities probably underestimates the broadband noise at low frequencies (see Sec. 3.3), the noise signature may become slightly less sharp due to an increased acoustic energy content at lower frequencies if measured directivities are considered. However, the perception and its impact on annoyance also depends on the expectations people have on the sound. This becomes evident from the studies by Feldmann *et al.* [31] and Schäffer *et al.* [77], which yield different results for different types of sound as to whether hissing or humming sounds are associated with higher annoyances. For airtaxis, no studies are available yet, which show that a certain sound quality characteristic (i.e. hissing, humming) is associated with increased annoyance. According to Schütte *et al.* [78], an appropriate semantic differential helps to identify, which sound characteristics lead to an annoying impression. These results would then have to be related to psychoacoustic parameters, such as sharpness.

In order to potentially decrease sharpness by design, the rotor blade count could be reduced, for future fan designs. In this case, at the same rotational speed, the blade passing frequency and its harmonics would decrease due to the reduced rotor blade count. However, these designs would no longer necessarily be low-count OGV fans. Nevertheless, the tonal energy would be shifted to lower frequencies leading to a reduction in sharpness.

An interesting result exceeding the answer of the research question is that both low-count OGV fans not only achieve similar aerodynamic efficiencies but also

provide similar loudness values while showing differences for other sound quality metrics (see Tab. 6 from publication II in Sec. 2.2 and Fig. 18 from publication III in Sec. 2.3). Since the annoyance model formulated by Di *et al.* [18] mainly depends on loudness, Boucher *et al.* [10] propose to conduct listening experiments with sounds presented at the same loudness. As this is automatically achieved for the designed low-count OGV fans, these are well suited to investigate the impact of sound quality metrics on human noise perception without any further adjustments.

Chapter 4

Summary and conclusions

This section summarizes the key findings of this work with regard to answering the research question. It was investigated how low-speed fan engines with fewer stator than rotor blades can be designed for urban air mobility applications, which are not only quieter than conventional fan engines but also perceived as less unpleasant for human hearing. An analytical method based on virtual flyover simulations and binaural sound syntheses was developed to evaluate the psychoacoustic sound quality characteristics of propulsion systems. This method was applied to the distributed propulsion system of an UAM vehicle in order to assess the impact of tonal noise reduction mechanisms on its noise signatures. Using this method, the following three questions were addressed:

a) Which tonal noise reduction measures can be taken for low-speed fan stages with fewer stator than rotor blades?

b) How can the effects be applied to fan designs for an urban air mobility vehicle?

c) Which tonal noise reduction potential arises and what is the impact on the sound quality for a distributed propulsion system?

To answer the first question, analytical blade count variations were performed in order to narrow the low-count OGV design space to blade count combinations with reduced tonal noise excitation. This allowed to identify three acoustically promising blade count areas. Using analytical and numerical predictions, it was evaluated, which acoustic effects cause the reduction in tonal noise excitation within

the identified rotor–stator blade count design spaces. A major contribution of this work was to numerically and experimentally validate these effects, which were already theoretically known, to transfer them to low-speed fans designed for an UAM vehicle powered by 26 distributed, ducted fans and to investigate the resulting sound quality characteristics. The results showed that the following two mechanisms can efficiently reduce the tonal noise excitation.

1) An inverse cut-off can be used to suppress the excitation of the blade passing frequency tone for low-speed, low-count OGV fan stages. Unlike the conventional cut-off, the inverse cut-off is achieved even though fewer stator than rotor blades are considered provided that the rotor tip Mach number is low-enough. A design rule was derived to quantify the limiting rotor tip Mach number. Depending on the axial Mach number M_x, the azimuthal mode order m and the rotor blade count B, the rotor tip Mach number has to fulfill the condition $M_{\text{tip}} < \sqrt{1 - M_x^2}\,|m|/B$.

2) The propagation angle of the dominantly excited mode directly impacts the tonal noise excitation of low-count OGV fan stages. A tonal benefit occurs when the modal propagation angle is aligned with the stator leading edge angle. If this condition is achieved for the dominant mode, a minimum of acoustic energy is excited since its modal propagation angle is perpendicular to the dipole radiation axis. The design rule $20\log_{10}(\sin(|\Delta|))$ was derived to quantify the noise reduction potential of this effect, where Δ is the difference between the stator leading edge angle and the modal propagation angle. The noise reduction potential and the validity of the formulated design rule were verified and confirmed using experimental results.

To address the second question, both identified tonal noise reduction mechanisms were applied to two low-count OGV fan stages for an urban air mobility vehicle. Since the impact of both effects is determined by the rotor–stator blade numbers, these were initially examined with the objective that both fan stages use at least one of the identified effects for tonal noise reduction. Thus, the formulated design rules were evaluated while iterating the rotor and stator blade numbers. Once the blade numbers were defined, the three–dimensional shapes of the rotor and stator geometries were designed in a multidisciplinary optimization procedure targeting similar aerodynamic performances for all fan stages.

To achieve a tonal noise reduction using the modal propagation angle, the following iteration was applied: The input for the iteration are the rotor and stator blade numbers as these define the dominantly excited tonal mode orders. The mode orders in turn determine the modal propagation angles. Since the stator leading edge angle is predefined by the aerodynamic flow conditions, the blade numbers were iterated until exactly those tonal mode orders were excited whose propagation angles are preferably parallel to the stator leading edge angle in order to achieve a tonal noise reduction according to the formulated design rule.

Table 4.1: Rotor–stator blade count numbers for all three fan stages.

blade numbers	Baseline	Low-broadband	Low-tone
rotor	18	31	31
stator	21	10	21

Table 4.1 summarizes the blade numbers of the baseline fan and those of both low-count OGV fan stages. The baseline fan is a cut-on design and the acoustic results showed that the tonal noise excitation is more than 10 dB lower upstream than downstream. The reason is that the propagation angle of the upstream dominantly excited mode is almost aligned with the stator leading edge angle resulting in a low radiation efficiency. By contrast, for the low-broadband fan, the blade numbers were intentionally chosen such that modal propagation angle of the downstream dominantly excited mode is almost aligned to the leading edge angle resulting in a downstream tonal noise reduction. This leads to an opposite dominant tonal noise radiation direction compared to the baseline fan. Thus, the low-broadband design demonstrated that the modal propagation angle can not only be applied to reduce the tonal noise excitation but also to specifically modify the dominant tonal noise radiation direction. Moreover, the stator vane count is approximately halved compared to the baseline fan leading to a reduction of broadband noise by about 3 dB. For the low-tone fan, the blade numbers were chosen such that the blade passing frequency tone is inverse cut-off and that the excitation of the second harmonic is reduced upstream due to the impact of the modal propagation angle. The low-tone design demonstrates that combining the two identified tonal noise reduction mechanisms (modal propagation angle and inverse cut-off), the tonal noise excitation is decreased significantly without incorporating further passive noise reduction methods, such as acoustic liners.

Table 4.2: Acoustic noise radiation characteristics of all three fan stages.

Acoustic Design Criterion	Baseline	Low-broadband	Low-tone
dominant tonal noise radiation direction	downstream	upstream	downstream
tonal to broadband noise ratio	high	medium	low
blade passing frequency	1350 Hz	2325 Hz	4650 Hz

Table 4.2 summarizes the acoustic characteristics of all three fan designs and indicates that due to the application of the identified acoustic effects three fans with opposite acoustic noise radiation characteristics were designed. These fans are therefore well suited for psychoacoustic studies and sound quality assessments.
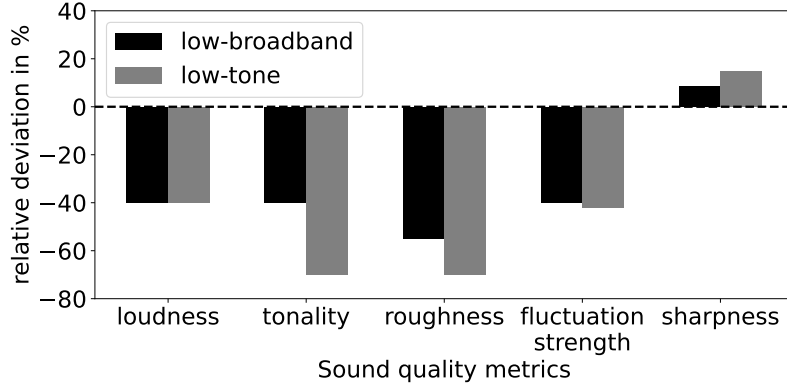
Figure 4.1: Relative deviation in sound quality characteristics of the low-count OGV fans compared to the baseline fan design according to Fig. 18 from publication III.

To address the third question, the three fan designs were each virtually integrated into a propulsion system for an urban air mobility vehicle consisting of 26 distributed fans. In order to assess the noise signature, an analytical auralization process was first extended for distributed propulsion systems and then applied to the propulsion system of the considered vehicle. For a take-off trajectory, the distributed low-broadband and low-tone fan stages achieved a reduction in effective perceived noise level (EPNL) compared to the baseline design of more than 6 dB and 11 dB, respectively. As visualized in Fig. 4.1, with the low-count OGV fan stages a sound quality improvement in terms of tonality, roughness, fluctuation strength and loudness was realized but an increase in sharpness was obtained compared to the baseline design at take-off conditions. The reductions were well above

one just noticeable difference. A unique characteristic of both low-count OGV fans is that similar loudness values were obtained while the other sound quality metrics are different. Compared to a turbofan engine at take-off, similar or even lower values of tonality, roughness and fluctuation strength were reached. The sharpness increased by a factor of 2 compared to the turbofan engines due to a tonal and broadband energy content at high frequencies.

All in all, in this work, two tonal noise reduction mechanisms were investigated analytically and numerically and, where possible, validated with experimental data from a low-speed fan test rig. The tonal noise reduction mechanisms were transferred to two new low-speed, low-count OGV fan stages, which were developed for the virtual integration into a distributed propulsion system of an UAM aircraft. An analytical process for psychoacoustic assessments using virtual flyover simulations was developed and applied to examine the impact of fan design on the noise signature of the distributed propulsion system. This work indicates that aerodynamically equivalent fan designs may produce different noise signatures, demonstrating that there is a wide latitude in the acoustic design of urban air mobility fan engines. The following key findings were published:

- The inverse cut-off effect and the modal propagation angle can efficiently reduce the tonal noise excitation for low-speed, low-count OGV fan stages.

- The inverse cut-off occurs if the rotor tip Mach number is lower than the critical value $M_{\text{tip, crit}} \approx \sqrt{1 - M_x^2}\, |m|/B$.

- The tonal noise reduction potential due to the impact of the modal propagation angle relative to the stator leading edge angle can be estimated using $20 \log_{10}(\sin(|\Delta|))$.

- The modal propagation angle can not only be applied to reduce tonal noise but also to modify the dominant tonal noise radiation direction.

- By applying the identified noise reduction mechanisms to low-count OGV fan stages of a distributed propulsion system representative of an urban air mobility application, the radiated noise levels were reduced and the sound quality characteristics were improved in terms of tonality, roughness, fluctuation strength and loudness, whereas an increase in sharpness is obtained.

Chapter 5

Outlook

Based on the limitations evaluated in Chap. 3, this section identifies open research demands that exceed the formulated research question and outlines possible follow-up approaches for future studies:

1. Experimental validation of the noise reduction mechanisms identified analytically and numerically.

   In future measurements both low-count OGV fan stages will be experimentally tested in DLR's CRAFT facility under realistic and representative conditions for urban air mobility applications providing data to validate the noise emission results. Experimental testing of the low-broadband design allows to further verify the impact of the modal propagation angle on noise excitation and to validate its tonal noise reduction potential for a low-count OGV fan. Experimental testing of the low-tone design provides two insights: First, an additional validation of the impact of the modal propagation angle on noise excitation and second, a verification of the inverse cut-off effect and its application to a low-speed fan. In addition, it can be evaluated whether non-uniform blades, e.g. due to manufacturing tolerances, and thus the generation of non-uniform wakes affect the tonal noise reduction potential obtained from the modal propagation angle or the inverse cut-off effect. Thereby it can be investigated to which extent the excitation of additional acoustic modes affects the identified tonal noise reduction mechanisms. Alongside with the measurements, the influence of non-uniform wakes could be investigated using analytical noise prediction. Initial measurement cam-

paigns including both low-count OGV fan stages are scheduled for the second quarter of 2025.

2. Verify the trends obtained from sound quality analysis using listening experiments.

Using sound quality metrics, a differentiated analysis of the noise signature is carried out and initial indications regarding the aural impression are obtained. However, the evaluation of these metrics cannot replace listening experiments in laboratory environments. Therefore, the predicted trends from sound quality assessment should be verified and validated using listening experiments with human subjects. Listening experiments with synthesized flyovers of the distributed propulsion system equipped with either low-broadband, low-tone or baseline fans are scheduled for the first quarter of 2026.

3. Verify the auralization results using measurement data.

In order to perform virtual flyover simulations and auralizations noise directivities are need as input data. So far, these noise amplitudes are calculated either fully analytical or based on RANS-informed analytical noise prediction. This is reasonable as the analytical noise prediction is a fast prediction method well-suited for pre-design processes and with turnaround times enabling to evaluate a variety of different configurations, as for example for blade count variations. However, for future studies, noise directivities obtained from measurements should also be considered as input data for the flyover simulation. Considering measured noise directivities as an input would allow (1) a step-by-step comparison of the virtual flyover and auralization results and (2) an analysis of how the excitation of additional modes present in the experimental data changes the aural perception. Thus, the noise emission, noise immission as well as the noise signatures could be compared between virtual flyovers with measured input and those with analytical input. Therefore, a new interface allowing to process measurement data should be developed for the flyover simulation. This interface is planned for the third quarter of 2025 so that, after completion of the measurement campaign, the measured noise directivities of the baseline, low-broadband and low-tone fans can be processed with the virtual flyover and auralization

method. Comparing the noise signals obtained with measured and predicted input is the first step regarding the verification of the auralization results. Provided that data from airtaxi flyovers are available in the future, these should be used to validate the predicted noise exposure using microphone data.

4. Conduct a sensitivity study to estimate the robustness of the virtual flyover results.

   In order to obtain a deeper understanding of how the boundary conditions and input parameters impact the noise immission results, a sensitivity study should be performed for all free parameters of the virtual flyover simulation. For instance, this study should address the impact of

   - weather and atmospheric conditions,
   - ground characteristics (e.g. hard surface or grass surface),
   - rotor and stator clocking positions,
   - variable operating conditions along the flight path

   on the resulting noise immission.

5. Verify the impact of fan installation effects on the tonal noise excitation.

   Future studies should include effects resulting from the fan installation positions, such as boundary layer ingestion or noise shielding. The fan engines of the considered propulsion system are mounted on the wings. Therefore, the boundary layer that is formed on the wing is continuously ingested into the engine during all flight phases. The resulting inhomogeneous inflow creates an additional noise source and it should be evaluated to what extent the excitation of additional modes mitigate the tonal noise reduction obtained from the investigated mechanisms. As an initial assessment, representative wing inflow distortions for cruise flight are included in the measurements scheduled for the second quarter of 2025. Moreover, due to the installation of the engines above the wing, it is expected that a part of the sound will be scattered or reflected by the wing. For certain radiation angles, the noise is shielded between the engine and the observer on the ground. This changes

97

the noise signature of the distributed propulsion system and thus its subjective aural perception. Therefore, a shielding model should be developed and included in the virtual flyover simulations in order to estimate the impact of noise shielding on the noise signature.

6. Include additional noise sources and trajectories in the virtual flyover simulation.

   So far, for the virtual flyover simulation and the subsequent noise syntheses, only engine noise sources are considered. This is reasonable as only take-off trajectories are considered within this work and for take-off conditions, the engines are expected to be the dominant noise source. However, in future studies, additional trajectories, such as approach or flyover flight paths, should be used and additional noise sources, such as airframe noise, should be included.

7. Assessment of noise emission when additional reduction measures are combined with the investigated effects.

   For the low-tone fan design, the tonal noise radiation is decreased without passive noise reduction technologies. Therefore, this fan design could be used to test liner geometries which are designed to attenuate a broader frequency range instead of the attenuation of discrete tonal frequencies. If it is possible to reduce the broadband noise using a liner an even quieter fan design would be achievable. These investigations could be addressed experimentally within the CRAFT facility and should be included in future measurement campaigns. Moreover, future studies should evaluate the expected additional noise reduction potential if stator sweep and lean are combined with the tonal noise reduction mechanisms investigated within this work.

Bibliography

[1] ISO 532-1. Acoustics – Method for calculating loudness – Zwicker method, 2017. URL: https://www.iso.org/standard/63077.html.

[2] M. Arntzen, L. Bertsch, and D. G. Simons. Auralization of novel aircraft configurations. *5th CEAS Air and Space Conference*, 2015. URL: https://resolver.tudelft.nl/uuid:e95b169a-6516-4859-9941-d9dccd59460e.

[3] K. Atci, P. Weiand, and F. Guner. Understanding the fixed pitch RPM-controlled rotor modeling for the conceptual design of UAM vehicles. *CEAS Aeronautical Journal*, 15:409–422, 2024. doi:10.1007/s13272-023-00703-9.

[4] W. Aures. Berechnungsverfahren für den sensorischen Wohlklang beliebiger Schallsignale. *Acta Acustica united with Acustica*, 59(2):130–141, 12 1985.

[5] Joby Aviation. Joby media kit, 2025. https://www.jobyaviation.com/ [Accessed: 20 March 2025].

[6] S. Bartels, F. Márki, and U. Müller. The influence of acoustical and non-acoustical factors on short-term annoyance due to aircraft noise in the field — the COSMA study. *Science of The Total Environment*, 538:834–843, 2015. doi:https://doi.org/10.1016/j.scitotenv.2015.08.064.

[7] M. Behn, U. Tapken, P. Puttkammer, R. Hagmeijer, and N. Thouault. Comparative study of different analytical approaches for modelling the transmission of sound waves through turbomachinery stators. *22nd AIAA/CEAS Aeroacoustics Conference*, 2016. doi:10.2514/6.2016-2927.

[8] G. Bernardini, F. Centracchio, M. Gennaretti, U. Iemma, C. Pasquali, C. Poggi, M. Rossetti, and J. Serafini. Numerical characterisation of the aeroacoustic signature of propeller arrays for distributed electric propulsion. *Applied Sciences*, 10(8), 2020. doi:10.3390/app10082643.

[9] J. J. Berton and W. J. Haller. A noise and emissions assessment of the N3-X transport. *52nd Aerospace Sciences Meeting*, 2014. doi:10.2514/6.2014-0594.

[10] M. Boucher, A. Christian, S. Krishnamurthy, T. Tracy, D. Begault, K. Shepherd, and S. Rizzi. Toward a psychoacoustic annoyance model for urban air mobility vehicle noise. *NASA/TM–20240003202*, 06 2024. doi:10.13140/RG.2.2.32111.24480.

[11] M. Boucher, M. Rafaelof, D. Begault, A. Christian, S. Krishnamurthy, and S. Rizzi. A psychoacoustic test for urban air mobility vehicle sound quality. *SAE International Journal of Advances and Current Practices in Mobility*, 6(2):972–985, 05 2023. doi:10.4271/2023-01-1107.

[12] D. Broszat, T. Selic, and A. Marn. Verification of the inverse cut-off effect in a turbomachinery stage - part 1 - numerical results. *18th AIAA/CEAS Aeroacoustics*

Conference (33rd AIAA Aeroacoustics Conference), 2012. AIAA 2012-2306. `doi:10.2514/6.2012-2306`.

[13] D. Broszat, T. Selic, and A. Marn. Verification of the inverse cut-off effect in a turbomachinery stage - part 2 - comparison to experimental results. *19th AIAA/CEAS Aeroacoustics Conference*, 2013. AIAA 2012-2306. `doi:10.2514/6.2013-2103`.

[14] F. Casagrande Hirono, A. J. Torija, S. D. Grimshaw, D. Cousins, J. Farman, and J. V. Taylor. Aerodynamic and aeroacoustic design of electric ducted fans. *Aerospace Science and Technology*, 153:109411, 2024. `doi:10.1016/j.ast.2024.109411`.

[15] S. Castegnaro. Aerodynamic design of low-speed axial-flow fans: A historical overview. *Designs*, 2(3), 2018. `doi:10.3390/designs2030020`.

[16] P. Daniel and R. Webber. Psychoacoustical Roughness: Implementation of an Optimized Model. *Accustica – acta acustica*, 83:113–123, 1997.

[17] M. Daroukh, C. Polacsek, and M. Carini. Acoustic assessment of BLI effects on airbus nautilius engine integration concept - part I: Noise generation. *28th AIAA/CEAS Aeroacoustics 2022 Conference*, 2022. `doi:10.2514/6.2022-2943`.

[18] G.-Q. Di, X.-W. Chen, K. Song, B. Zhou, and C.-M. Pei. Improvement of Zwicker's psychoacoustic annoyance model aiming at tonal noises. *Applied Acoustics*, 105:164–170, 2016. `doi:10.1016/j.apacoust.2015.12.006`.

[19] J. H. Dittmar, J. N. Scott, B. R. Leonard, and E. G. Stakolich. Effects of longchord acoustically treated stator vanes on fan noise. 1: Effect of long chord (taped stator). *NASA Technical Note TN D-8062*, 1975. URL: `https://ntrs.nasa.gov/api/citations/19760003044/downloads/19760003044.pdf`.

[20] J. H. Dittmar and R. P. Woodward. An evaluation of some alternative approaches for reducing fan tone noise. *NASA Technical Memorandum TM 105356*, 1992. URL: `https://ntrs.nasa.gov/api/citations/19920009040/downloads/19920009040.pdf`.

[21] P. E. Duncan and B. Dawson. Reduction of interaction tones from axial flow fans by suitable design of rotor configuration. *Journal of Sound and Vibration*, 33(2):143–154, 1974. `doi:10.1016/S0022-460X(74)80102-1`.

[22] EASA. Study on the societal acceptance of urban air mobility in Europe, 05 2021. URL: `https://www.easa.europa.eu/en/full-report-study-societal-acceptance-urban-air-mobility-europe`.

[23] EASA. Environmental protection technical specifications applicable to VTOL-capable aircraft powered by tilting rotors. *consultation paper*, 1, 2023. URL: `https://www.easa.europa.eu/en/document-library/product-certification-consultations/consultation-paper-environmental-protection-0`.

[24] European Union Aviation Safety Agency EASA. UAM ten key findings, 2025. Accessed 29th January 2025. URL: `https://www.easa.europa.eu/en/uam-10-key-findings`.

[25] European Union Aviation Safety Agency EASA. What is UAM?, 2025. Accessed 29th January 2025. URL: `https://www.easa.europa.eu/en/what-is-uam`.

[26] H. Eißfeldt and M. Stolz. Public perception of air taxis in Germany: anticipated risks, benefits, and noise sensitivity. *Proceedings of Meetings on Acoustics*, 54(1), 09 2024. `doi:10.1121/2.0001947`.

[27] UBER Elevate. Fast-forwarding to a future of on-demand urban air transportation. *white paper*, 2016. URL: `https://evtol.news/__media/PDFs/UberElevateWhitePaperOct2016.pdf`.

[28] E. Envia, D. Huff, and C. Morrison. Analytical assessment of stator sweep and lean in reducing rotor-stator tone noise. *Aeroacoustics Conference*, 1996. `doi:10.2514/6.1996-1791`.

[29] E. Envia and M. Nallasamy. Design selection and analysis of a swept and leaned stator concept. *Journal of Sound and Vibration*, 228(4):793–836, 1999. `doi:https://doi.org/10.1006/jsvi.1999.2441`.

[30] Department of Transportation Federal Aviation Administration. Noise standards: Aircraft type and airworthiness certification, CFR Title 14, Part 36, 2016 Edition. URL: `https://www.ecfr.gov/current/title-14/chapter-I/subchapter-C/part-36`.

[31] C. Feldmann, T. Carolus, and M. Schneider. A semantic differential for evaluating the sound quality of fan systems. *Turbo Expo Volume 1: Aircraft Engine; Fans and Blowers; Marine; Honors and Awards*, 06 2017. `doi:10.1115/GT2017-63172`.

[32] D. Giacche, T. P. Hynes, S. Baralon, J. Coupland, N. Humphreys, and P. Schwaller. Acoustic optimization of ultra-low count bypass outlet guide vanes. *19th AIAA/CEAS Aeroacoustics Conference*, 2013. `doi:10.2514/6.2013-2295`.

[33] S. Guerin and A. Moreau. Accounting for sweep and lean in the design-to-noise of rotor-stator stages. *Fortschritte der Akustik DAGA 2010. 36. Deutsche Jahrestagung für Akustik*, 2010. URL: `https://elib.dlr.de/68802/`.

[34] S. Guérin, C. Kissner, P. Seeler, R. Blázquez, P. Carrasco Laraña, H. de Laborderie, D. Lewis, P. Chaitanya, C. Polacsek, and J. Thisse. ACAT1 benchmark of RANS-informed analytical methods for fan broadband noise prediction: Part II—influence of the acoustic models. *Acoustics*, 2(3):617–649, 2020. `doi:10.3390/acoustics2030033`.

[35] S. Guérin and D. Tormen. A contribution to the investigation of acoustic interferences in aircraft distributed propulsion. *CEAS Aeronautical Journal*, 14:965–982, 2023. `doi:10.1007/s13272-023-00679-6`.

[36] D. Y. Gwak, D. Han, and S. Lee. Sound quality factors influencing annoyance from hovering UAV. *Journal of Sound and Vibration*, 489:115651, 2020. `doi:10.1016/j.jsv.2020.115651`.

[37] D. Hanson. Acoustic reflection and transmission of rotors and stators including mode and frequency scattering. *3rd AIAA/CEAS Aeroacoustics Conference*, 1997. `doi:10.2514/6.1997-1610`.

[38] D. B. Hanson. Theory for broadband noise of rotor and stator cascades with inhomogeneous inflow turbulence including effects of lean and sweep. *NASA/CR–2001-210762*, 2001. URL: `https://ntrs.nasa.gov/api/citations/20010071812/downloads/20010071812.pdf`.

[39] B. P. Hill, O. DeCarme, M. Metcalfe, C. Griffin, S. Wiggins, C. Metts, B. Bastedo, M. D. Patterson, and N. L. Mendonca. UAM vision concept of operations (ConOps) UAM maturity level (UML) 4. *NASA Contractor or Grantee Report prepared by Deloitte Consulting LLP*, 2020. URL: `https://ntrs.nasa.gov/citations/20205011091`.

[40] R. Jaron. *Aeroakustische Auslegung von Triebwerksfans mittels multidisziplinärer Optimierungen*. Dissertation, Technical University of Berlin, Berlin, Germany, 2018. `doi:10.14279/depositonce-7057`.

[41] J. Y. Jeon, J. You, C. Il Jeong, S. Y. Kim, and M. J. Jho. Varying the spectral envelope of air-conditioning sounds to enhance indoor acoustic comfort. *Building and Environment*, 46(3):739–746, 2011. `doi:10.1016/j.buildenv.2010.10.005`.

[42] M. G. Jones, F. Simon, and R. Roncen. Broadband and low-frequency acoustic liner investigations at NASA and ONERA. *AIAA Journal*, 60(4):2481–2500, 2022. `doi:10.2514/1.J060862`.

[43] H. Kim and M.-S. Liou. Flow simulation and optimal shape design of N3-X hybrid wing body configuration using a body force method. *Aerospace Science and Technology*, 71:661–674, 2017. `doi:10.1016/j.ast.2017.09.046`.

[44] H. D. Kim, A. T. Perry, and P. J. Ansell. A review of distributed electric propulsion concepts for air vehicle technology. *2018 AIAA/IEEE Electric Aircraft Technologies Symposium*, 2018. URL: `https://www1.grc.nasa.gov/wp-content/uploads/2018EATS-Review-of-DEP-Hyun-D.-6.2018-4998.pdf`.

[45] L. Klähn, L. Caldas, R. Meyer, A. Moreau, and U. Tapken. Experimental investigation of inflow-distortion-induced tonal noise in a sub-sonic fan test rig. *29th International Congress on Sound and Vibration, ICSV 2023*, 07 2023. URL: `https://elib.dlr.de/194810/`.

[46] L. Klähn, A. Moreau, L. Caldas, and U. Tapken. Assessment of in-duct fan broadband noise measurements in a modern low-speed test rig. *International Conference of Fan Noise, Aerodynamics, Applications and Systems 2022*, 2022. `doi:10.26083/tuprints-00021709`.

[47] L. Klähn, R. Meyer, and U. Tapken. Inflow distortion noise and turbulence measurements in a low speed fan test rig. *30th AIAA/CEAS Aeroacoustics Conference (2024)*, 2024. `doi:10.2514/6.2024-3157`.

[48] H. Kobayashi and J. F.Groeneweg. Effects of inflow distortion profiles on fan tone noise. *AIAA Journal*, 18(8):899–906, 1980. `doi:10.2514/3.50832`.

[49] F. Kohlenberg, A. Schulz, L. Enghardt, and K. Knobloch. Modeling of advanced helmholtz resonator liners with a flexible wall. *AIAA Journal*, 61(7):3108–3118, 2023. `doi:10.2514/1.J062227`.

[50] S. Krishnamurthy, S. Rizzi, R. Cheng, D. D. Boyd, and A. W. Christian. Prediction-based auralization of a multirotor urban air mobility vehicle. *AIAA Scitech 2021 Forum*, 2021. `doi:10.2514/6.2021-0587`.

[51] G. Kröger, R. Schnell, and N. D. Humphreys. Optimised aerodynamic design of an OGV with reduced blade count for low noise aircraft engines. *Turbo Expo: Power for Land, Sea, and Air*, Volume 8: Turbomachinery, Parts A, B, and C:407–418, 06 2012. `doi:10.1115/GT2012-69459`.

[52] U. Landström, E. Åkerlund, A. Kjellberg, and M. Tesarz. Exposure levels, tonal components, and noise annoyance in working environments. *Environment International*, 21(3):265–275, 1995. `doi:10.1016/0160-4120(95)00017-F`.

[53] J. Lee. *The effects of tones in noise on human annoyance and performance*. Dissertation, ETD collection for University of Nebraska-Lincoln, 2016. AAI10102764. URL: `https://digitalcommons.unl.edu/dissertations/AAI10102764`.

[54] Lilium. Lilium media kit, 2025. `https://lilium.com` [Accessed: 20 March 2025].

[55] F. B. Metzger, R. W. Menthe, and C. J. Mccolgan. Performance and noise of a low pressure ratio variable pitch fan designed for general aviation applications. *NASA Contractor Report CR-159246*, 1980. URL: `https://ntrs.nasa.gov/citations/19810018561`.

[56] S. More and P. Davies. Human responses to the tonalness of aircraft noise. *Noise Control Engineering Journal*, 58(4):420–440, 2010. `doi:10.3397/1.3475528`.

[57] A. Moreau. *A unified analytical approach for the acoustic conceptual design of fans for modern aero-engines*. Dissertation, Technical University of Berlin, Berlin, Germany, 2017. `doi:10.14279/depositonce-5935`.

[58] A. Moreau and S. Guerin. Similarities of the free-field and in-duct formulations in rotor noise problems. *17th AIAA/CEAS Aeroacoustics Conference (32nd AIAA Aeroacoustics Conference)*, 2011. AIAA 2011-2759. `doi:10.2514/6.2011-2759`.

[59] A. Moreau, S. Guérin, and S. Busse. A method based on the ray structure of acoustic modes for predicting the liner performance in annular ducts with flow. *International Conference on Acoustics NAG/DAGA 2009*, conference proceedings:1248–1251, 2009. URL: `http://pub.dega-akustik.de/NAG_DAGA_2009/data/articles/000268.pdf`.

[60] A. Moreau, S. Guérin, L. Enghardt, A.-L. Le Denmat, E. Nicke, S. Weber, S. Diehl, and P. Koch. The new NWB ventilator: a practical case of design-to-noise. *18th AIAA/CEAS Aeroacoustics Conference (33rd AIAA Aeroacoustics Conference)*, 2012. `doi:10.2514/6.2012-2178`.

[61] A. Moreau, A. Prescher, S. Schade, M. Dang, R. Jaron, and S. Guérin. A framework to simulate and to auralize the sound emitted by aircraft engines. *InterNoise conference 2023*, conference proceedings, 2023. `doi:10.3397/IN_2023_1073`.

[62] M. Nallasamy, E. Envia, S. Thorp, and A. Shabbir. Fan noise source diagnostic test - computation of rotor wake turbulence noise. *8th AIAA/CEAS Aeroacoustics Conference & Exhibit*, 2002. AIAA-2022-2489. `doi:10.2514/6.2002-2489`.

[63] P. Nathen. *Architectural performance assessment of an electric vertical take-off and landing (e-VTOL) aircraft based on a ducted vectored thrust concept*, 2021. URL: `https://investors.lilium.com/static-files/c355ba0f-662c-466c-aa6a-43072b3d34c3`.

[64] International Civil Aviation Organization. Annex 16 to the Convention on International Civil Aviation, Environmental Protection, Volume I, Aircraft Noise (7th Edition), 2014.

[65] H. Pak, L. Asmer, and P. Kokus et al. Can urban air mobility become reality? Opportunities and challenges of UAM as innovative mode of transport and DLR contribution to ongoing research. *CEAS Aeronautical Journal*, 2024. `doi:10.1007/s13272-024-00733-x`.

[66] R. Pieren, L. Bertsch, D. Lauper, and B. Schäffer. Improving future low-noise aircraft technologies using experimental perception-based evaluation of synthetic flyovers. *Science of The Total Environment*, 692:68–81, 2019. `doi:10.1016/j.scitotenv.2019.07.253`.

[67] C. Poggi, M. Rossetti, J. Serafini, G. Bernardini, M. Gennaretti, and U. Iemma. Neural network meta–modelling for an efficient prediction of propeller array acoustic signature. *Aerospace Science and Technology*, 130:107910, 2022. `doi:10.1016/j.ast.2022.107910`.

[68] S. Rizzi. Toward reduced aircraft community noise impact via a perception-influenced design approach. *45th International Congress and Exposition on Noise Control Engineering INTER-NOISE 2016*, 08 2016. URL: `https://ntrs.nasa.gov/api/citations/20160011152/downloads/20160011152.pdf`.

[69] S. Rizzi and A. Christian. A psychoacoustic evaluation of noise signatures from advanced civil transport aircraft. *22nd AIAA/CEAS Aeroacoustics Conference*, 2016. `doi:10.2514/6.2016-2907`.

[70] S. Rizzi and A. K. Sahai. Auralization of air vehicle noise for community noise assessment. *CEAS Aeronautical Journal*, 10:313–334, 2019. `doi:10.1007/s13272-019-00373-6`.

[71] S. A. Rizzi, D. L. Huff, D. D. Boyd, P. Bent, B. S. Henderson, K. A. Pascioni, D. C. Sargent, D. L. Josephson, M. Marsan, H. He, and R. Snider. Urban air mobility noise: Current practice, gaps, and recommendations. *NASA/TP-2020-5007433*, 2020. URL: `https://ntrs.nasa.gov/api/citations/20205007433/downloads/NASA-TP-2020-5007433.pdf`.

[72] S. Schade, J. Ludowicy, P. Ratei, M. Hepperle, A. Stürmer, K.-S. Rossignol, S. de Graaf, and T. F. Geyer. Conceptual design of electrically-powered urban air mobility vehicles for aeroacoustic studies. *under review for CEAS Aeronautical Journal, presented at German Aerospace Congress DLRK 2024*, 2025.

[73] S. Schade, R. Merino-Martinez, P. Ratei, S. Bartels, R. Jaron, and A. Moreau. Initial study on the impact of speed fluctuations on the psychoacoustic characteristics of a distributed propulsion system with ducted fans. *30th AIAA/CEAS Aeroacoustics Conference (2024)*, 2024. `doi:10.2514/6.2024-3273`.

[74] B. Schiltgen, M. Green, D. Hall, A. Gibson, T. Foster, and M. Waters. Split-wing propulsor design and analysis for electric distributed propulsion. *49th AIAA Aerospace Sciences Meeting including the New Horizons Forum and Aerospace Exposition*, 2011. `doi:10.2514/6.2011-224`.

[75] S. Schoder, J. Schmidt, A. Fürlinger, R. Klaus, and M. Paul. An affordable acoustic measurement campaign for early prototyping applied to electric ducted fan units. *Fluids*, 8(4), 2023. `doi:10.3390/fluids8040116`.

[76] P. Schwaller, A. Parry, M. Oliver, and A. Eccleston. Far-field measurement and mode analysis of the effects of vane/blade ratio on fan noise. *9th Aeroacoustics Conference*, 1984. `doi:10.2514/6.1984-2280`.

[77] B. Schäffer, R. Pieren, M. Brink, and S. J. Schlittmeier. Development and application of a semantic differential for perception-based optimization of wind turbine and other broadband sounds. *Applied Acoustics*, 211, 2023. `doi:https://doi.org/10.1016/j.apacoust.2023.109493`.

[78] M. Schütte, U. Müller, S. Sandrock, B. Griefahn, C. Lavandier, and B. Barbot. Perceived quality features of aircraft sounds: An analysis of the measurement characteristics of a newly created semantic differential. *Applied Acoustics*, 70(7):903–914, 2009. `doi:10.1016/j.apacoust.2009.01.004`.

[79] A. M. Stoll, E. V. Stilson, J. Bevirt, and P. P. Pei. Conceptual design of the Joby S2 electric VTOL PAV. *14th AIAA Aviation Technology, Integration, and Operations Conference*, 2014. `doi:10.2514/6.2014-2407`.

[80] D. L. Sutliff, D. M. Nark, and M. G. Jones. Multi-degree-of-freedom liner development: Concept to flight test. *International Journal of Aeroacoustics*, 20(5-7):792–825, 2021. `doi:10.1177/1475472X211023860`.

[81] U. Tapken. *Analyse und Synthese akustischer Interaktionsmoden von Turbomaschinen*. Dissertation, Technical University of Berlin, Berlin, Germany, 2016. `doi:10.14279/depositonce-5124`.

[82] U. Tapken, L. Caldas, R. Meyer, M. Behn, L. Klähn, R. Jaron, and A. Rudolphi. Fan test rig for detailed investigation of noise generation mechanisms due to inflow disturbances. *AIAA AVIATION 2021 FORUM*, 2021. `doi:10.2514/6.2021-2314`.

[83] A. J. Torija and C. Clark. A psychoacoustic approach to building knowledge about human response to noise of unmanned aerial vehicles. *International Journal of Environmental Research and Public Health*, 18(2), 2021. `doi:10.3390/ijerph18020682`.

[84] A. J. Torija, Z. Li, and P. Chaitanya. Psychoacoustic modelling of rotor noise. *The Journal of the Acoustical Society of America*, 151(3):1804–1815, 03 2022. `doi:10.1121/10.0009801`.

[85] J. M. Tyler and T. G. Sofrin. Axial flow compressor noise studies. *SAE Technical Paper 620532*, 01 1962. `doi:10.4271/620532`.

[86] A. Osses Vecchi, R. García León, and A. Kohlrausch. Modelling the sensation of fluctuation strength. *Proceedings of Meetings on Acoustics*, 28(1):050005, 04 2017. `doi:10.1121/2.0000410`.

[87] G. von Bismark. Sharpness as an attribute of the timbre of steady sounds. *Acta Acustica united with Acustica*, 30(3):159–172, 1974. URL: `https://www.semanticscholar.org/paper/Sharpness-as-an-attribute-of-the-timbre-of-steady-Bismarck/9576a2a74bff46ee0cded25bfd9e4302b4fb0470`.

[88] M. Vorländer. *Auralization - Fundamentals of Acoustics, Modelling, Simulation, Algorithms and Acoustic Virtual Reality*. Springer Berlin, Heidelberg, 1 edition, 2008. `doi:10.1007/978-3-540-48830-9`.

[89] Y. Wang, G. Shen, Y. Gong, and W. Wu. Correlation study on the subjective and objective evaluation indices of sound quality based on vehicle noises. *Research Journal of Applied Sciences, Engineering and Technology*, 4(22), 2012. URL: `https://maxwellsci.com/print/rjaset/v4-4851-4855.pdf`.

[90] D. Weintraub, J. Koppelberg, J. Köhler, and P. Jeschke. Ducted fans for hybrid electric propulsion of small aircraft. *CEAS Aeronautical Journal*, 13:471–485, 2022. `doi:10.1007/s13272-022-00573-7`.

[91] R. Woodward, C. Hughes, R. Jeracki, and C. Miller. Fan noise source diagnostic test – far-field acoustic results. *8th AIAA/CEAS Aeroacoustics Conference & Exhibit*, 2002. `doi:10.2514/6.2002-2427`.

[92] R. Worobel and M. G. Mayo. Q-FANSTM for general aviation aircraft. *NASA Contractor Report CR-114665*, 1973. URL: `https://ntrs.nasa.gov/citations/19740005613`.

[93] T. Zhang and G. N. Barakos. Review on ducted fans for compound rotorcraft. *The Aeronautical Journal*, 124(1277):941–974, 2020. `doi:10.1017/aer.2019.164`.

[94] R. Meier zu Ummeln. *Aeroakustische Bewertung von Fanstufen im Rahmen des Vorentwurfs von Triebwerken*. Dissertation, Technical University of Berlin, Berlin, Germany, 2024. `doi:10.14279/depositonce-19827`.

Associated Publications

R. Merino-Martinez, S. Schade. *Psychoacoustic analysis of the perceptual influence of rotational speed fluctuations in an urban air mobility vehicle with distributed ducted fans*, 54th International Congress & Exposition on Noise Control Engineering, InterNoise, Brazil, 2025.

S. Schade, J. Ludowicy, P. Ratei, M. Hepperle, A. Stürmer, K.-S. Rossignol, S. de Graaf, T. F. Geyer. *Conceptual design of electrically-powered Urban Air Mobility vehicles for aeroacoustic studies*, presented at Deutscher Luft- und Raumfahrtkongress 2024.

S. Schade, R. Merino-Martinez, A. Moreau, S. Bartels, R. Jaron. Psychoacoustic evaluation of different fan designs for an urban air mobility vehicle with distributed propulsion system. *J. Acoust. Soc. Am.* 26 March 2025; 157 (3): 2150–2167. doi: 10.1121/10.0036228

D. Straub, S. Schade, R. Al Mahmudur, S. Bartels. *Novel Approach to assess the link between engine design parameters and noise perception.* In: Proceedings of Quiet Drones 2024, Manchester, Großbritannien, 2024.
`https://elib.dlr.de/207235/`

S. Schade, R. Merino-Martinez, P. Ratei, S. Bartels, R. Jaron and A. Moreau. *Initial Study on the Impact of Speed Fluctuations on the Psychoacoustic Characteristics of a Distributed Propulsion System with Ducted Fans*, AIAA 2024-3273. 30th AIAA/CEAS Aeroacoustics Conference (2024). June 2024. doi: 10.2514/6.2024-3273

S. Schade, R. Jaron, L. Klähn, A. Moreau. Smart Blade Count Selection to Align Modal Propagation Angle with Stator Stagger Angle for Low-Noise Ducted Fan Designs. *Aerospace* 2024, 11, 259. doi: 10.3390/aerospace11040259

A. Prescher, A. Moreau, S. Schade. Model for random atmospheric inhomogeneities in engine noise auralization, *CEAS Aeronaut J* 15, 1111–1125 (2024). doi: 10.1007/s13272-024-00764-4

A. Moreau, A. Prescher, S. Schade, M. Dang, R. Jaron, S. Guérin. *A framework to simulate and to auralize the sound emitted by aircraft engines.* INTER-NOISE and NOISE-CON Congress and Conference Proceedings, 125 (1), 2023, ISSN 0736-2935. doi: 10.3397/IN_2023_1073

S. Schade, L. Klähn, R. Jaron. *Analytische, numerische und experimentelle Untersuchung des tonalen Rotor-Stator Interaktionsschalls in einer langsam drehenden, ummantelten Fanstufe.* In: Proceedings of DAGA 2023 - 49. Jahrestagung für Akustik, pp. 526-529, Hamburg, 2023. `https://pub.dega-akustik.de/DAGA_2023/data/articles/000341.pdf`

S. Schade, R. Jaron, A. Moreau, S. Guérin. Mechanisms to reduce the blade passing frequency tone for subsonic low-count OGV fans. *Aerospace Science and Technology*, Volume 125, SI: DICUAM 2021, 2022, ISSN 1270-9638. doi: 10.1016/j.ast.2021.107083

S. Schade, R. Jaron, S. Guérin. *Einfluss der Schaufelzahlpaarung auf den Rotor-Stator-Interaktionslärm unter Berücksichtigung einer Lärmbewertungsmethode.* Deutsche Gesellschaft für Akustik e.V.. DAGA 2020 - 46. Jahrestagung für Akustik, Hannover, 2020. `https://elib.dlr.de/135044/`.